DOT/FAA/AR-95/110

Office of Aviation Research
Washington, D.C. 20591

Fiber Reinforced Structures for Small Turbine Engine Fragment Containment (Phase II)

July 1996

Final Report

This document is available to the U.S. public through the National Technical Information Service, Springfield, Virginia 22161.

U.S. Department of Transportation
Federal Aviation Administration

DISCLAIMER NOTICE

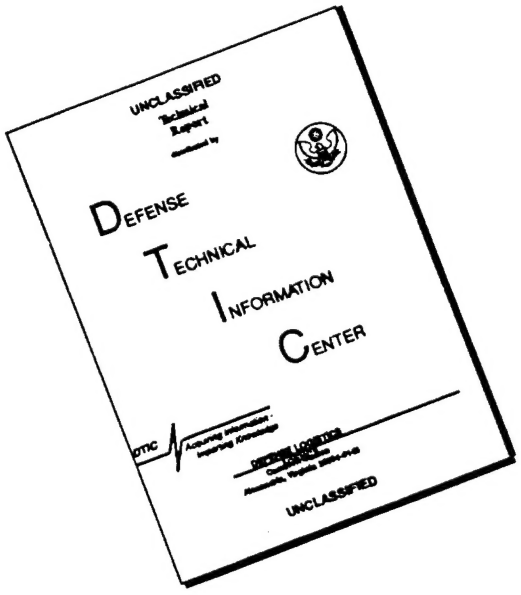

THIS DOCUMENT IS BEST QUALITY AVAILABLE. THE COPY FURNISHED TO DTIC CONTAINED A SIGNIFICANT NUMBER OF PAGES WHICH DO NOT REPRODUCE LEGIBLY.

NOTICE

Technical Report Documentation Page

1. Report No.	2. Government Accession No.	3. Recipient's Catalog No.
DOT/FAA/AR-95/110		

4. Title and Subtitle	5. Report Date
FIBER REINFORCED STRUCTURES FOR SMALL TURBINE ENGINE FRAGMENT CONTAINMENT (PHASE II)	July 1996
	6. Performing Organization Code
7. Author(s)	8. Performing Organization Report No.
9. Performing Organization Name and Address Pepin Associates, Inc. 15 Holly Street Scarborough, ME 04074	10. Work Unit No. (TRAIS)
	11. Contract or Grant No. DTRS-57-90-C-00025
12. Sponsoring Agency Name and Address U.S. Department of Transportation Federal Aviation Administration Office of Aviation Research Washington, DC 20491	13. Type of Report and Period Covered Final Report
	14. Sponsoring Agency Code AAR-431

15. Supplementary Notes

FAA COTR: John Reinhardt

16. Abstract

This Phase II program developed two fiber reinforced structures for lightweight containment of turbine rotor failures. The first is a hybrid core sandwich panel capable of being used both as a part of the airframe or nacelle structure and as a containment panel, if required. The second is a collar or ring placed close to the turbine case wall of a turbofan, turboprop, or turboshaft engine. The program focused on the design of these structures to contain a 1 million in-lb. T-53 tri-hub rotor burst using the lowest weight containment structure possible.

These goals were accomplished by sandwich panel and ring design tasks, test article fabrication, and spin pit testing. Design modification and subsequent testing developed an understanding of the relationship between reinforcement architecture, static/elastic behavior, and dynamic/impact behavior of the ring and panel. Additional spin pit testing was performed to evaluate changes in geometry and panel-to-panel joint designs.

The hybrid panel structure is composed of facesheets connected by many rigid rods which penetrate a dry fabric laminate. The core was shown to be mechanically equivalent to typical aerospace grade honeycombs as well as effective in stopping high velocity fragments. Kevlar 29 Polybenzbisoxazole (PBO) fabrics were used to absorb fragment energies while graphite/epoxy was used as the structural material. For particular containment designs and fiber architectures, ply count thresholds were obtained which just contained the tri-hub rotor burst. This allowed comparison to determine how the architecture and fiber choice affected the performance.

The program results indicate containment structure design characteristics to stop small rotor disk bursts, and these results can guide engine and airframe structure design to minimize the weight/space penalty for containment of internal turbine engine failures.

17. Key Words	18. Distribution Statement
Uncontained turbine engine failure, Kevlar, Polybenzbisoxazole, Containment ring, Spin pit testing	This document is available to the public through the National Technical Information Service, Springfield, Virginia 22161

19. Security Classif. (of this report)	20. Security Classif. (of this page)	21. No. of Pages	22. Price
Unclassified	Unclassified	91	N/A

TABLE OF CONTENTS

LIST OF FIGURES

LIST OF TABLES

EXECUTIVE SUMMARY

This Phase II program sought to develop a hybrid sandwich panel structure capable of supporting mechanical loads like a honeycomb panel but also capable of preventing the penetration of high velocity fragments as from a failed turbine engine disk. Such a panel could be applied to nacelles, cowlings, firewalls, or other airframe structure to prevent blade or disk fragments from a failed rotor from damaging critical components of an aircraft. This goal was accomplished by mechanical tests to establish the compressive, shear, and flexure properties of the new core and spin chamber tests to evaluate its ability to stop high velocity disk fragments. A second objective of the program was to determine the potential of polybenzbisoxazole (PBO) fiber as a material for lightweight containment structures in areas exposed to high temperatures such as near an engine hot section. The spin test program included a PBO ring whose results were compared directly to a Kevlar 29 ring of similar geometry and fiber architecture. Other results of this program included the effect of fiber architecture on containment performance and initial joint designs for containment panels.

The hybrid sandwich panel consists of a dry, unimpregnated fabric laminate with several closely spaced rigid rods penetrating through its thickness. These rods are mechanically attached to rigid facesheets. This concept was tested mechanically using Kevlar fabric for the dry laminate and graphite/epoxy for the rigid structure. The results showed that the mechanical properties of such a structure are equivalent to those for commonly used aerospace honeycomb cores. Using the same Kevlar fabric and graphite/epoxy materials, panel and ring structures were fabricated and tested in a spin Chambers. Ten spin tests were performed using a T-53 rotor precut to fail in a tri-hub burst mode at one million in-lb. of rotor energy. The sandwich panel core performed as well or better than similar structures without the rigid rod architecture showing that no containment performance penalty is paid for including these rods in the structure.

The PBO ring tested contained the tri-hub burst at the same weight and number of fabric plies as one of the Kevlar rings; however, the real advantage of PBO fiber containment structures will be realized at elevated temperatures where they could be used near engine hot sections. At this time PBO is still being developed by Toyobo Inc. and is not yet commercially available.

Energy absorbing fiber architecture was also varied and showed the potential of off-axis designs to reduce weight if larger distances to stop the fragments could be tolerated. Other design issues included the necessity of crushing blades to prevent their being driven through a containment structure wall by a disk segment and avoiding massive objects in the expansion zone of the structure to prevent its being pinched between the object and the high velocity fragment.

These Phase II results, then, show the potential of the hybrid sandwich panel for application to containment barrier structures on aircraft and helicopters and the issues which must be addressed when specific installations are designed. These include geometry, constituents, fiber architecture, and joints.

1. BACKGROUND.

1.1 OVERVIEW.

Since the advent of turbine powered aircraft, the risk of turbine engine rotor failures and damage from resulting high-energy fragments has been present. Although uncontained rotor failures are thankfully rare, significant damage can result when these events do occur. In some cases high-energy rotor fragments have severed control cables, fuel lines, and other critical systems. Such fragments have also penetrated fuel tanks, pressurized fuselage skin and frames, and other engines on the aircraft. The Federal Aviation Administration (FAA) has established regulations and design guidelines for containment of rotor failures in Federal Aviation Regulation (FAR) 33 subpart B which defines engine design requirements and FARs 23 and 25 which include design precautions to minimize hazards from uncontained engine and auxiliary power units (APU) failures. Advisory Circulars (AC) also serve as design guidelines for location critical systems and components relative to the engine rotors and fan blades.

Current regulations require that the failure of a fan, compressor, or turbine blade be contained and that the engine safely shutdown after such a failure. A single blade failure may lead to the failure of other blades or other components in the engine. Engine manufacturers must demonstrate that an engine can lose a critical rotor blade and be successfully shutdown after 15 seconds without a fire, case flange separation, or excessive mount loads.

Containment of a rotor disk failure has so far been impractical due to very high disk energy levels and the weight and volume required for a structure to contain a disk rupture. Design guidance in this area [1] focuses on saving the aircraft after a disk failure. Specific approaches include evaluation of critical system locations relative to engine rotor planes and fragment paths. Critical components and areas are:

a. Other engines - High-energy fragments from a rotor failure on one engine could impact an adjacent engine causing its failure as well.

b. Fuselage, wing and empennage, primary structure, and pressure sections.

c. Flight crew area.

d. Fuel system and tanks - Fuel spillage inside the aircraft in the event of a ruptured tank must be avoided.

e. Electrical, hydraulic, fuel, and engine control systems.

f. Flight control systems - The aircraft must be controllable following engine rotor failure.

g. Engine fire extinguisher systems.

h. Instrumentation critical for continued safe flight and landing.

The design guidance given in reference 1 suggests locating critical components outside probable fragment paths. For large 1/3 disk fragments the impact zone is given as a ±3° conical angle on either side of the disk plane. This angle originates at the engine longitudinal axis. For other large fragments, this angle increases to ±5° and for smaller fragments the spread angle is ±15°. Important components in these vulnerable areas can be duplicated to provide redundancy or can be protected by airframe structure. Critical structures themselves must have redundant design to sustain fragment impact.

In cases where it is difficult to relocate or protect critical components, shield structures can be used. Fragment energies in rotation and translation must be considered when designing such shield structures. The worst case design condition for a disk failure, for example, would be a 1/3 segment failure at the critical rotating speed. This energy level can vary from 0.5 to 6 million in-lbs. and greater depending on engine size. Experience with fan blades has also shown that the most severe failures involve 4-lb. (17.8 N) tip fragments which spiral forward of the engine fan plane with velocities up to 900 feet/sec (274 m/sec). Smaller fragments of about 0.6 lb. (2.67 N) have been ingested and thrown forward. Average velocities of these fragments are about 400 ft/sec (121.9 m/sec). Shield structures of Kevlar are common around the fan case and are being considered for other applications such as fuselage protection for prop-fan installations, engine cowling patches, and APU/starter containment.

Although the containment issue is broad in scope and covers many complex questions, the FAA is particularly interested in developing lightweight containment structures for turbine disks on small turboprop, turboshaft, and turbofan engines as well as APUs. The reasons for this focus are that a relatively high uncontained failure rate exists in this category especially among turbine powered helicopters and that a small disk failure in the one million in-lb. energy range may be containable with a relatively lightweight structure. A 1987 Society of Automotive Engineers (SAE) report [2] covering aircraft and helicopter turbine engine failures between 1976 and 1983 concludes that the greater severity of helicopter noncontainment events was due to the close proximity of helicopter engines to critical systems and structures. Helicopters also operate at low altitudes and over rough terrain making successful auto rotation difficult. The demands on helicopter engines can also be very high such as when the helicopter is used for heavy log lifting, electrical tower lifting, and similar missions. In these cases a 6:1 factor is used on time change of turbine wheels; i.e., one hour of heavy lifting is equal to six hours of normal operation [3]. The SAE report did suggest a fairly good record for general aviation turbine aircraft over the period covered, but more recent incidents of hot section failure on turboprop commuter aircraft show the potential need for containment structures on small fixed-wing aircraft as well.

1.2 THE NEED FOR LIGHTWEIGHT CONTAINMENT STRUCTURES.

Engine manufacturers are striving to improve their products and meet the FAA requirements for blade containment along with the many other engine requirements. To prevent disk rupture a bladed disk is sometimes designed so that a noncatastrophic failure mode, such as blade failure, occurs first to prevent disk overspeed and possible failure. A mechanical fuel shutoff and electronic overspeed shutdown can also be included as additional safety measures. In spite of these efforts, however, uncontained failures do occur. Containment structures may be useful

until safety modifications are made to an engine or to routinely protect vital components as a means of compliance with FAA guidelines.

The source of turbine disk failure can be overheating, rubbing, defects in components, or overspeed due to some power train failure. Design, manufacturing, maintenance, and operation can all play a significant role in engine reliability and can each or most probably, in some combination, lead to uncontained failure. The Allison A250 engine which powers some S-76 helicopters as well as many other aircraft had developed internal oil fires due to leaking seals. Component overheating resulted in uncontained failures in this engine. While changes were being made, a containment ring was installed to prevent possible fragment damage to critical components. Internal containment was then built into the engine using Inconel 625. The Lycoming LTS 101 engine has had a few uncontained failures, reportedly maintenance and operation related. Some involved ignoring a chip light detector warning of metal particles in the engine oil [4]. According to Lycoming, an egg shaped containment collar prototype was fitted to the LTS 101 engine in the Bell 222 helicopter but the containment structure was abandoned after Airworthiness Directives (AD) were issued to solve the LTS 101 problems. In some Bell 222 operations several chip light warnings continue to occur and frequent engine changes are common while in others the experience has been good. The type of operation is probably partly responsible for these differences [5]. As mentioned, the helicopter installation is very sensitive to uncontained failure due to the proximity of the other engine, tail rotor shaft, fire extinguishers, and other critical systems.

Fixed-wing commuter and small turbofan powered aircraft have also experienced uncontained failures. The General Electric CT-7 engine was originally designed as a helicopter engine but was then adapted to turboprop aircraft and it now powers the SAAB 340. It is a very high-efficiency engine but hot section reliability and longevity have not been as good as some operators would like. Both contained and uncontained turbine rotor failures have occurred on the turboprop version of the CT-7. The PT-6 engine is very common and has an excellent record but on rare occasions it has released blade fragments. Since many turboprop corporate and commuter aircraft have wing-mounted engines whose disk planes are aligned with the crew area, uncontained failures such as these potentially threaten the safety of the entire aircraft. Lightweight containment rings near an engine or structures integral with a cowling could serve to block any fragment release from an engine compartment.

Containment structures have also been considered for direct, built-in applications on new aircraft to satisfy FAA requirements for noncatastrophic turbine rotor failure. Garrett and Embraer considered cowling patches for the Embraer 123 to protect the pressurized fuselage and fuel system. Since the aircraft is a pusher, contained fragments must not impact propeller blades. Such a failure mode may cause propeller blade failure and blade fragment penetration of the fuselage. However Embraer did not feel that appropriate containment technology was available and they chose to analyze potential fragment paths and move systems to comply with FAA guidelines.

Uncontained failures also occur on large turbofan engines. The most tragic example in recent times is the CF-6 fan disk failure on the United DC-10 which caused loss of most control and

lead to the eventual crash at Sioux City. Containment of such a failure has been investigated but not yet pursued because of the high-energy levels and, hence, large weight penalties involved. Better disk reliability, inspection procedures, and aircraft and engine system integration are current areas of focus to prevent such accidents in the future; however, in some very specific areas such as protecting computer control systems from possible wing-mounted engine failure, containment of such a large disk is still begin considered.

Other important applications for containment structures are on starters, air turbines, and APUs. An air turbine starter can overspeed if it becomes disengaged from the engine too early or does not disengage when the engine drives the starter. Optimal failure modes include blade rubbing or failure thereby eliminating the driving force accelerating the rotor; however, tri-hub burst containment may be required for some of these components. A similar air turbine device is often used to drive auxiliary systems. For example, the L1011 has an air turbine motor which runs on bleed air and drives a hydraulic pump used during takeoff and landing. Lockheed specified that the turbine rotor be notched such that it would fail at 20 percent of overspeed instead of a much higher value. This has caused reliability concerns for the notched turbine rotors now operating. If problems should occur a lightweight containment structure could be added as a barrier to rotor fragments.

APU's are sometimes located in particularly sensitive areas of aircraft and require disk containment structures for safety. These structures are usually metal, but advanced, lightweight disk containment structures made from high strength fibers could save 30 lbs (133 N) or more in some APU installations. Although further development of metal containment structures continues to support current needs, the lighter weight composite containment structures could eventually replace them given appropriate attention to fiber temperature stability. For example, near the compressor case a 400-600°F (204-315°C) environment is present while the turbine case wall is near 1200°F (649°C). The compressor core could be handled with fiber forms currently available while a hybrid layer design to provide thermal insulation for the energy absorbing fibers would be an approach for the hot section.

These few examples indicate that a lightweight containment system whose materials and design lend themselves to many engine installations would have significant benefit as an off-the-shelf measure to protect critical aircraft systems from rotor fragment impact. Such containment designs would be especially useful in situations where a particular turbine disk failure has many causes requiring several engine modifications. A containment structure would protect vital components while the problems were being sorted out and the corrections implemented. Lightweight containment designs would also be useful in new installations of both engines and APUs where the design constrains the engine and system location and consequences of uncontained failure would be particularly serious.

2. RESEARCH OBJECTIVES.

2.1 PANEL CONCEPT.

The first objective of this Phase II program was to evaluate the potential of the hybrid sandwich panel concept shown in figure 1 as a containment structure for turbine engines. This concept

would support structural loads like other sandwich panels but would also act as a barrier to high-velocity fragment impacts. The core of this sandwich panel is composed of many rigid, small-diameter rods piercing a multi-ply, dry fabric laminate. The rod ends are firmly attached to the facesheets providing the structural connection between one facesheet and the other. The dry, unimpregnated fabric laminate of the core is designed to absorb the energy of high-velocity fragment impacts at minimum weight. The structural performance of this panel was evaluated by mechanical testing while the containment potential was determined through spin pit testing of panel and ring structures surrounding a turbine rotor.

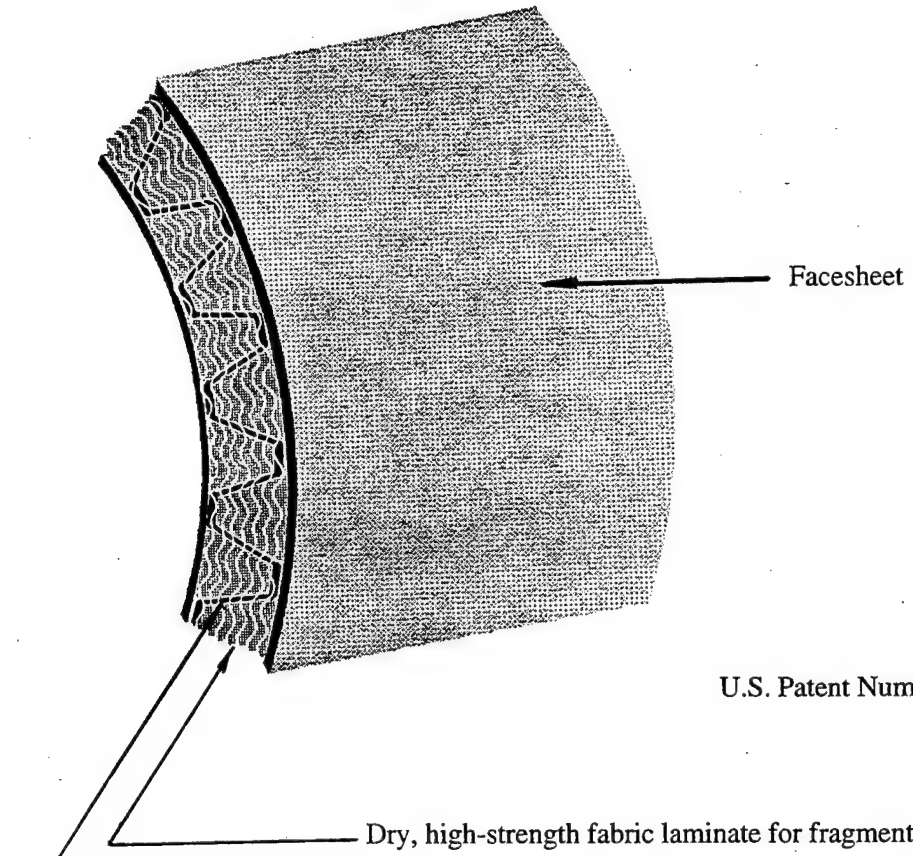

FIGURE 1. HYBRID STRUCTURAL ENERGY ABSORBING PANEL

2.2 INTERMEDIATE TEMPERATURE FIBER FOR RING STRUCTURE.

The second objective of this research program was to test the energy absorbing capability of polybenzbisoxazole (PB0) fiber. This fiber's high toughness, tensile strength, and especially its potential temperature stability to 572°F (300°C) make it attractive for a containment structure near the engine. Spin test results of a PB0 ring structure were compared with those of a Kevlar 29 ring.

3. RESEARCH WORK PERFORMED.

3.1 MECHANICAL TEST PROGRAM.

3.1.1 Goal and Testing Approach.

The broad goal of the mechanical test program was to determine if a through-thickness rod architecture as envisioned could efficiently transmit mechanical loads across the core of a sandwich panel. Mechanical properties of other core materials commonly used for aircraft and space structures were used for comparison with current results to assess the hybrid panel's mechanical efficiency. More specific goals for this test program include examining how changes in the rod geometry affected the mechanical properties and what failure modes occurred.

To begin to learn how the hybrid panel behaves mechanically, three different architectures were each tested in three modes - through-thickness compression, flexure, and shear. The testing was done in an iterative fashion so that test results on one type of architecture could be used to help select the rod array for the next series of tests. Three replicates of each property and rod array combination were performed.

3.1.2 Test Specimen Design.

The mechanical test specimens were small, hybrid core sandwich panels whose exterior dimensions coincided with those required for the particular test. They all had a dry, unimpregnated fabric laminate core of Kevlar 29 style 745 fabric plies. This dry laminate was wrapped with a 1-mil Teflon film and covered on each face by a graphite/epoxy prepreg fabric laminate which becomes part of the facesheet. The Teflon is a barrier to resin flow into the dry Kevlar. This stack of dry Kevlar, Teflon, and graphite/epoxy was then sewn through with 12K AS4/3501-6 towpreg in a stitch pattern which became the rigid rod array after the precursor form was molded. After all the rods were inserted, further plies of graphite/epoxy prepreg were added to cover the loops at the top and bottom. These loops were then trapped inside the facesheet to mechanically lock the rods to the facesheets.

An expanded cross section schematic of the typical test specimen lay-up is shown in figure 2. It shows the core of 24 plies of Kevlar 29 fabric encapsulated by a 1-mil Teflon film as described. The rods penetrate the fabric, the film, and three plies of the five-ply facesheet laminate to mechanically lock them into the facesheets themselves. The 12K (12000 filament) AS4/3501-6 unidirectional graphite/epoxy towpreg is from Hercules while the Kevlar fabric is style 745 from Clark Schwebel. The facesheets are laminates of either AS4/8553 3K plain weave fabric prepreg or AS/3501-6 6K five harness satin, dependent on the specimen.

These prepregs are also from Hercules. The 8553 resin was used on the flexure specimens because it is a tougher system. There were also some variations to the baseline lay-up sequence for some specimens and these will be noted as the test results are discussed.

A cutaway view of one of the shear specimens is shown in figure 3. The specimen was chiseled apart along its mid plane breaking many of the rods, but about half remain and these give a good view of the hybrid panel core structure with Kevlar fabric and graphite/epoxy rods.

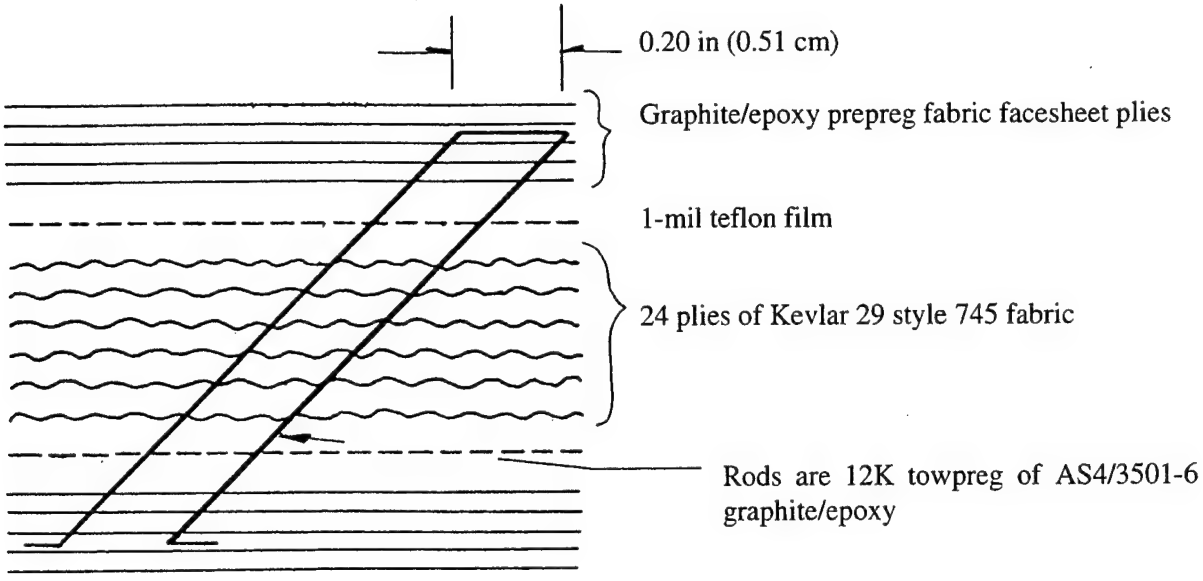

FIGURE 2. TYPICAL TEST SPECIMEN LAY-UP SHOWING A PAIR OF THROUGH-THICKNESS RODS WHOSE LOOP IS TRAPPED IN THE FACESHEET LAMINATE.

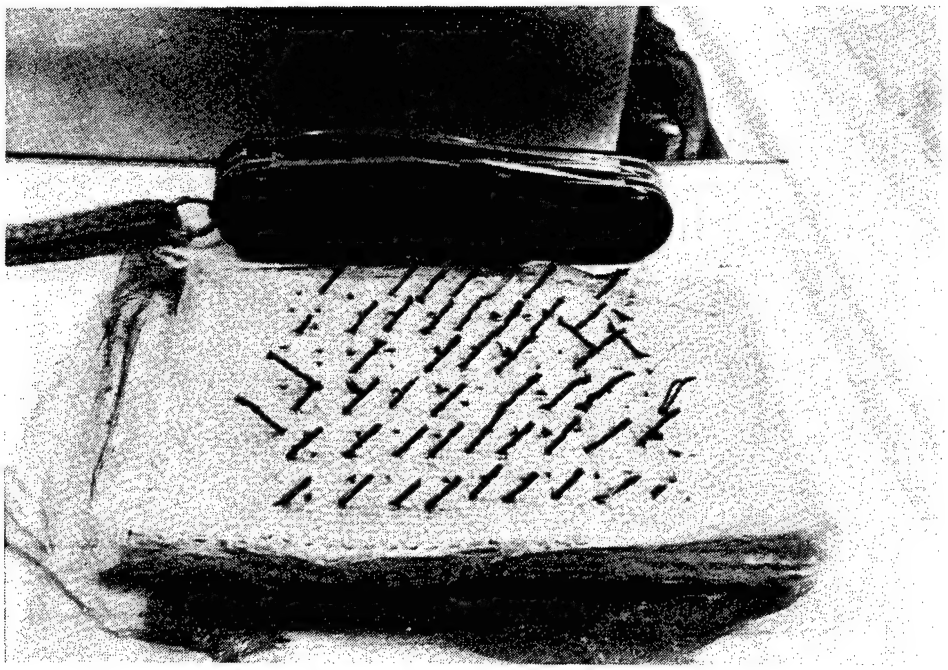

FIGURE 3. CUTAWAY OF SHEAR SPECIMEN SHOWING MANY OF THE ±45° 12K UNIDIRECTIONAL GRAPHITE/EPOXY RODS PENETRATING SOME OF THE DRY KEVLAR FABRIC LAMINATE PLIES. MOST OF THE -45° RODS WERE DAMAGED AS THIS SPECIMEN WAS SPLIT.

Three candidate rigid rod architectures were developed during the testing program. Candidate A is shown in figure 4. This figure shows the compression specimen with Candidate A architecture. A set of three rows of rods forms the building block of this core. The first row contains rods at +45°, the second row at 90°, and the third row at -45°. This sequence is repeated across the width of the specimen. The length of the loops on the surface is 0.20 in (0.51 cm) and distance between rows is also 0.20 in. (0.51 cm). Candidate B is the same as Candidate A except the 90°, rows are replaced by 45° rows so the rod architecture consists entirely of alternating ±45° rows. Candidate C is somewhat more complex in that, although the rods pierce the facesheet planes at 45°, they are not lined up in rows along a specimen axis. As figure 5 shows, the planes which contain the rods are at a 55° angle with respect to the facesheet planes providing shear strength and stiffness in both XY and XZ planes. The length of the loop at the surface is again 0.20 in (0.51 cm).

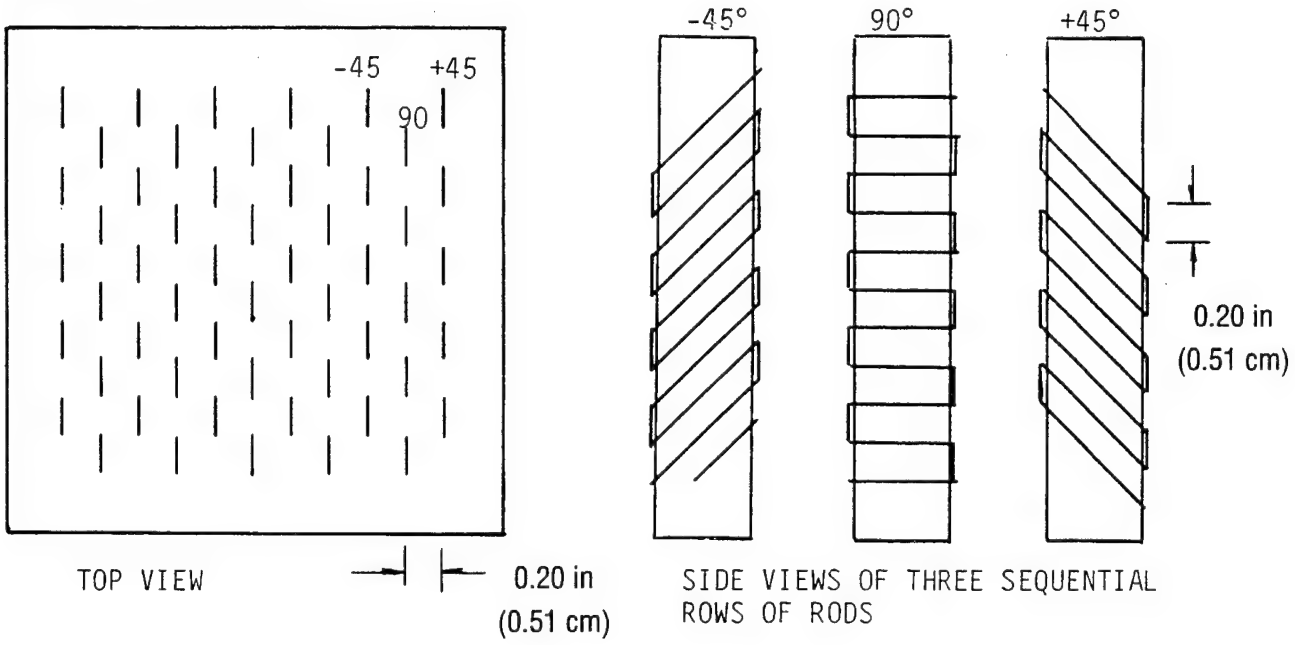

FIGURE 4. COMPRESSION SPECIMEN WITH CANDIDATE A THROUGH-THICKNESS ROD ARCHITECTURE. ROWS ALTERNATE +45°, 90°, AND -45° ROD PENETRATION ANGLES THROUGH THE DRY FABRIC LAMINATE

The specimen dimensions and test procedures follow Hexcel's TSB 120, Mechanical Properties of Hexcel Honeycomb Materials, which is based on MIL-STD401 and applicable ASTM standards. This allows direct comparison of mechanical properties obtained for the hybrid sandwich panel core to those of honeycomb cores commonly used in the aerospace industry. Nominal hybrid core panel specimen dimensions are given in table 1 while actual dimensions of each specimen are found in table A.1 of the appendix. These hybrid core panel dimensions differ slightly from those used by Hexcel for honeycomb panels. For example the flexure and compression specimens were slightly narrower to accommodate fabrication constraints but their surface areas were still large enough to allow accurate measurement of flexure and compression properties. The Kevlar laminate extended slightly beyond the area of the rigid rods to ensure support of all of the rods by the tightly woven area of the fabric.

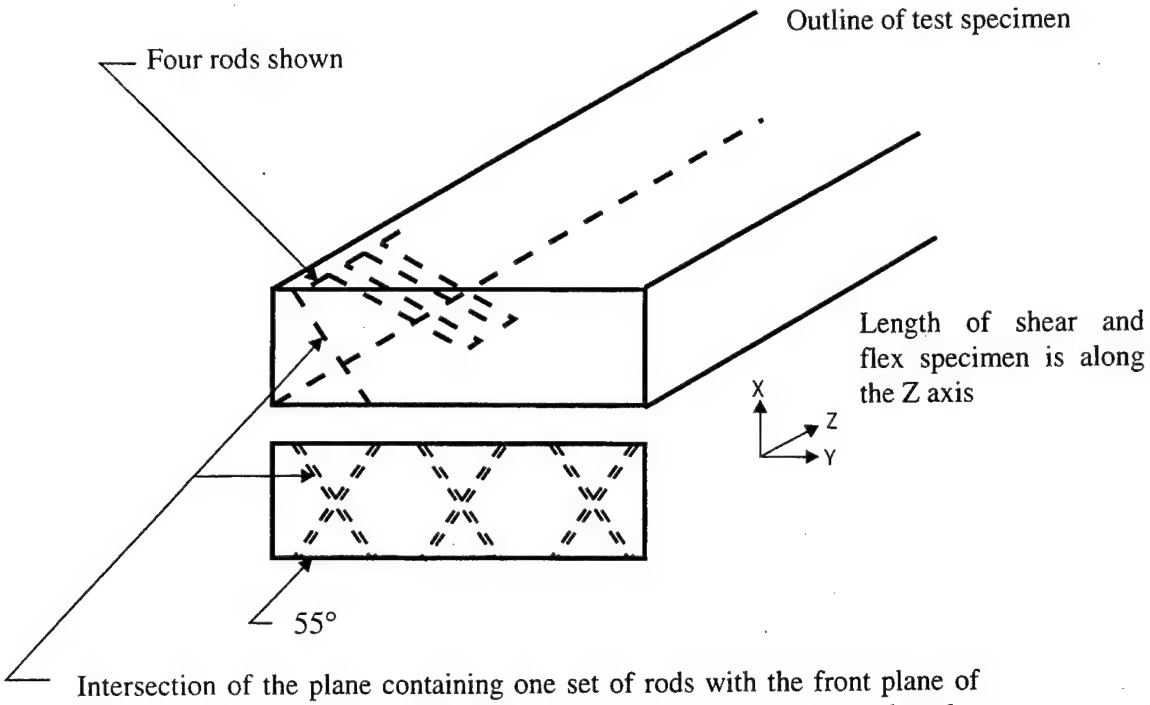

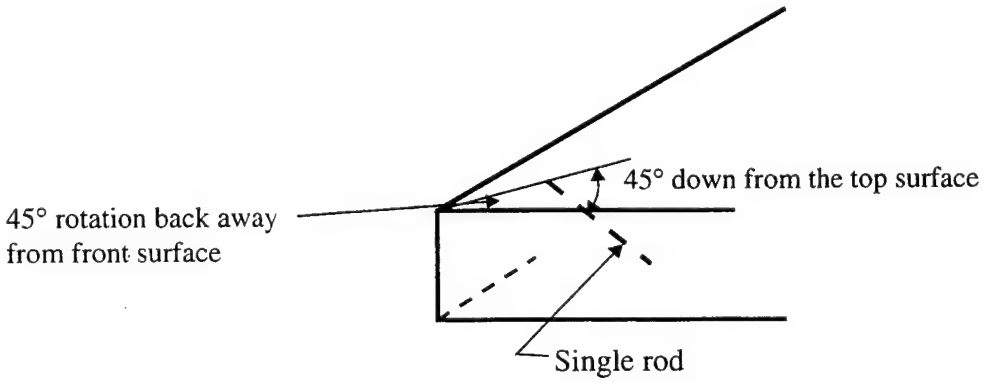

FIGURE 5. CANDIDATE C THROUGH-THICKNESS ROD ARCHITECTURE

TABLE 1. MECHANICAL TEST SPECIMEN NOMINAL DIMENSIONS

	Thickness in (cm)	Kevlar Core Width x Length in (cm)	Graphite/Epoxy Facesheet Width x Length in (cm)
Compression	0.60 (1.52)	2.75 (6.99) square	2.0 (5.08) square
Shear	0.60 (1.52)*	2.6 (6.60) x 3.8 (9.65)	2.0 (5.08) x 3.8 (9.65)
Flexure	0.60 (1 52)	2.3 (5.84) x 9 (22.86)	2.0 (5.08) x 8.75 (22.23)

*Candidate A is 0.37 inch thick

3.1.3 Test Specimen Fabrication.

The test specimens were fabricated by manually cutting and laying up the Kevlar, teflon film, and graphite/epoxy prepeg plies. The lay-up was sewn at the corners and taped around the edges to hold the plies in place. The rods connecting the facesheets were then inserted by manually sewing towpeg through the plies at the required spacing and angles guided by sliding them in grooves cut into angled blocks placed against the specimen as shown in figures 6 and 7. A grid was drawn on the prepreg surface to locate needle position. After the rods were all inserted into a particular specimen)the required additional plies of prepreg fabric were added on both sides to cover and trap the towpreg loops.

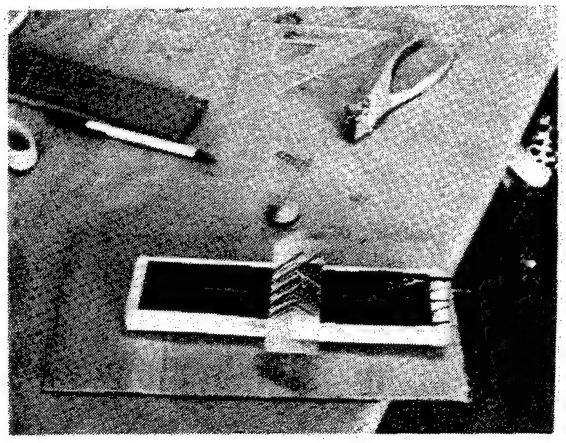

FIGURE 6. FLEXURE SPECIMEN BEING SEWN SHOWING LEXAN TOOL TO GUIDE NEEDLES AT THE PROPER ANGLE

The sewn lay-up preform was then molded by compressing and heating in a tooling fixture. The fixture, shown in figure 8 in small and large versions, consisted of flat aluminum plates constrained to move toward and away from each other while remaining parallel. This was done by means of linear bearings mounted in one plate riding on rods mounted in the other. The specimen to be molded was placed in between the plates and the entire fixture was sealed in a vacuum bag against a heated plate as shown in figure 9.

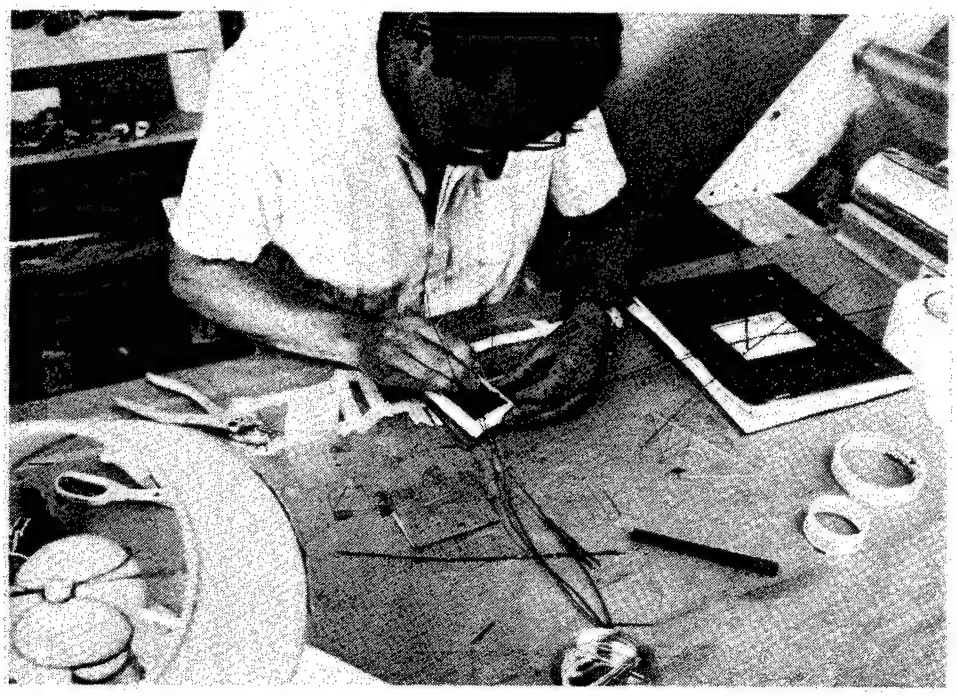

FIGURE 7. MANUAL INSERTION OF TOWPREG THROUGH TEST SPECIMEN LAY-UP

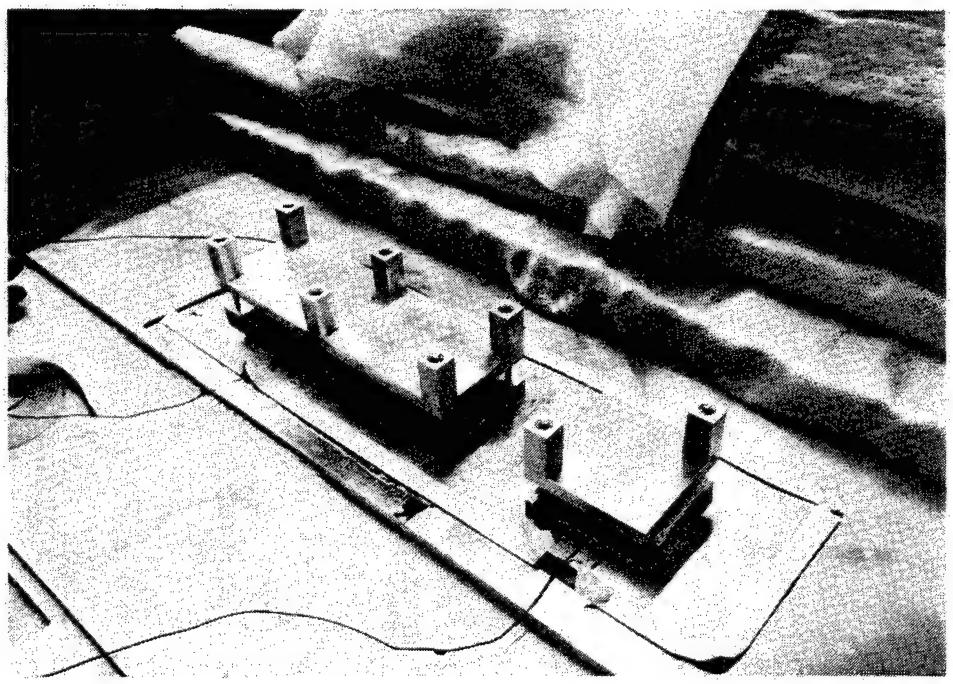

FIGURE 8. MOLDING FIXTURE FOR MECHANICAL TEST SPECIMENS

Vacuum was then applied to the bag to compress the specimen between the two tooling plates and the assembly heated to 350°F to cure the resin. The heating, held at 350°F, and cooling each took one hour.

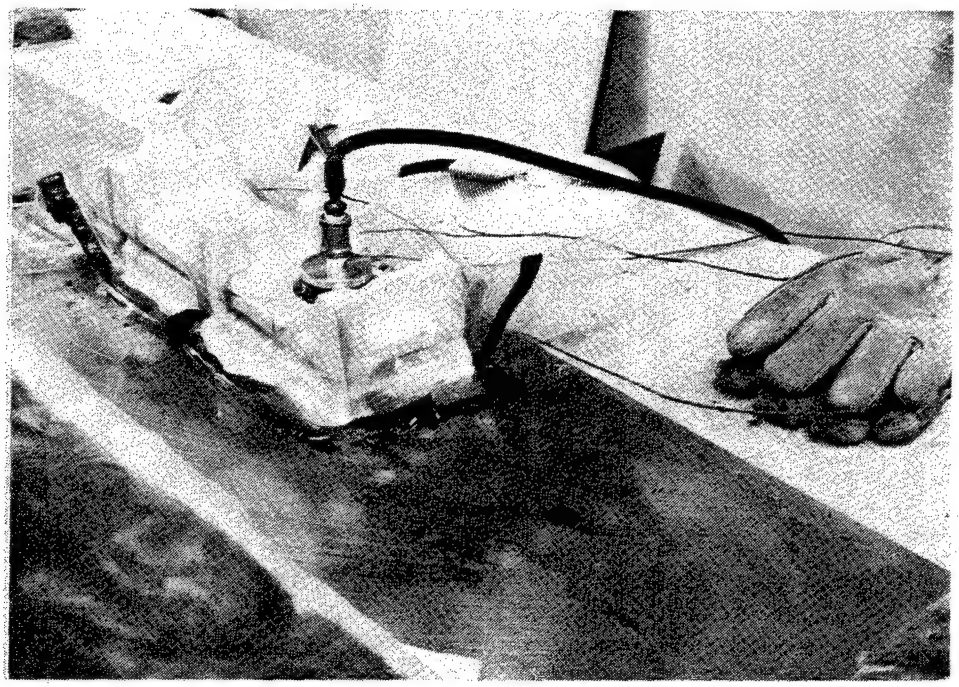

FIGURE 9. MOLDING FIXTURE FOR MECHANICAL TEST SPECIMENS SHOWN IN VACUUM BAG ON HEATED PLATE

3.1.4 Test Procedures.

All mechanical testing was done at the Massachusetts Institute of Technology (MIT) Technology Laboratory for Advanced Composites (TELAC). TELAC has two MTS servo hydraulic load frames with computer data acquisition systems. Load versus deformation was also plotted directly on an X-Y plotter during each test.

3.1.4.1 Compression.

The through-thickness compression test was performed by placing the specimen flat between two parallel loading platens mounted to the mechanical test machine. The compressive load was applied by the test machine and recorded by the load cell while the linear compressive deformation was measured by a linear variable differential transformer (LVDT). Load versus deformation was recorded and stress and modulus values were calculated using the facesheet area and thickness of the specimen as follows:

$$\sigma_C = \frac{P}{A_C} \quad and \quad \varepsilon_C = \frac{\Delta_t}{t} \tag{1}$$

where:

σ_c = compressive stress
P = applied load
A_c = facesheet area of specimen
ε_c = compressive strain
Δ_t = change in specimen thickness
t = original specimen thickness

Figure 10 shows a schematic and a photo of the compression test setup.

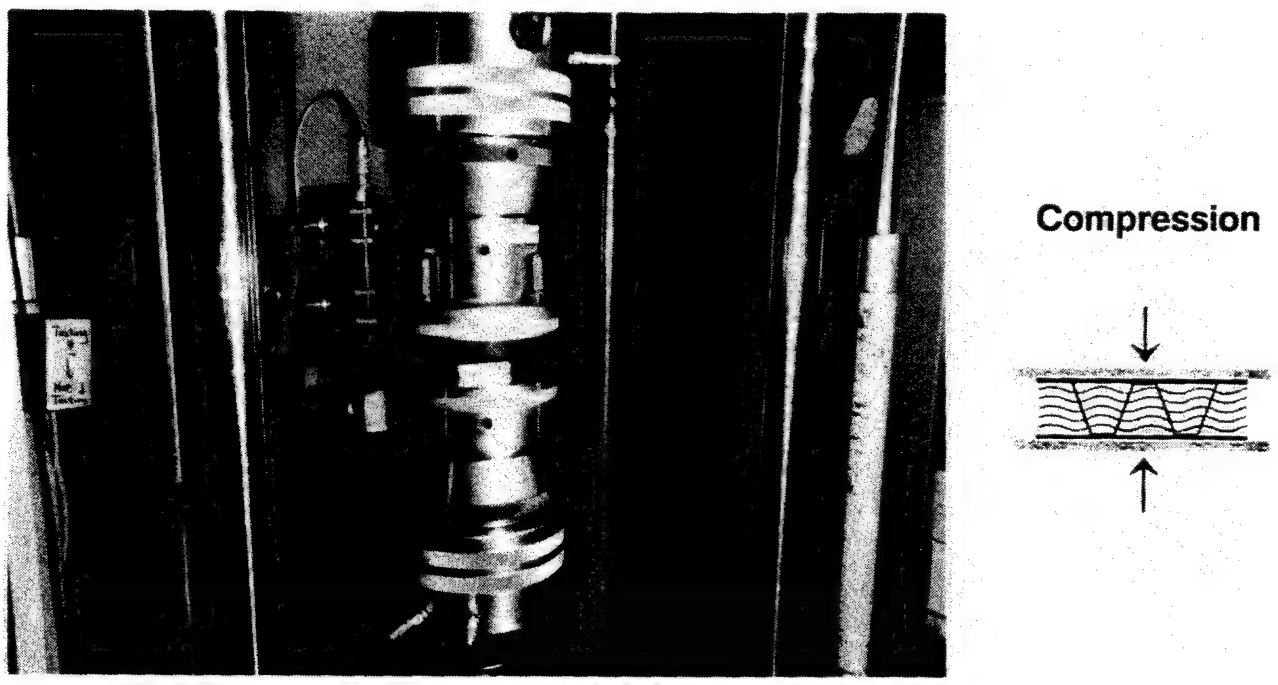

FIGURE 10. COMPRESSION TEST SETUP SHOWING LOWER STATIONARY AND UPPER FLEXIBLE PLATENS. THE SPECIMEN IS SHOWN ON THE LOWER PLATEN

3.1.4.2 Shear.

The shear properties of the hybrid core panel were measured by directly applying a shear force to the facesheets. This was done by sandwiching the test specimen between two steel plates, one bonded to one facesheet and one bonded to the other. One edge of each steel plate was beveled to a knife edge across which a compressive force was applied. The compressive force line of action passes through both knife edges so that the assembly as a whole had no moment about it. The force and relative platen displacement were recorded during the test and the shear stress/strain are calculated from the geometry as follows:

$$\tau = \frac{P}{A} \quad and \quad \gamma = \frac{\delta}{t} \tag{2}$$

where:

τ = shear stress
P = applied load
A = facesheet area
γ = shear strain
δ = shear displacement of one facesheet relative to the other
t = specimen thickness

The shear modulus was obtained by dividing shear stress by shear strain over the linear portion of the stress-strain curve. The platen relative displacement, instead of the facesheet relative displacement, was the parameter actually measured but the error is negligible since the angle of the specimen is only 8°. A sketch and photo of the test setup is shown in figure 11.

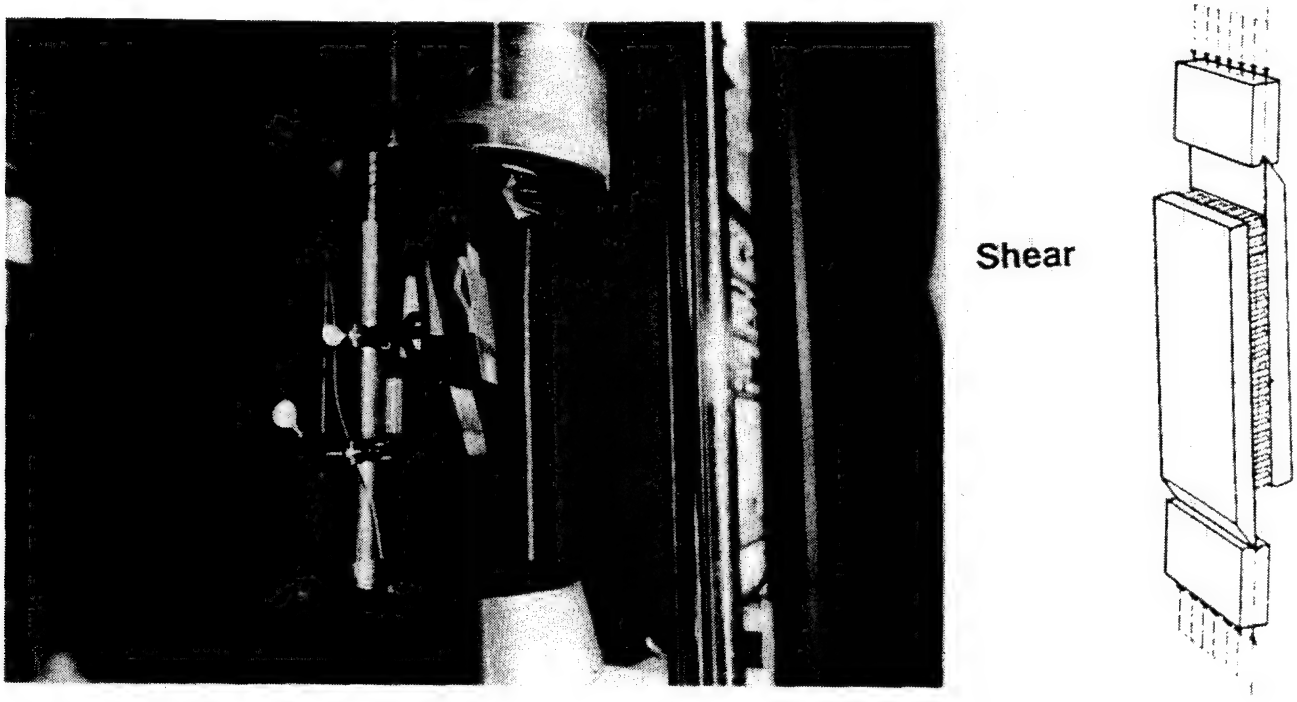

FIGURE 11. SHEAR TEST SETUP SHOWING SPECIMEN BONDED TO STEEL PLATES. PLATES ARE WRAPPED WITH TAPE TO HOLD THEM TOGETHER IN CASE OF A SUDDEN BOND FAILURE BETWEEN THE PLATES AND THE SPECIMEN

3.1.4.3 Flexure.

The three point flexure test was performed by placing the specimen across supports seven inches apart and loading the specimen in bending halfway between the supports. Load was plotted directly versus midpoint deflection on the X-Y plotter. Longitudinal strain on the upper and lower facesheets was also measured at midspan. The following equation (from Hexcel TSB 124) relates midspan deflection to sandwich panel design and loading. Shear modulus was computed from this equation using data from the Candidate C specimen and compared to directly measured shear modulus. These two values did not always agree because the facesheets carry some shear loading but they were close for low density, 4 lbs/ft^3 (0.06 g/cc), honeycomb cores.

$$\delta = \frac{2K_b PL^3 \lambda}{E_f t_f h^2 b} + \frac{K_s PL}{G_c h b} \qquad (3)$$

where:

δ = midspan deflection

K_b = bending constant = 0.02083 for 3 point bending

K_s = shear constant = 0.25

P = midpoint load

L = span length, 7 in (17.78 cm)

$\lambda = 1-\mu^2$ where μ is facesheet Poisson's ratio

E_f = facesheet modulus, 10×10^6 psi (69 GPa)

t_f = facesheet thickness = 0.07 in (0.18 cm)

$h = \frac{t_{f1}}{2} = \frac{t_{f2}}{2} + t_c = 0.07 + 0.55 = 0.62$ in (1.57 cm)

b = panel width, 1.8 in (4.57 cm)

G_c = core shear modulus

A schematic and photo of the flexure test setup is shown in figure 12.

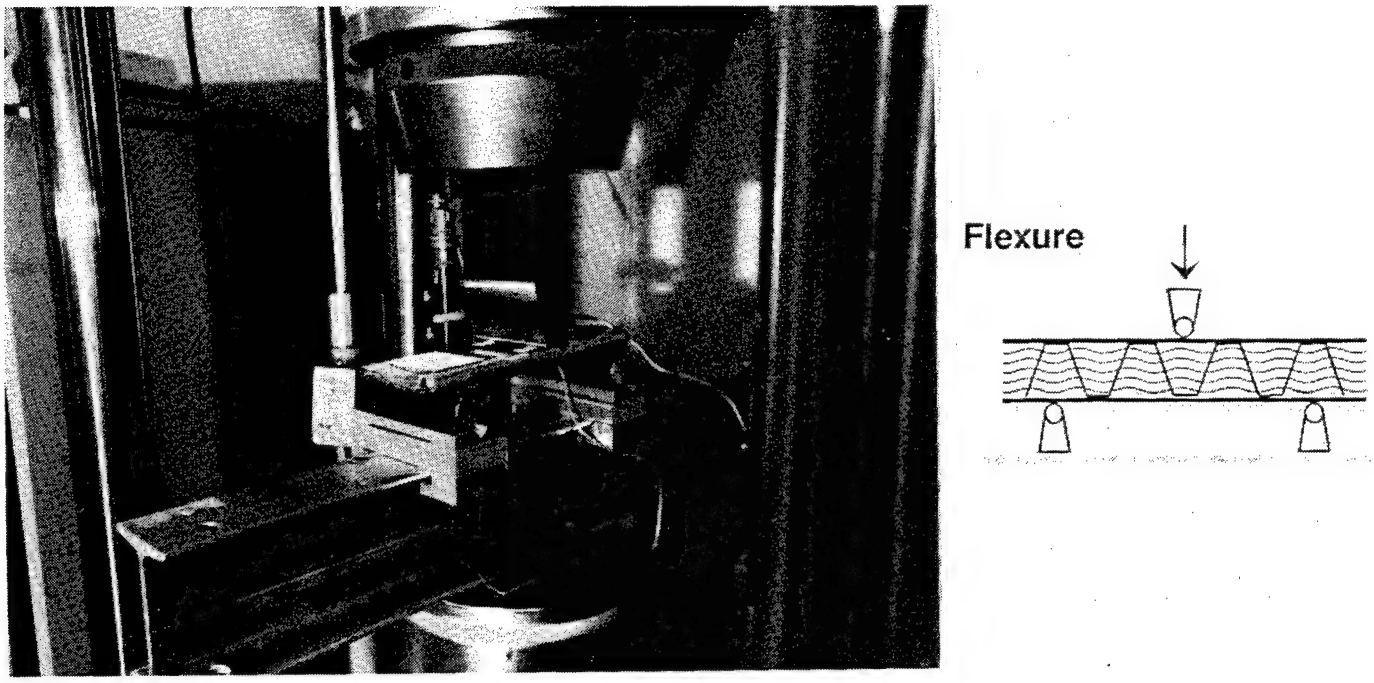

FIGURE 12. FLEXURE TEST SETUP SCHEMATIC AND PHOTO

3.1.5 Mechanical Test Results for Each Candidate Architecture.

3.1.5.1 Candidate A.

3.1.5.1.1 Candidate A Compression.

Candidate A has -45°, 90°, +45° rows of facesheet connecting rods. This compression specimen was constructed from the standard 24-ply Kevlar fabric core encapsulated by the one-mil teflon film. It differs from the baseline construction as follows. One ply of E glass fabric separated the graphite/epoxy facesheet laminate from the teflon. The facesheets each contained four plies of five harness satin graphite/epoxy molded prepreg plies. This AS4/3501-6 fabric was woven with 6K tows. The 12K graphite/epoxy towpreg which forms the rods was sewn through the glass, teflon, and Kevlar laminate. Two graphite/epoxy prepreg laminates were added to form the facesheets and the specimen was then molded. These variations in facesheet construction were done to check fabrication parameters like resin flow, but since a facesheet anchor is all that is required to impart a compression load to a rod, the precise facesheet lay-up has a minimal effect on through-thickness compression test results.

Figure 13 shows the load versus deformation curves for each of the Candidate A compression specimens. With the exception of A1 the load was recorded for both the loading and unloading process. The load was increased until well into the failure zone where the rods were continually crushing. The linear portion of the loading curve was used to obtain modulus, and the failure stress was taken as the first point where obvious permanent damage was being done to the rods.

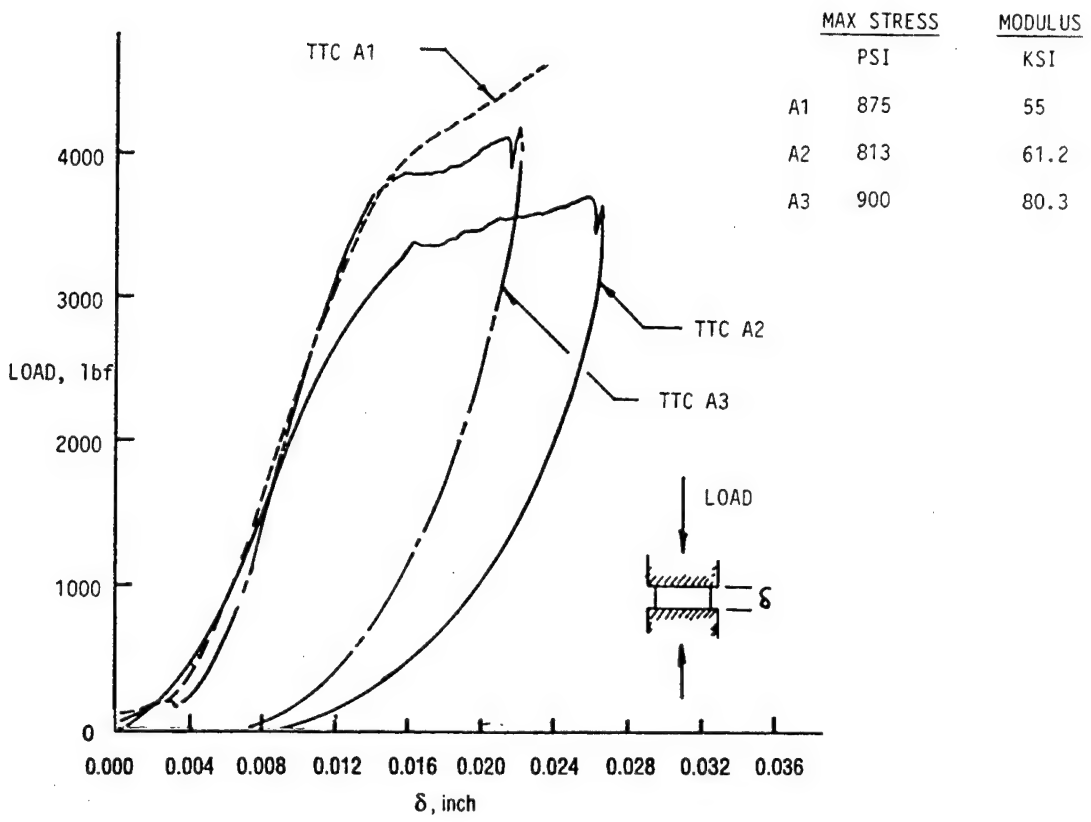

FIGURE 13. LOAD VERSUS DEFLECTION FOR CANDIDATE A THROUGH-THICKNESS COMPRESSION SPECIMENS

The permanent internal damage causes the large hysteresis in the curves. The maximum stress is seen to range from 813-900 psi (5.6-6.2 MPa) and modulus from 55-80 ksi (379-552 MPa).

3.1.5.1.2 Candidate A Shear.

The Candidate A shear specimen consisted of 12 Kevlar fabric plies encapsulated in Teflon film and covered by five AS4/8553 graphite/epoxy plies on each face to form the facesheets. Rods were sewn through three of the five facesheet plies on each side. The thickness of B and C shear specimens was increased to 24 Kevlar plies to conform with the recommended thickness for honeycombs but this 12<-ply specimen allowed qualitative evaluation of the effect of thickness on shear strength and stiffness of the hybrid core. The thinner lay-up was originally designed for a double lap shear specimen but this was later changed to conform to the test procedure used for honeycomb cores. Two of the three sandwich panel specimens were bonded to the steel plates with a room temperature epoxy while the third (A2) was bonded with a film adhesive at 350°F. The room temperature epoxy debonded at low load levels while the film adhesive, FM 355, held the plates to the specimen for the entire test. The debonded specimens, A1 and A3, were rebonded with the film adhesive and retested. This film adhesive was used for all remaining shear specimens.

The curves of figure 14 show the modulus and strength to be fairly consistent among the three specimens. A very slight bimodular behavior was noticed so two moduli were recorded for each specimen. This behavior could be due to straightening of these 45° rods which are in tension from an initially kinked or bent position. Their stiffness contribution would increase as they became straighter. Shear strength ranged from 525-617 psi (3.62-4.25 MPa) while the modulus spanned 13.4-17.6 ksi (92.4-121.4 MPa). Failure was due to buckling and tensile failure of the rods internally.

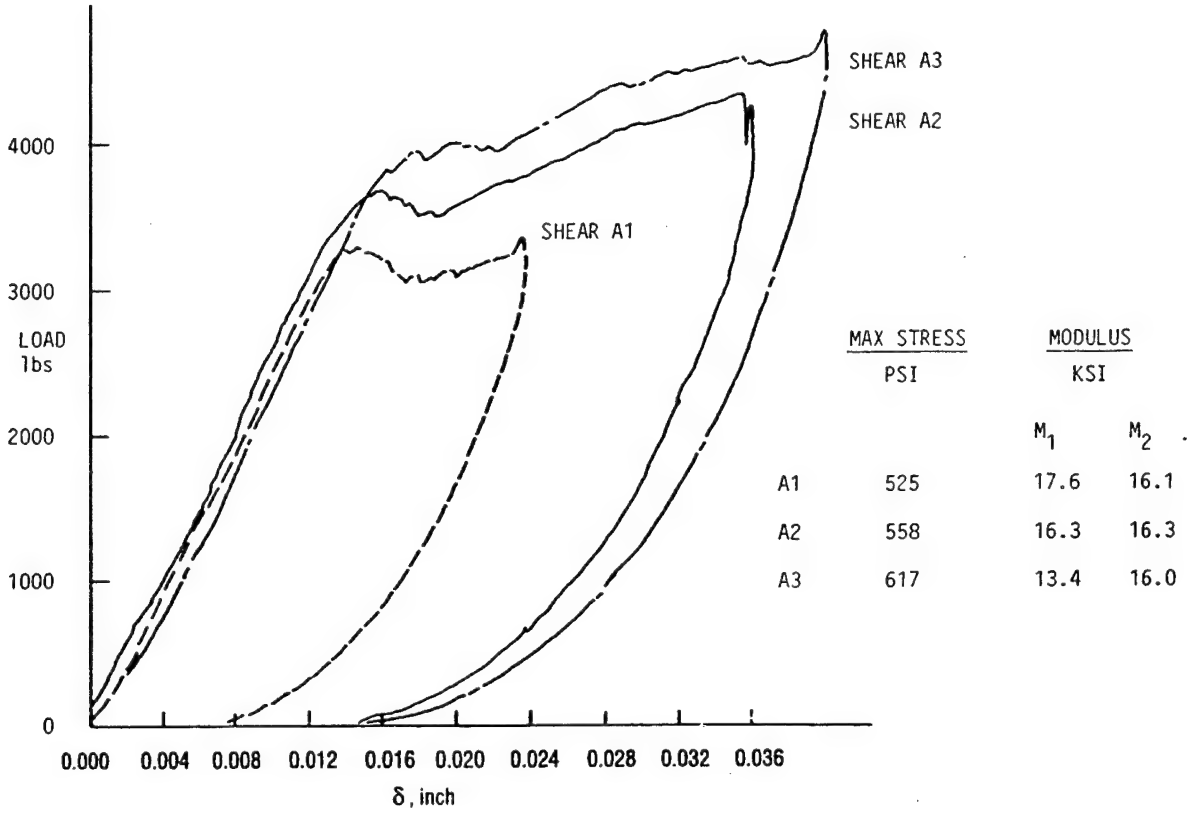

FIGURE 14. LOAD VERSUS DEFLECTION FOR CANDIDATE A SHEAR SPECIMENS

3.1.5.1.3 Candidate A Flexure.

All flexure specimens used the baseline lay-up of 24 Kevlar plies, teflon, and seven AS4/8553 facesheet plies, three of which are sewn through to trap the rods. The balanced plain weave facesheet plies are 0°, 90° lay-ups with 0° being the specimen's longitudinal axis. The facesheets were thick enough, 0.07 in (0.18 cm), such that virtually all flexure specimens failed in a shear mode with the rods buckling or crushing in compression and failing in tension. The rows of rods as depicted in the description of the Candidate A architecture are aligned with the specimen's long axis to support the shear loading and give maximum flexure stiffness and strength.

Figures 15 and 16 show the load versus deflection and surface strains of the three flexure specimens of Candidate A. Load and deflection were recorded at the point of first obvious internal failure and at the highest load reached. The tests were terminated well beyond points of significant damage and usually after a maximum load had been reached. The three specimens behaved in much the same fashion reaching a load of over 1000 lb (4448 N) at a deflection of 0.10 in. (0.25 cm) and continuing to support load after initial rod damage was experienced. This could be due to rod misalignment causing some rods to fail before others. As the deflection further increased the load was supported by the remaining rods which, in this case, resulted in an even higher load being supported by the beam. This suggests that a highly damage tolerant structure may be designed with a rod reinforced core given proper design and precise control of rod angles.

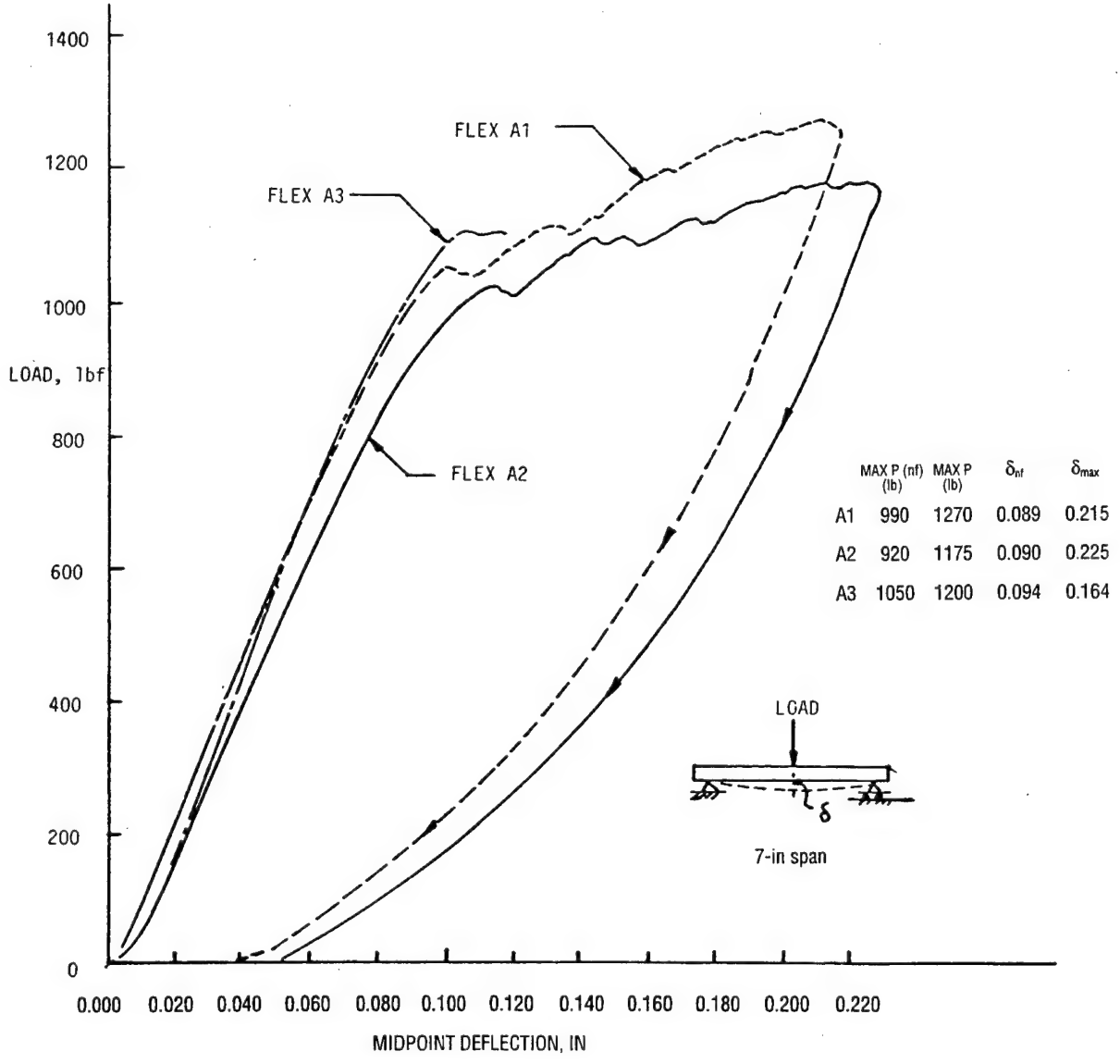

FIGURE 15. LOAD VERSUS MIDPOINT DEFLECTION FOR CANDIDATE A FLEXURE SPECIMENS

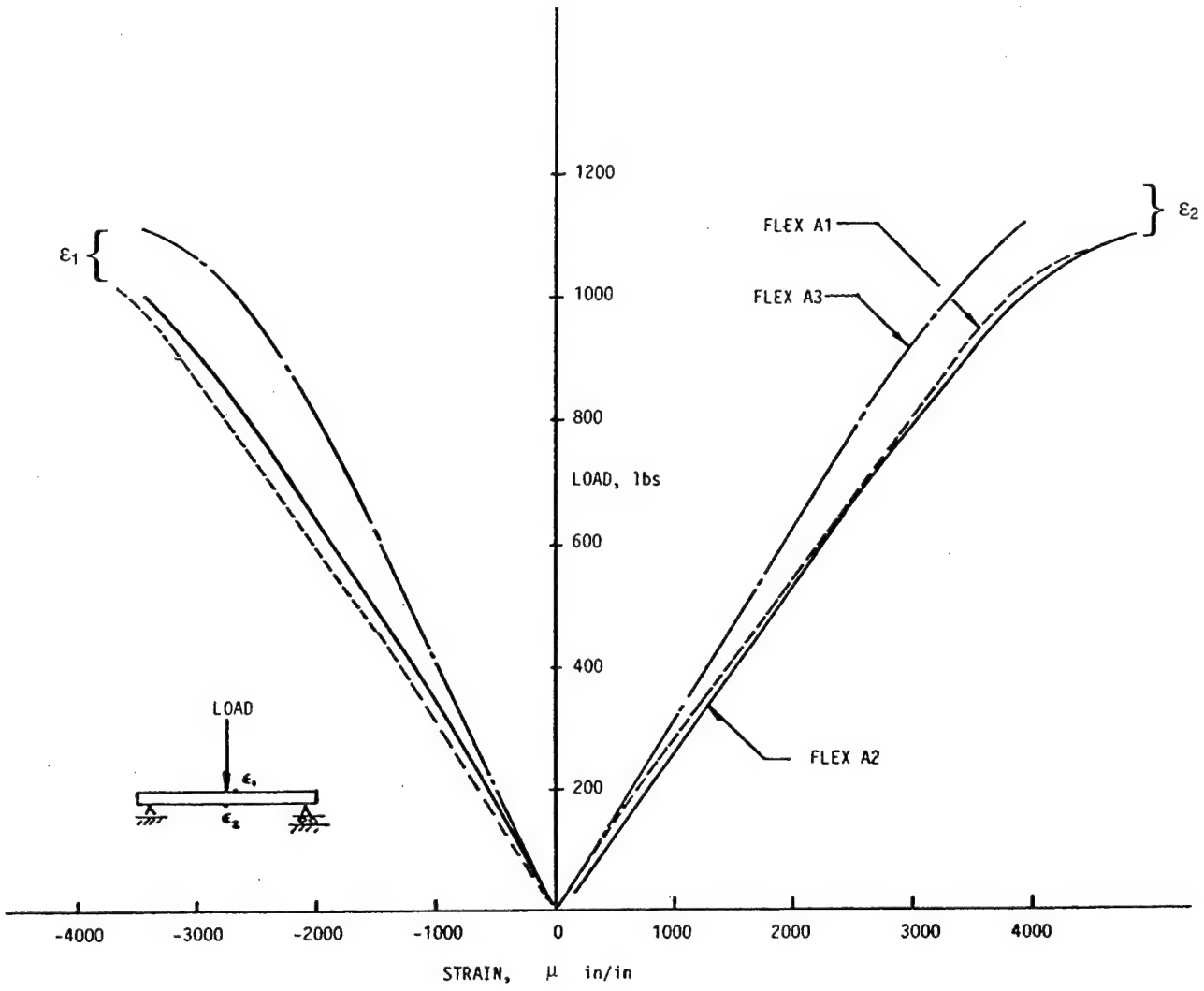

FIGURE 16. LOAD VERSUS UPPER AND LOWER SURFACE LONGITUDINAL STRAIN FOR CANDIDATE A FLEXURE SPECIMENS

Surface strains reached reasonably high operating levels for a graphite/epoxy laminate. The top middle surface longitudinal strain (displaced slightly to allow room for the loading ram) reflects both the longitudinal compressive strain due to facesheet bending and the longitudinal compressive strain imposed by the rods through shear. The strain of the tensile side of the beam also reflects similar contributions of facesheet bending and rod inputs. The curves also indicate that the facesheets did not fail before the core which was the intended result so that the strength, stiffness, and failure mode of the core could be determined.

3.1.5.2 Candidate B.

The Candidate B architecture simply removed the straight 90° through thickness rods from Candidate A and replaced them with ±45° rods to make the entire rod reinforcement a set of alternating ±45° rods. This reduces the through-thickness compression strength or stiffness but

improves the shear properties which are important for this type of core design. This is especially true if a hybrid core sandwich panel is applied to areas where thick sections are exposed to shear or flexure loading.

3.1.5.2.1 Candidate B Compression.

The facesheet construction of the Candidate B compression specimens differed from the standard design but, again, due to the nature of this test, the changes in facesheet lay-up did not affect the compression results. In this case the standard 24-ply Kevlar core with teflon overwrap was covered with three plies of AS4/8553 plain weave fabric prepreg on each side to form the facesheet base. All these plies were sewn through with the rod precursor 12K tow. Before a final ply was added, however, a layer of American Cyanamid FM 350 series film adhesive was added to determine how it would process and bond to adjacent plies. Its compatibility was good and it seemed to provide good bonding at the interface containing the loops.

The Candidate B compression test results are shown in figure 17. Both strength and modulus are lower as expected with strength ranging from 500-563 psi (3.45-3.88 MPa) and modulus from 36.7-48.4 ksi (253-333 MPa). Again the strength is taken at the point of initial failure and modulus is calculated using the initial linear part of the loading curve. The number of rods actually inserted was counted for most Candidate B specimens. As shown in the inset table of figure 17, several rods were inadvertently omitted in specimens B2 and B3 and this effect is seen as a lower modulus, but strength values did not seem to be significantly affected. Small variation in actual rod angle could be responsible for this observation.

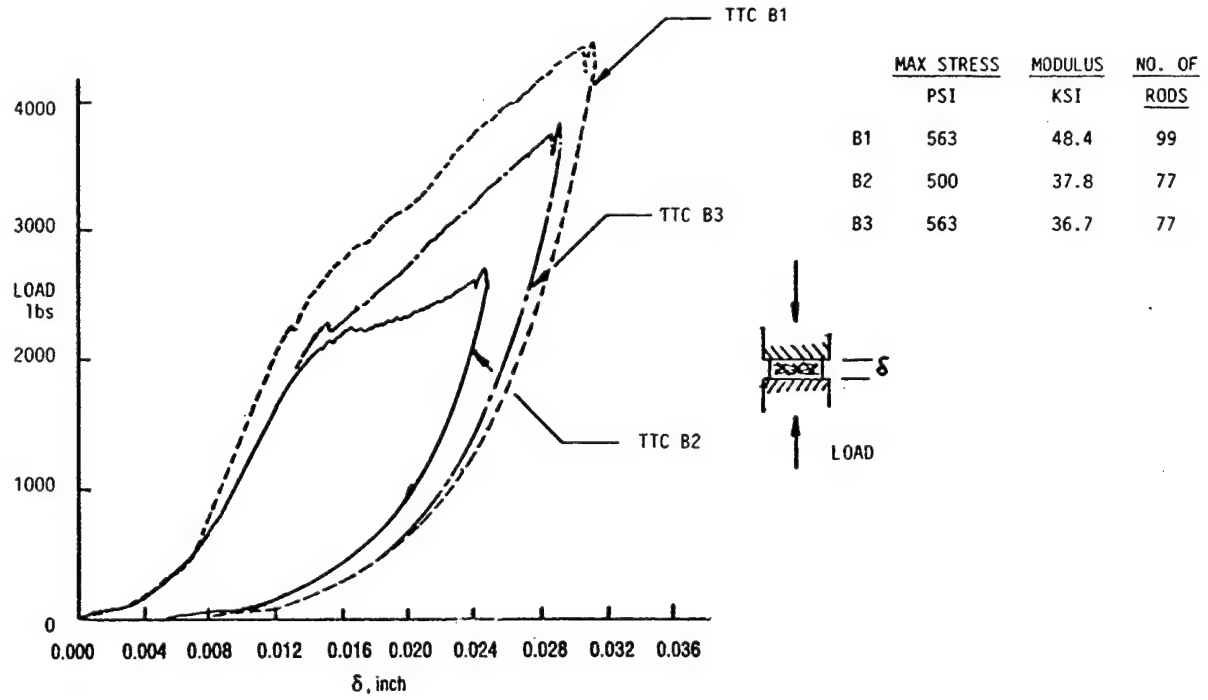

	MAX STRESS PSI	MODULUS KSI	NO. OF RODS
B1	563	48.4	99
B2	500	37.8	77
B3	563	36.7	77

FIGURE 17. LOAD VERSUS DEFLECTION FOR CANDIDATE B THROUGH-THICKNESS COMPRESSION SPECIMENS

3.1.5.2.2 Candidate B Shear.

The Candidate B shear specimen lay-up included the standard 24 plies of Kevlar fabric and had the same facesheet lay-up as Candidate A. Figure 18 shows a bimodular behavior of the load-deflection curve which again indicates that rod load sharing is probably a function of strain level. Slight kinking in the rods supporting tensile loads may also be responsible since they would appear stiffer as they became stretched out. Two shear strengths are reported—one at the upper level of the linear region and one at the load level where permanent damage occurs. The higher shear strength level varies between 350-459 psi (2.4-3.1 MPa) while the high modulus ranges from 22.4-25.4 ksi (154-175 MPa). The modulus values are higher than A values as expected because the 90° rods were replaced with ±45° rods but the strength is lower than A. This might also be expected since the longer rods of the thicker B specimen have a lower buckling strength so the rods which are in compression fail at a lower load level. If the rods are initially kinked or bent, the longer length would increase the bending moment lowering the rod's compression strength.

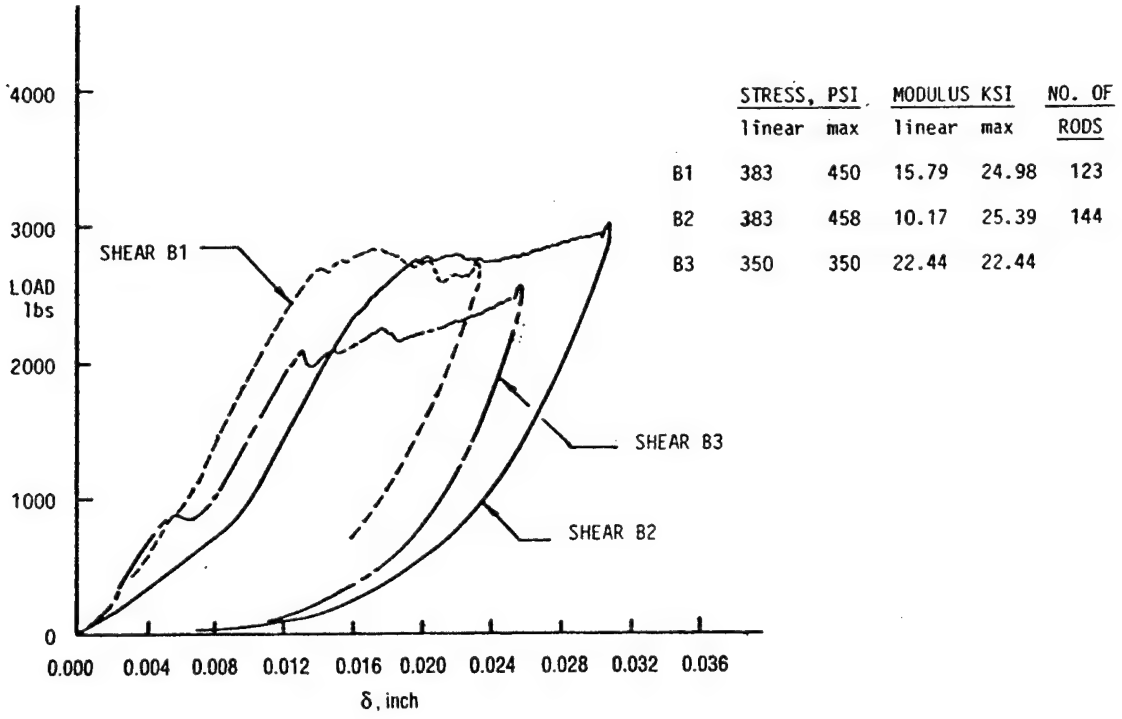

	STRESS, PSI		MODULUS KSI		NO. OF
	linear	max	linear	max	RODS
B1	383	450	15.79	24.98	123
B2	383	458	10.17	25.39	144
B3	350	350	22.44	22.44	

FIGURE 18. LOAD VERSUS DEFLECTION FOR CANDIDATE B SHEAR SPECIMENS

3.1.5.2.3 Candidate B Flexure.

The Candidate B flexure specimens were fabricated using the baseline materials and lay-up sequence of the other flexure specimens. Results are shown in figures 19 and 20. In this case three maximum loads are reported—the maximum load in the linear range, the maximum load at which no obvious failure occurs, and the maximum load reached at any point. Midspan deflections corresponding to these load points are also given. The flexural stiffness and strength

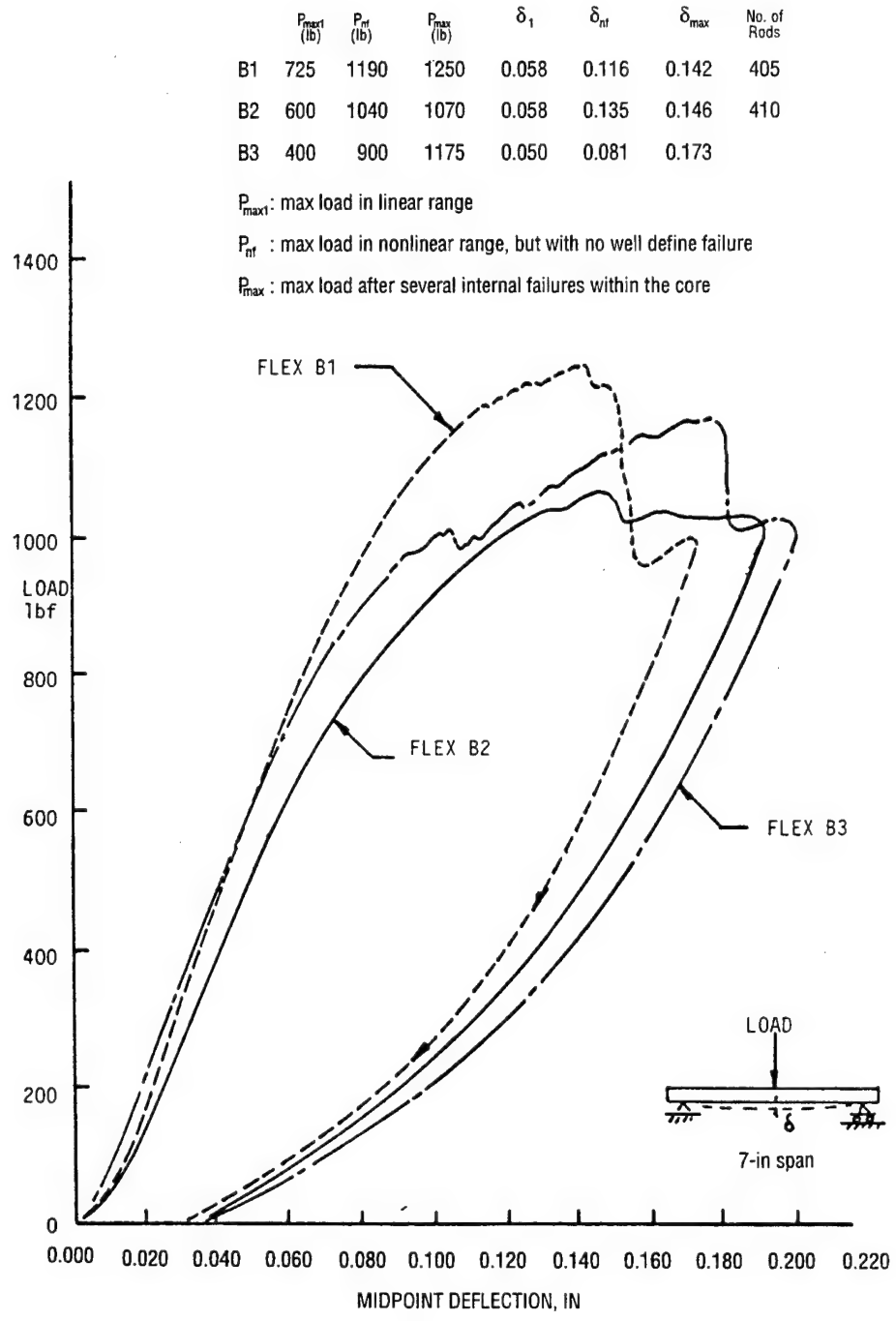

FIGURE 19. LOAD VERSUS MIDPOINT DEFLECTION FOR CANDIDATE B FLEXURE SPECIMENS

were close to A values. The difference between the two was that the Candidate B design had a sharper failure mode and reached its maximum load at lower deflection level.

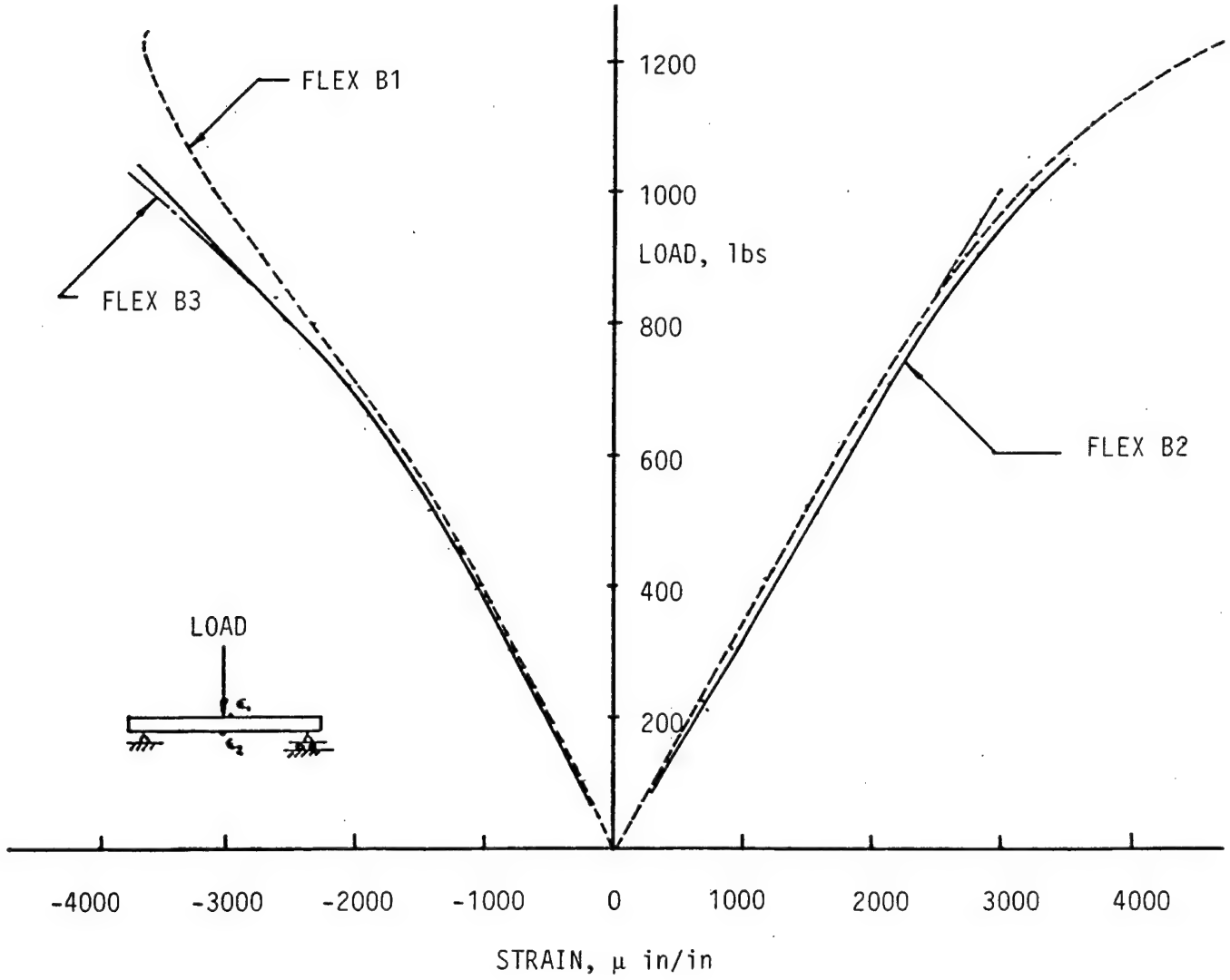

FIGURE 20. LOAD VERSUS UPPER AND LOWER SURFACE LONGITUDINAL STRAIN FOR CANDIDATE B FLEXURE SPECIMENS

3.1.5.3 Candidate C.

Like Candidate B, the Candidate C design uses rods which are at 45° to the facesheet plane but, unlike B, they do not form a plane which is normal to the facesheet plane. Instead, the rods lie in a plane which is tilted at 55° to the facesheet plane providing facesheet-to-facesheet shear stiffness in both lateral and longitudinal specimen directions. The C geometry also allowed a larger number of rods to be inserted over a given area than the other two geometries—an average of 8 more rods (8%) for the compression specimen, 30 more rods (20%) for the shear specimen, and 80 more rods (16%) for the flexure specimen.

3.1.5.3.1 Candidate C Compression.

Figure 21 gives the load versus deformation curves for the three Candidate C compression specimens. The loading curves are quite consistent and reflect strengths between 650 and 788 psi (4.48-5.43 MPa) and moduli in the range 52.8-60.1 ksi (364-414 MPa). These are both slightly higher than the Candidate B specimens. This could be due to the eight extra rods on average for the C specimens or better quality of fabrication due to experience gained with the first two series of specimens.

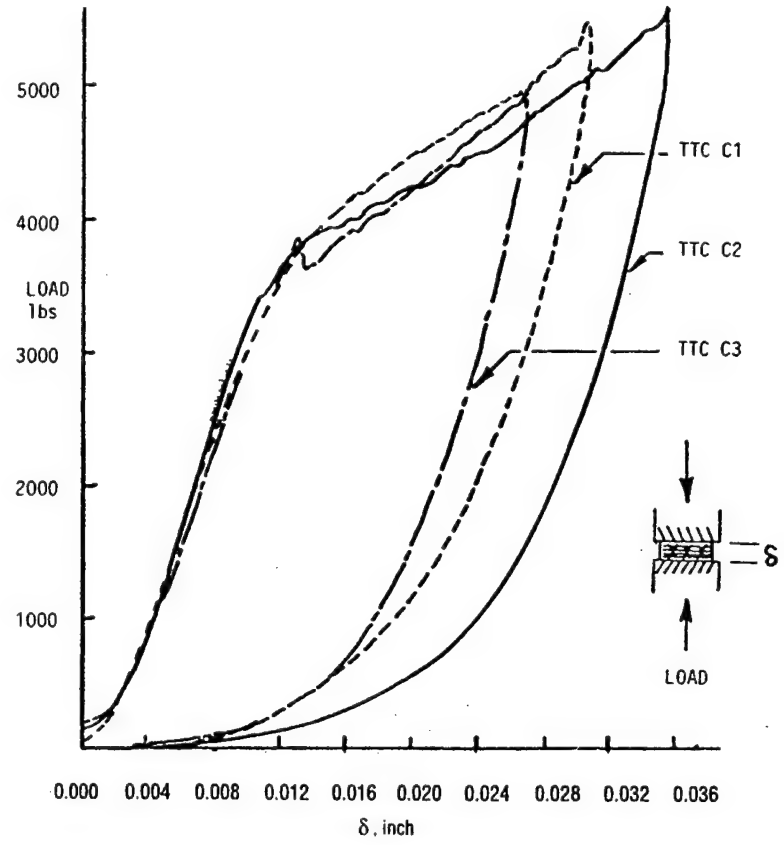

	STRESS PSI	MODULUS KSI	NO. OF RODS
C1	650	52.8	106
C2	788	60.1	108
C3	750	57.7	107

FIGURE 21. LOAD VERSUS DEFLECTION FOR CANDIDATE C THROUGH-THICKNESS COMPRESSION SPECIMENS

3.1.5.3.2 Candidate C Shear.

The shear fixture was designed with beveled edges on both longitudinal and lateral sides of the plates so that specimens could be tested in both directions. Each specimen was first loaded in the Y or lateral direction to obtain a modulus. The force level was low enough so that the specimen was not damaged. The specimens were then loaded to failure in the longitudinal direction as before. The Y direction curves are shown in figure 22 and these shear modulus values range between 19.1 and 23.8 ksi (132-164 MPa) which are only slightly lower than B longitudinal values. The longitudinal shear curves are shown in figure 23 and these moduli range from 20.7 to 29.4 ksi (143-203 MPa)—somewhat higher than the transverse values. It appears that a small penalty was paid for reorienting the rods to support lateral shear loading even allowing that

Candidate C shear specimens had 20% more rods. This multidirectional form could be useful in designs requiring support of shear or bending loads applied in several axes. The longitudinal shear modulus was also calculated from flexure data to be discussed next. The average value of longitudinal shear modulus calculated from flexure data was 25.1 ksi (173 MPa) while the average directly measured value was 24.8 ksi (171 MPa) so the flexure data seems to support the directly measured value. As stated previously, however, these can differ depending on specimen geometry and relative shear stiffness of the core.

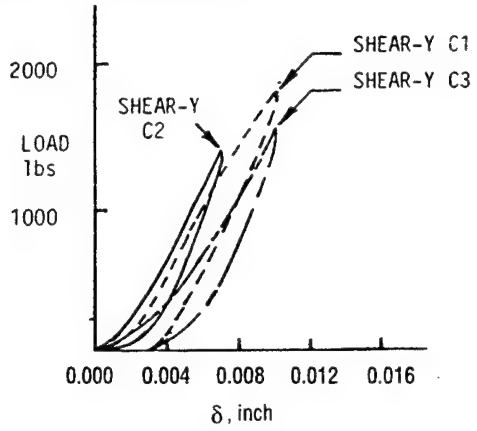

FIGURE 22. LOAD VERSUS TRANSVERSE DEFLECTION FOR CANDIDATE C SHEAR SPECIMENS

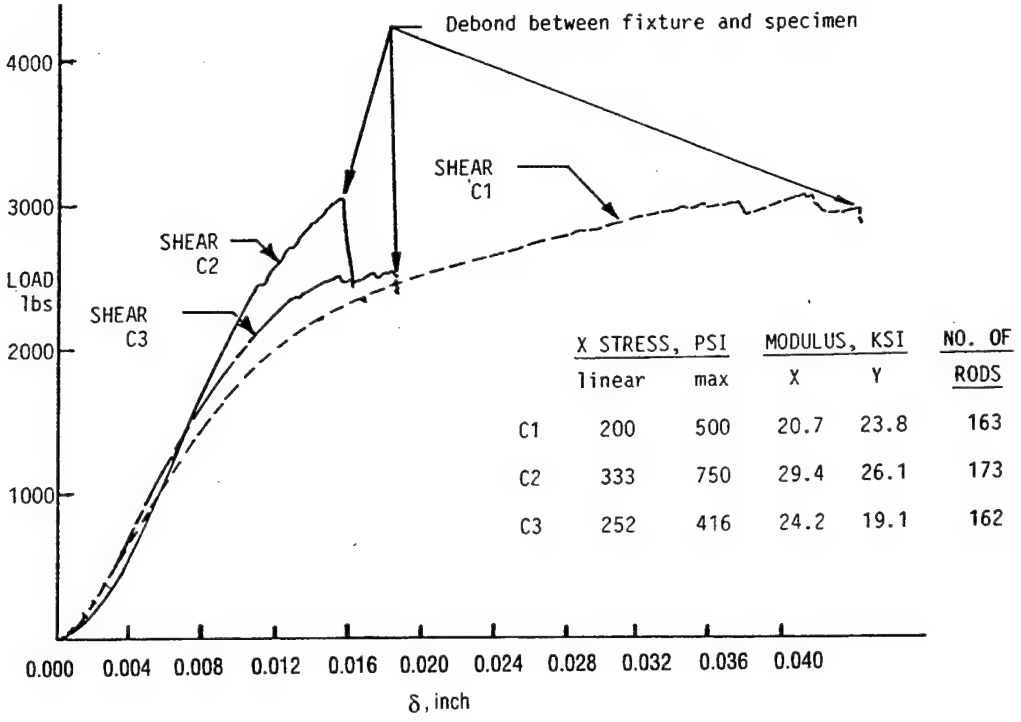

	X STRESS, PSI		MODULUS, KSI		NO. OF
	linear	max	X	Y	RODS
C1	200	500	20.7	23.8	163
C2	333	750	29.4	26.1	173
C3	252	416	24.2	19.1	162

FIGURE 23. LOAD VERSUS LONGITUDINAL DEFLECTION FOR CANDIDATE C SHEAR SPECIMENS. INSET TABLE GIVES DATA FOR BOTH TRANSVERSE (Y) AND LONGITUDINAL (X) DIRECTIONS.

3.1.5.3.3 Candidate C Flexure.

The Candidate C flexure results are given in figures 24 and 25. The initial slope of the load versus deflection curve is the same as for all the other specimens but this linearity is sustained at higher loads and deflections than for any of the previous specimens. Specimens C1 and C3 failed very abruptly indicating that many rods failed simultaneously or in very rapid succession. A loud bang was heard each time. After these failures each specimen still supported about 900 lbs (4003 N). Specimen C2 failed more gradually like the previous specimens of Candidates A and B. The rods of the C1 and C3 specimens were probably placed more precisely allowing many to share the high shear loading more equally and hence fail at nearly the same time. The maximum loads reached by the C1 and C3 specimens—1290 lbs (5738 N) and 1260 lbs (5604 N), were also slightly higher than that reached by C2, 1220 lbs (5427 N). Loads and deflections are given at the maximum load of the linear region, the maximum with no obvious failure, and the overall maximum.

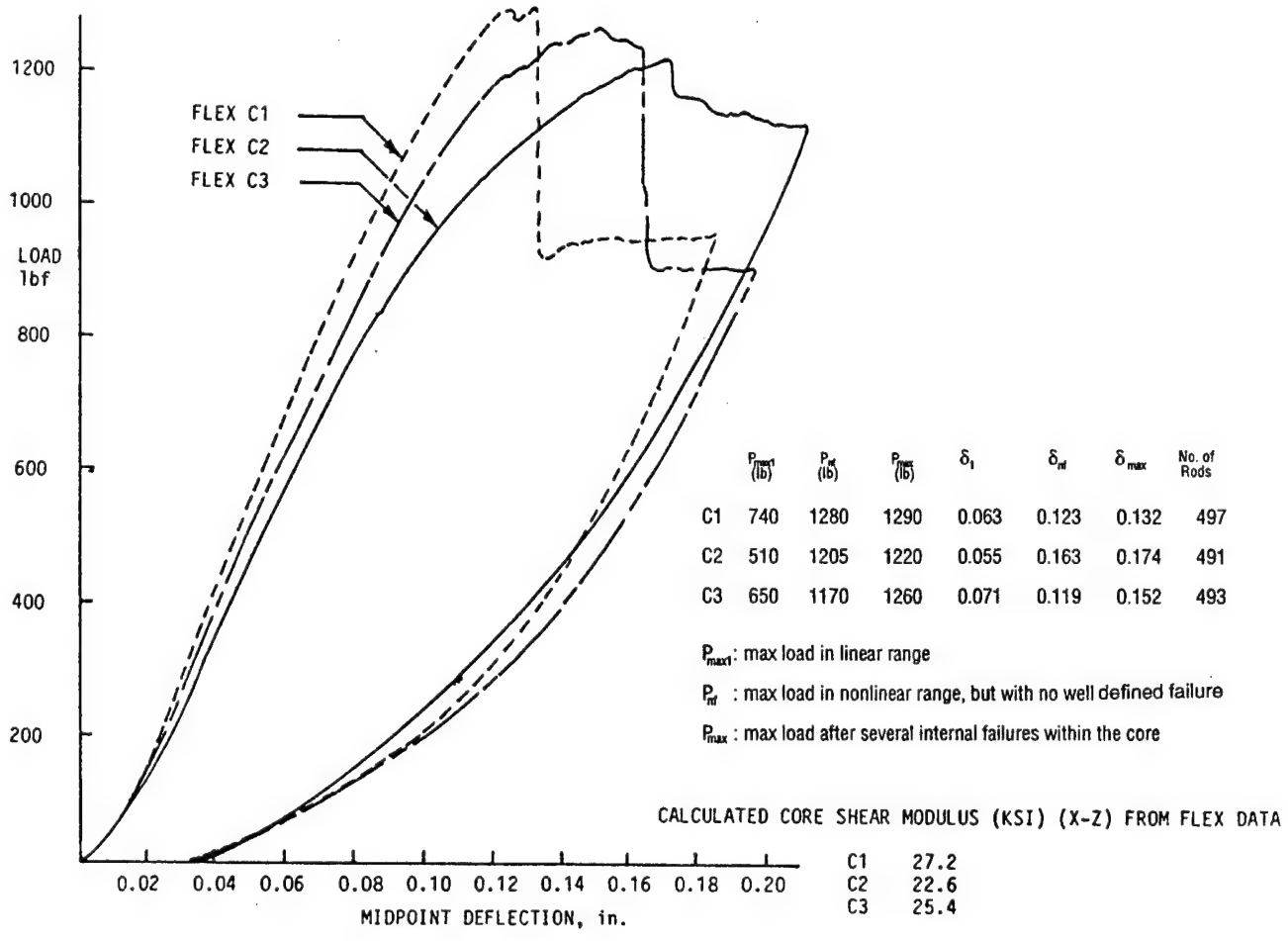

FIGURE 24. LOAD VERSUS MIDPOINT DEFLECTION FOR CANDIDATE C FLEXURE SPECIMENS

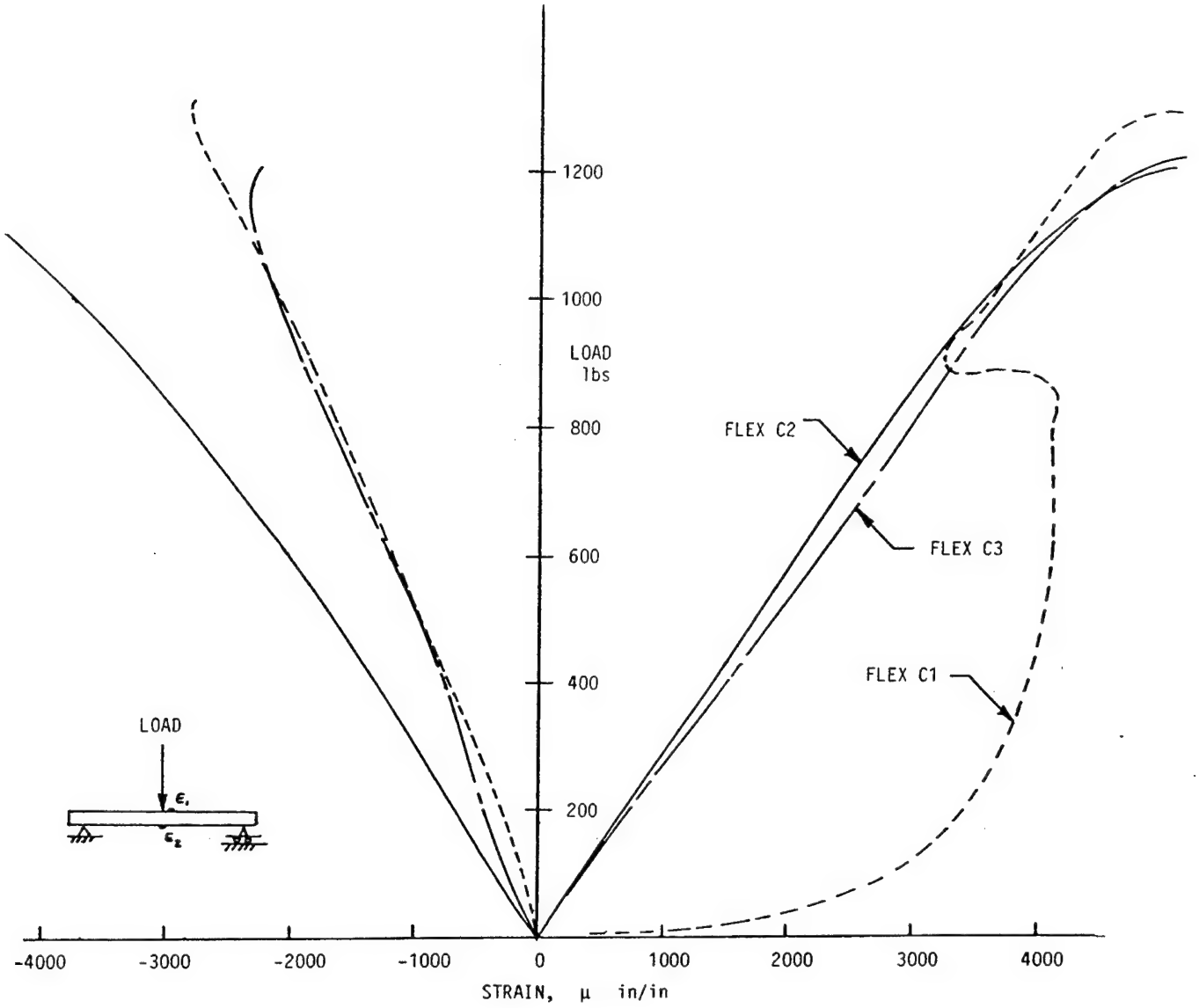

FIGURE 25. LOAD VERSUS UPPER AND LOWER SURFACE LONGITUDINAL STRAIN FOR CANDIDATE C FLEXURE SPECIMENS

The strain data from the facesheet surfaces was similar in form to the previous flexure specimens except that the tensile C1 signal was lost. The strain gage data shows that a reasonably high (4000-μ strain) strain level was reached in the facesheets and that, again, no obvious facesheet failures occurred before shear failure of the core.

3.1.6 Hybrid Core Mechanical Properties Compared to Those of Typical Aerospace Grade Honeycomb Cores.

The hybrid core mechanical properties measured in this test program are compared to Hexcel honeycomb core data in figures 26, 27 and 28. The honeycomb data is from Hexcel TSB 120. These figures are curves of stabilized compressive strength, shear strength, and shear modulus

versus core density for various honeycomb core types. The "stabilized" compressive strength refers to the honeycombs being bonded to the facesheet thereby supporting its edges. The hybrid core data points are plotted on the graphs at a density calculated by dividing rigid rod mass by the volume the rods reinforce. The Kevlar fabric laminate mass was omitted since it plays little or no role in the static mechanical properties of the core. The density of the dry Kevlar laminate is about 45 lbs/ft^3.

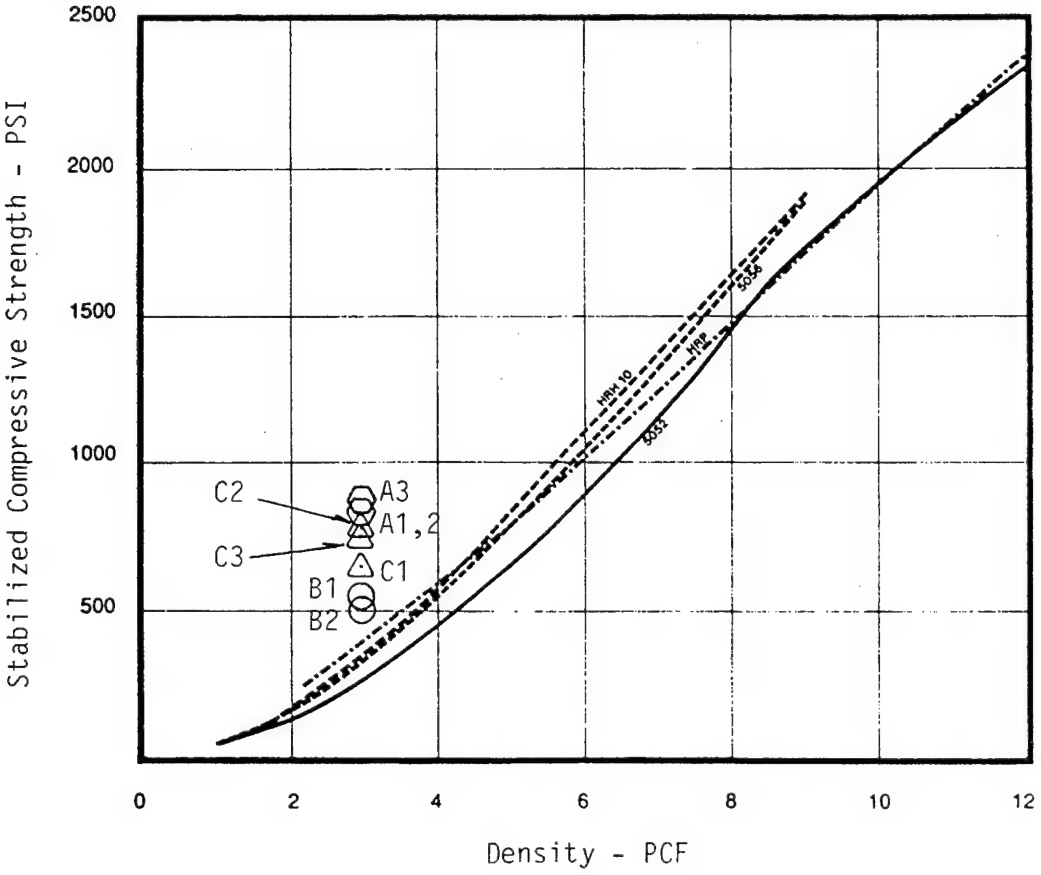

FIGURE 26. COMPARISON OF STABILIZED COMPRESSIVE STRENGTH VERSUS DENSITY FOR HYBRID PANEL TEST SPECIMENS AND TYPICAL HONEYCOMB CORES

Figure 26 shows the compressive strengths of the A, B, and C specimens to be higher than the strengths of comparable honeycomb cores. The average compressive strength of the honeycomb is 350 psi (2.41 MPa). The shear strength of the hybrid core is also higher than that for comparable honeycombs as shown in figure 27; however, figure 28 shows the hybrid core shear modulus data falling in the range of glass/phenolic and aramid honeycombs. Aluminum honeycombs have shear moduli about twice the hybrid core at equivalent densities.

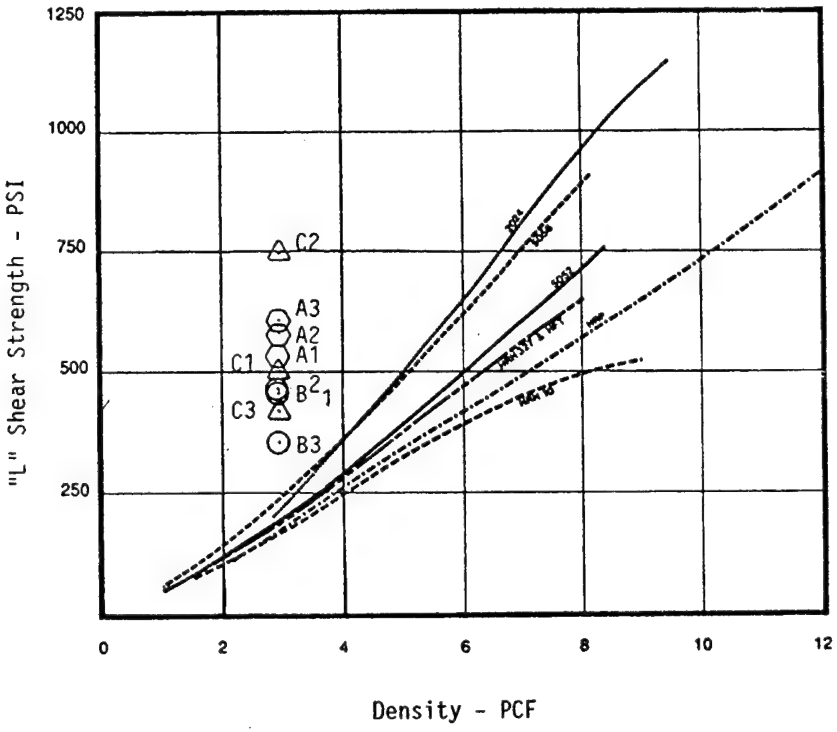

FIGURE 27. COMPARISON OF SHEAR STRENGTH VERSUS DENSITY FOR HYBRID SANDWICH PANEL SPECIMENS AND TYPICAL HONEYCOMB CORES

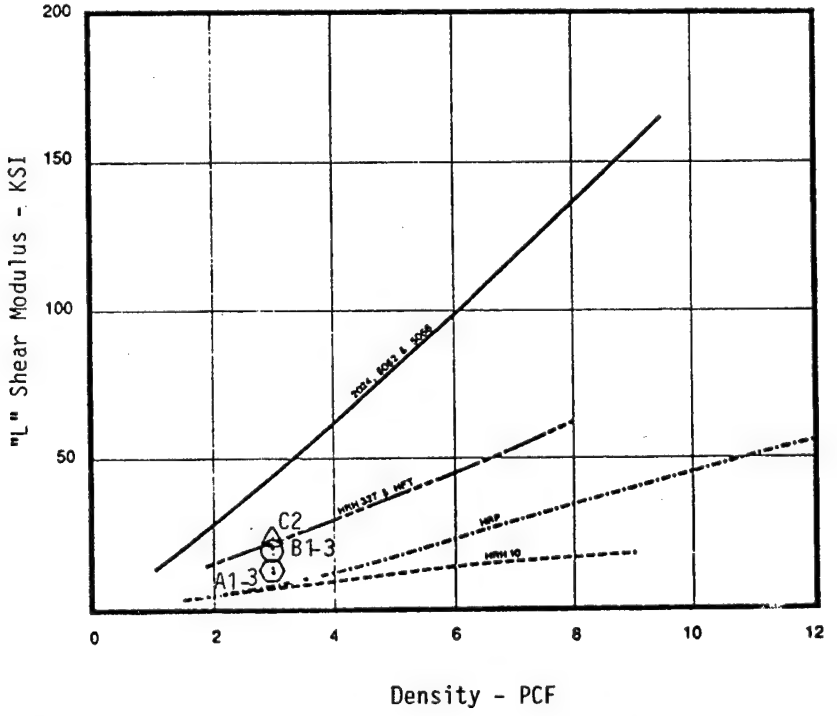

FIGURE 28. COMPARISON OF SHEAR MODULUS FOR HYBRID SANDWICH PANEL SPECIMENS AND TYPICAL HONEYCOMB CORES

From the data presented it appears that the hybrid core could be designed to support typical loading which might be encountered in airframe secondary structures. The honeycomb cores to which it has been compared are used in rotor blades, cowlings, landing gear doors, control surfaces, floor panels, and other similar structures requiring low weight and high stiffness. Not only are the static properties of the hybrid panel sufficient for these applications but the panel continues to support loading after it has suffered internal damage so its damage tolerance and resistance to core/facesheet debonding or separation are also desirable mechanical features.

3.2 TEST PROGRAM TO EVALUATE CONTAINMENT POTENTIAL OF HYBRID SANDWICH PANELS AND RINGS.

3.2.1 Overview.

The mechanical test program showed that the hybrid panel structure is capable of supporting static loads with a performance comparable to existing honeycomb cores. The efficiency of the panel with its soft core to stop high velocity fragments which impact it from a failed rotor was determined. Panel and ring structures were fabricated and each tested by placing them around a test rotor. The rotor was spun until it failed in a tri-hub burst mode at a predesigned speed and energy level. The surrounding containment structure was impacted by the released fragments and was examined after the test. Ten tests were performed with structures of varying fiber type, thickness, and fiber reinforcement architecture to determine which design provided the lightest weight structure. This section provides a description of the test procedure, specimen design and fabrication, and test results.

3.2.2 Test Procedure.

The rotor burst tests were performed in a spin test chamber at the Naval Air Warfare Center in Ewing, NJ. Figure 29 shows a schematic of the chamber and associated hardware required to perform the test. The test rotor is mounted inside the chamber to a shaft which penetrates vertically through the chamber's top cover. The rotor is driven by an air-drive turbine attached to the outside of the top cover. The containment structure is suspended from the cover and surrounds the rotor such that the rotor's disk plane coincides with the horizontal midplane of the structure. A thin aluminum sheet witness ring is also attached to the cover and surrounds the containment structure some distance away. Its purpose is to record fragment penetration of the containment structure. Fragments which penetrate the structure will also penetrate or, if at small energies, dent the witness ring. The rotor is partially cut radially inward in three places 120° apart such that it fails in a tri-hub burst mode upon reaching a predetermined rotational speed. The chamber is evacuated to 10-mm Hg to reduce aerodynamic forces on the rotor allowing the air turbine to quickly accelerate the rotor to its burst speed. The rotor used in these tests is a T-53 Model 13 second stage power turbine. It is cut to fail in three equal parts at 19,845 RPM giving a burst kinetic energy of one million in-lbs.

A Cordin high-speed camera records the impact event by viewing through a port at the side of the chamber and a 45° mirror inside which allows a view up at the rotor. The repeating electronic flash which actually activates the camera is initiated by signal interruption from a trigger strip

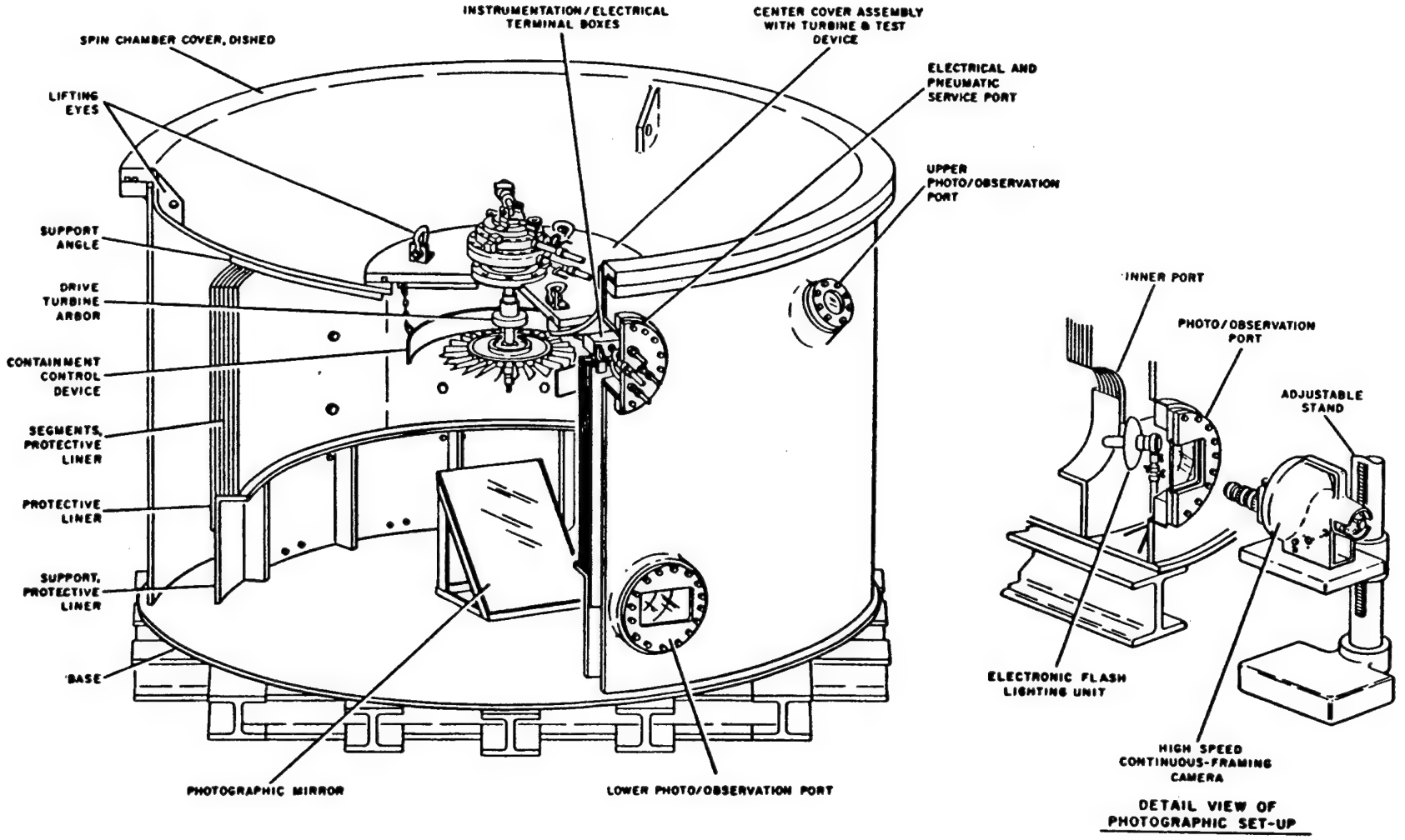

FIGURE 29. SPIN TEST CHAMBER AT THE NAVAL AIR WARFARE CENTER

bonded around the inside of the containment structure. This signal interruption also fixes the time at which the rotor speed is recorded. The nominal camera framing rate is 13,000 frames/sec and about 30 pictures are taken during the event.

3.2.3 Test Structures.

Ten test structures were designed and fabricated for spin chamber testing. With the exception of specimen 8, the energy absorbing material for all specimens was Kevlar 29 plain weave fabric. Specimen 8 used polybenzbisoxazole fiber with the same balanced plain weave configuration as the Kevlar style 745 so that test results could be directly compared. The first three test structures were constructed by bolting three flat, rectangular hybrid core panels together to form a triangular structure around the rotor. This configuration was used to test a possible application where a fragment shield is attached to airframe structures to provide a limited area barrier to high-energy fragments. Spin test structures 4 through 9 were rings. A ring is the most weight efficient containment structure and can be used as a collar around an engine. The final test structure consisted of two curved panels joined to form a lenticular geometry around the rotor. The joints in this structure were hinge type joints. Within these test structure geometries the number of energy absorbing plies and fiber orientations were varied to determine the effect of these changes on the containment performance. These details are discussed with the test results for the individual structures. The following drawings show nominal dimensions common to all the test structures of a given type. Figures 30, 31, and 32 show the triangular, ring, and curved panel structures respectively.

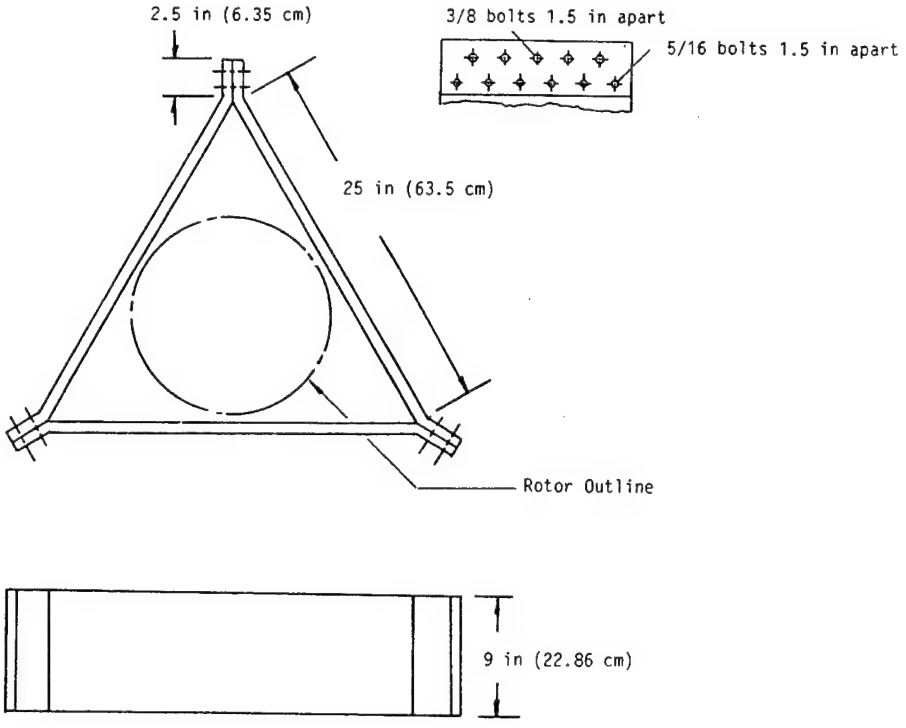

FIGURE 30. ARRANGEMENT OF TRIANGULAR TEST STRUCTURE

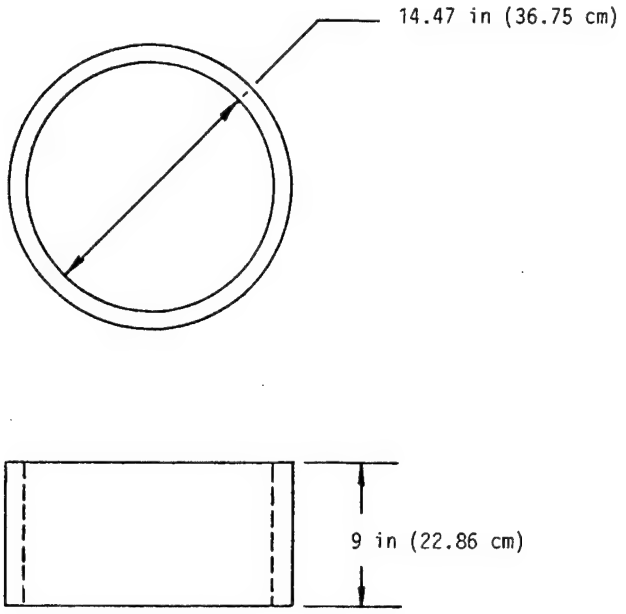

FIGURE 31. RING STRUCTURE GEOMETRY

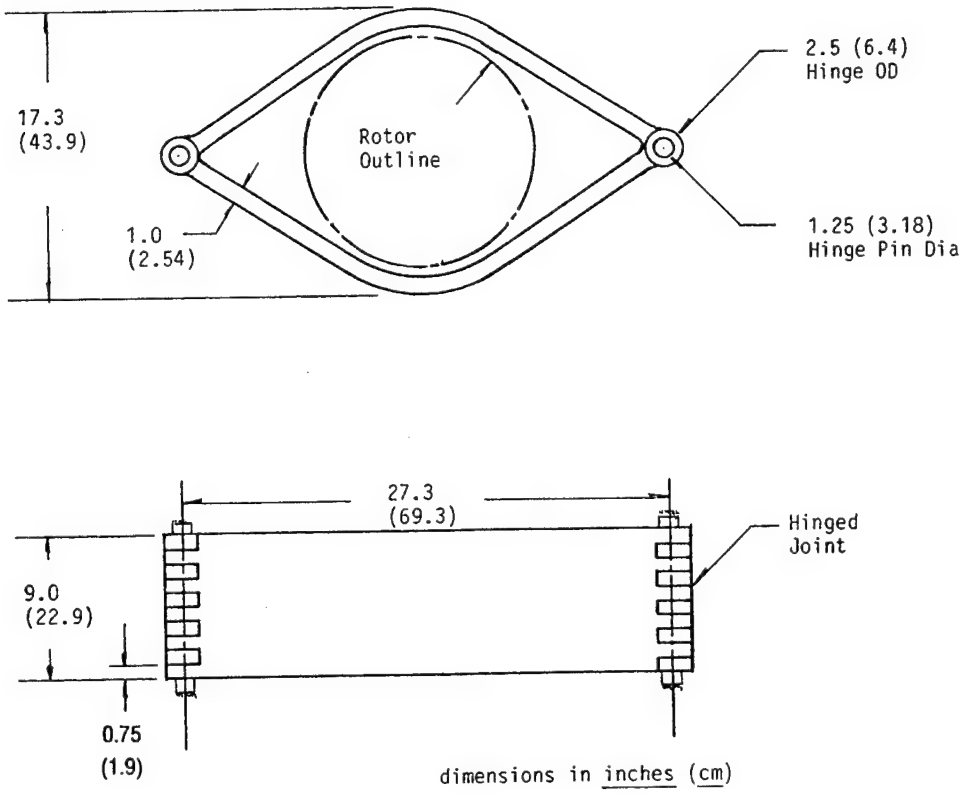

FIGURE 32. CURVED PANEL TEST STRUCTURE WAS THE TENTH CONTAINMENT STRUCTURE TESTED

3.2.4 Test Structure Fabrication.

The test structures were fabricated in much the same fashion as the mechanical test specimens only on a larger scale. The Kevlar plies were cut, stacked, and wrapped with Teflon film. Those panels with facesheets used the AS4/3501-6 five harness satin prepreg. Figure 33 shows a panel being sewn with graphite/epoxy 12K towpreg through two prepreg plies on each side of the core. The Candidate B rod architecture was used for all test structures since it had reasonably good mechanical properties and was easy to fabricate. The latter was an important consideration since many rods had to be inserted manually in the ten structures fabricated through the course of the program. The tooling shown in the figure guides the needles at the proper angle and separations. The needles are four inches (10.16 cm) long and have Kevlar leaders to help guide the carbon tow through the panel.

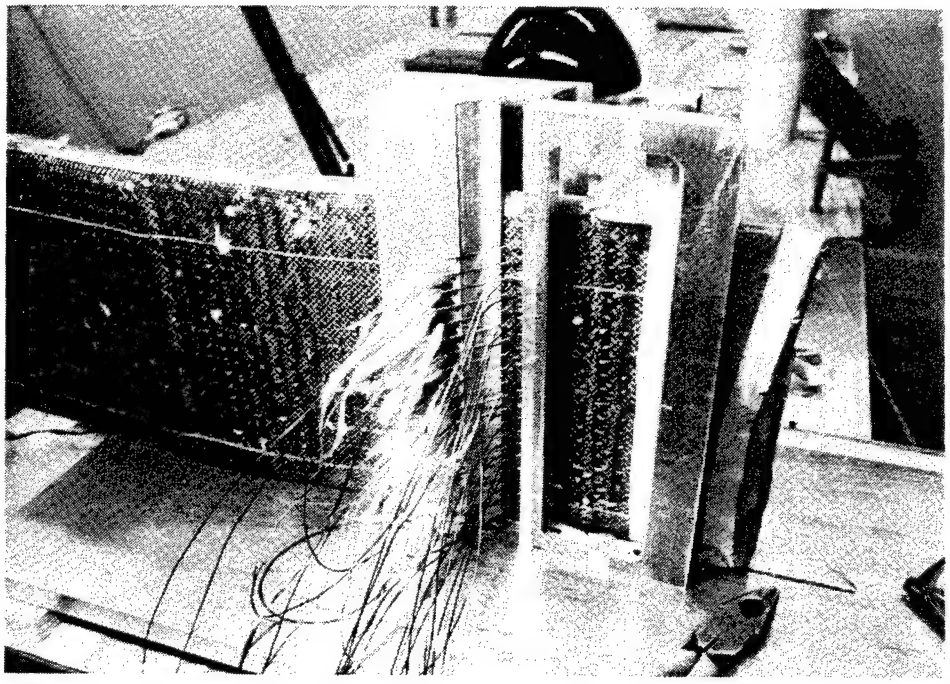

FIGURE 33. INSERTION OF PREPREG TOW INTO PANEL. PHOTO SHOWS GUIDES FOR NEEDLE ALIGNMENT

After stitching, the facesheet overlay plies were added and the panel was vacuum bag molded against a heated flat plate. Figure 34 shows the preformed panel on the plate without the overlay facesheet plies. The dry Kevlar tab ends on one of the structure 1 panels were impregnated by interleaves of FM 355 film adhesive during molding, but the mesh carrier on the adhesive caused excessive bulk. A wet lay-up approach using a room temperature cure epoxy resin was then used for the remaining panels. After molding the tab ends, the hole pattern was drilled and each pair of ends were bolted together. Grade eight 5/16-inch (0.79-cm) bolts were used for the inside bolt row and 3/8-inch (0.95-cm) bolts were used for the outside row, i.e., away from the rotor.

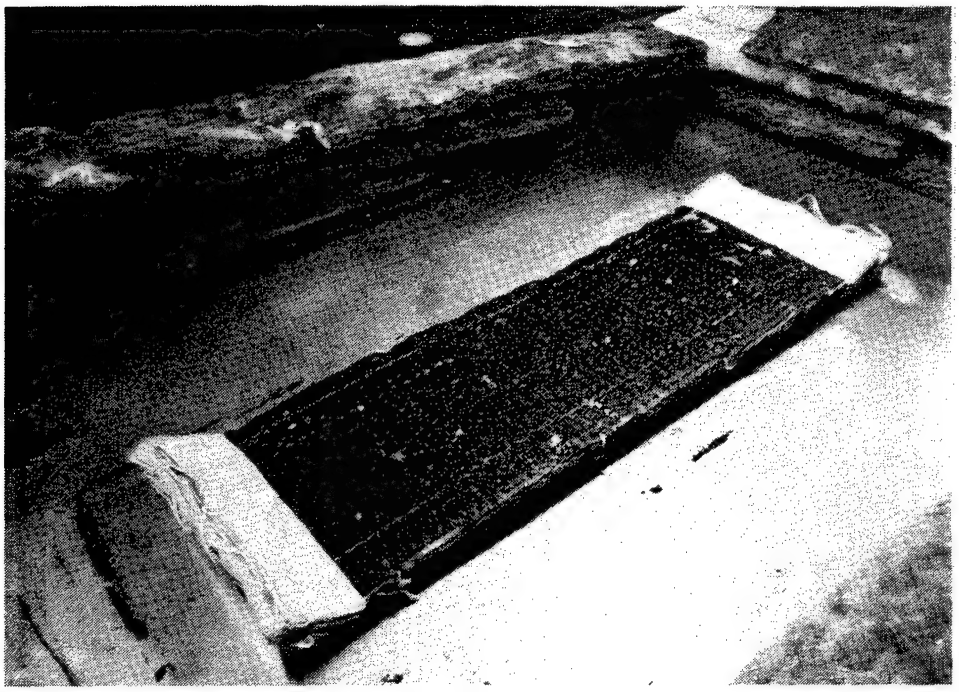

FIGURE 34. PREPARING PREFORM PANEL ON HOT PLATE FOR MOLDING

A 0.5-inch (1.27-cm) thick 4340 steel washer plate was used over all tabs for structure 1 but was replaced with Kevlar/epoxy for structures 2 and 3. This will be discussed further with the results.

The ring structures were fabricated by wrapping a 9-inch-wide Kevlar fabric onto a drum until the required number of plies was achieved. Splices were overlapped and sewn. A Teflon film was taped to the ring surfaces and the ring edges sewn with Kevlar or dacron to hold the dry ring laminate together while the 12K towpreg was inserted. The needle guides were similar to those shown in figure 33 except narrower so the ring could fit into them. A completely sewn ring is shown in a partially assembled molding tooling in figure 35. The ring is shown inside a steel ring tool wrapped with a silicone heater. Steel plate arc segments were placed against the inner diameter (ID) wall of the ring and held in place with ties. The entire assembly, shown in figure 36, was wrapped in a breather ply and then a vacuum bag. The vacuum forced the ID segments radially outward to mold the ring against the ID of the steel ring tool. Figure 37 was taken just after molding and shows the bag and outside thermal insulation.

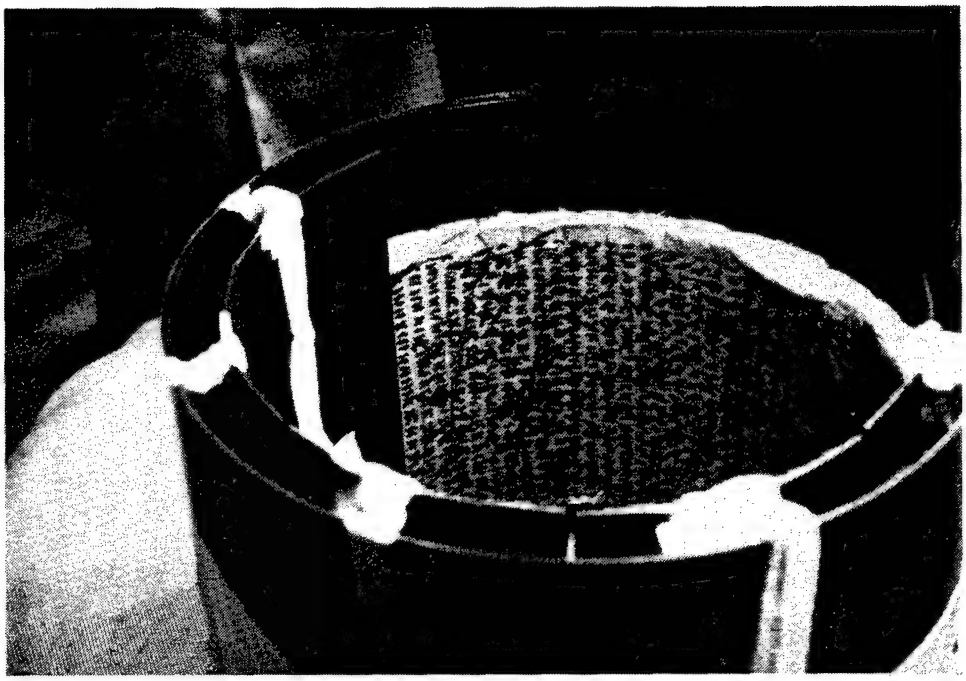

FIGURE 35. RING IS SHOWN INSIDE PARTIALLY ASSEMBLED MOLDING TOOLING

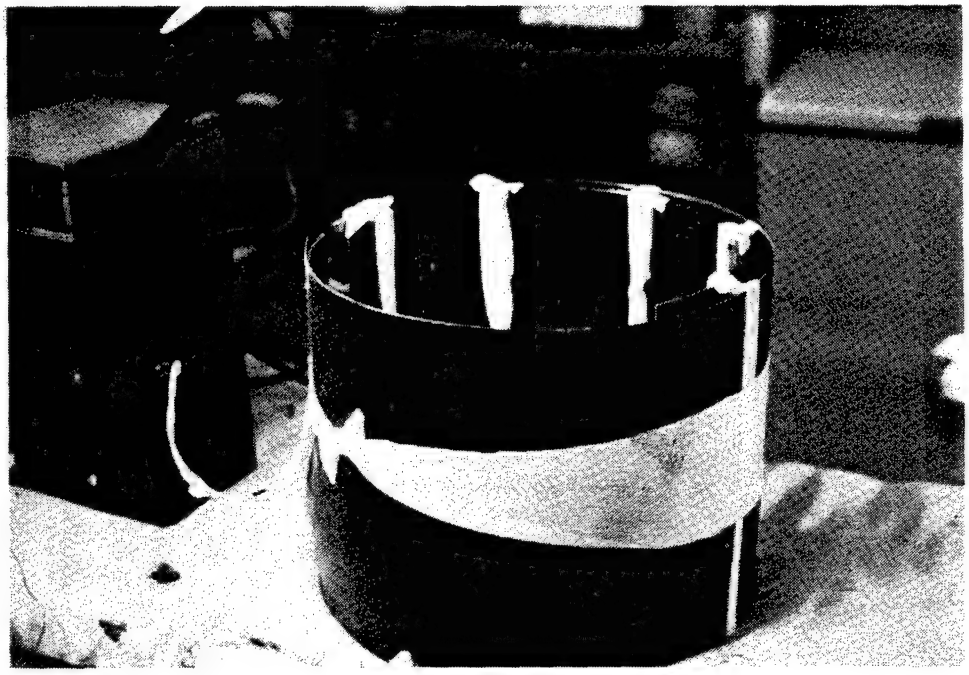

FIGURE 36. RING MOLDING ASSEMBLY AS ID SEGMENTS ARE PUT IN PLACE

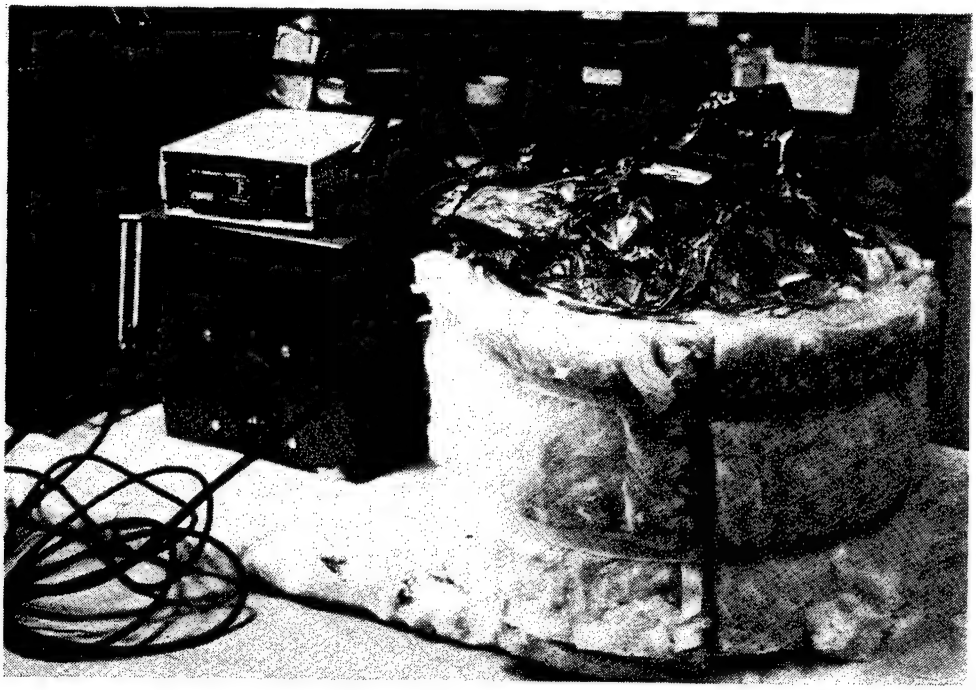

FIGURE 37. PHOTO AFTER MOLDING CYCLE SHOWING VACUUM BAG AND INSULATION. TOP AND ID INSULATION HAVE BEEN REMOVED.

3.3 SPIN TEST PROGRAM.

3.3.1 Overview.

Hybrid core panel and ring structures of various designs were tested in a rotor spin chamber at the Naval Air Warfare Center (formerly Naval Air Propulsion Center) in Ewing, NJ. The design, fiber architecture, or fiber type were varied to determine how these specific variables affected the ability of the structure to contain a rotor burst of a given energy level. The broad goal of this program was to determine if the hybrid panel could stop the high velocity fragments of the failed rotor with areal weight efficiencies comparable to those of the core without the rods or facesheets, i.e., a simple dry fabric laminate. Another specific goal was to compare the performance of PBO and Kevlar in the containment structure application. Each of the ten spin tests is discussed separately and a summary is then presented.

3.3.2 Discussion of Spin Test Results.

3.3.2.1 Spin Test Structure 1.

Test structure 1 was a triangular structure with bolted joints. The three 9- x 30-in. (22.9- x 76.2-cm) panels surrounded the rotor. The joints were formed by impregnating the 2½-in (6.35-cm) Kevlar tabs with resin, drilling holes, and bolting adjoining tabs together. The mating tab ends were sandwiched between 0.5-in. (1.27-cm) steel plates which formed the bearing surfaces for bolt heads and nuts. The tab ends of two panels were impregnated with a room temperature curing epoxy while the tabs of the third panel were impregnated with the 350°F curing film adhesive, FM 355.

The construction of the three panels was identical with 32 plies of Kevlar 29 style 745 plain weave fabric sandwiched between two plies of AS4/8553 3K graphite prepreg and sewn with AS4 12K towpreg using the candidate B architecture. Before molding, two additional plies of AS4/3501-6 6K graphite fabric prepreg were added to each side forming the sandwich panel with rigid rods locked into the facesheets. After molding, each 9- x 30-in. panel weighed 7 lbs with dry end tabs. Original thickness of the dry Kevlar fabric laminate was 0.700 in. (1.78 cm) while the final molded panel thickness averaged 0.88 in. (2.24 cm).

Total structure weight was 44.1 lbs (196.2 N) but 20.7 lbs (92 N) of that was the steel washer plate weight. The weight breakdown is given in table 2. Figure 38 shows the test structure mounted and ready for testing. The trigger strip can also be seen along the midplane of the inside surface.

TABLE 2. SPIN PIT TEST STRUCTURE 1 PANEL MATERIALS AND WEIGHT PER PANEL

Materials	Weight
Kevlar 29 style 745 plain weave 32, 9- x 30-in. plies 0.70 in. thick	5.5 lbs
Graphite/Epoxy facesheets and rigid rod members Candidate B architecture	1.5 lbs
Resin in two end tabs	0.8 lb
One set of bolts and two 0.5-in (1.27-cm) 4130 steel plates	6.9 lbs

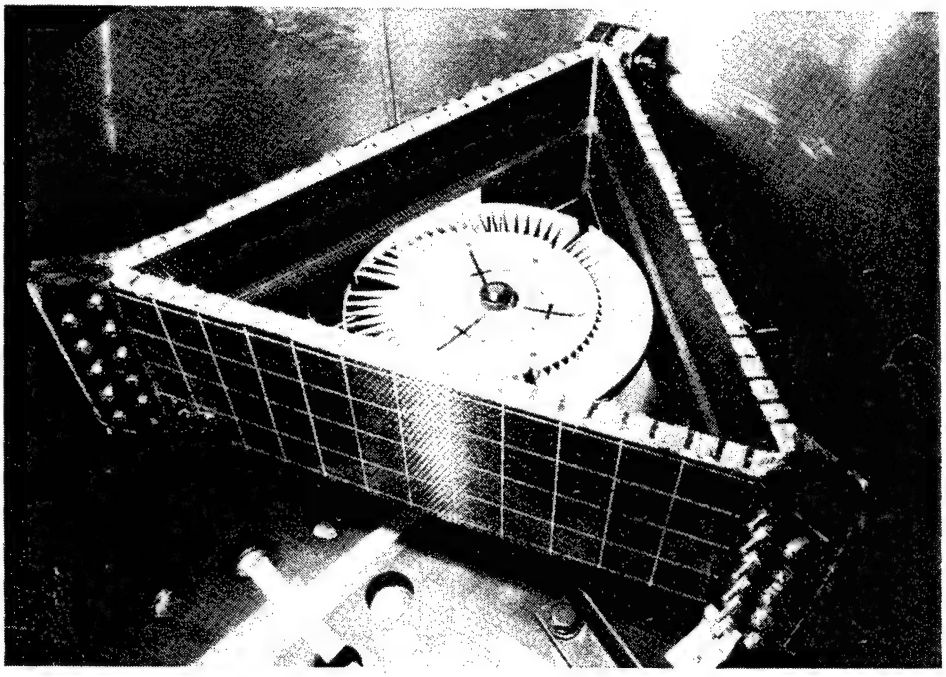

FIGURE 38. SPIN TEST STRUCTURE 1 MOUNTED IN CHAMBER AND READY FOR TEST

Figure 39 is a more vertical view which shows the radial saw cuts in the rotor to cause its failure at 20,000 RPM or one million in-lbs of rotor energy.

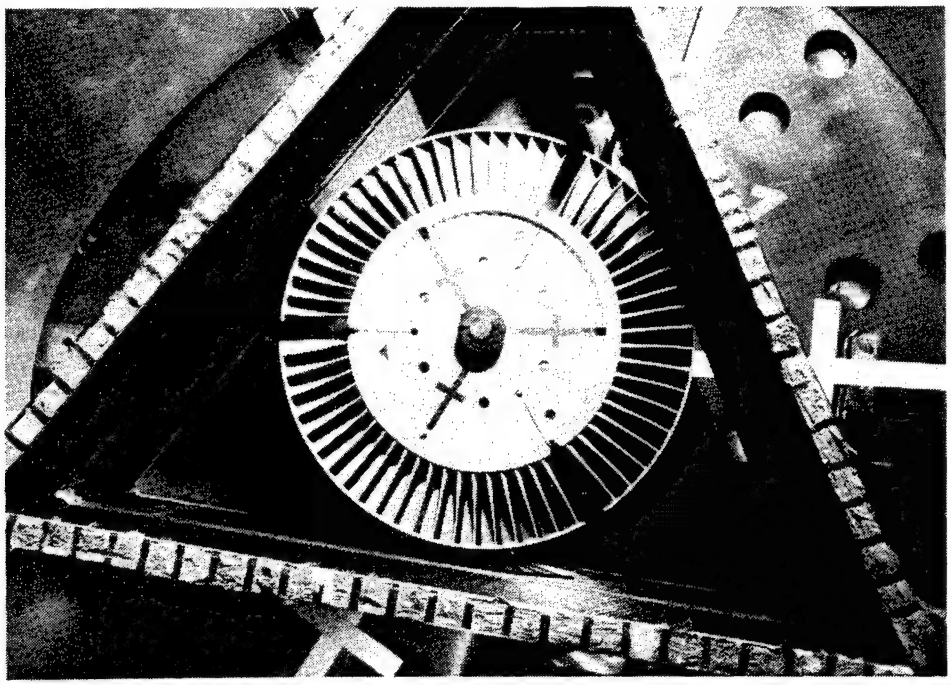

FIGURE 39. VERTICAL VIEW OF SPIN TEST STRUCTURE 1 AROUND ROTOR SHOWS RADIAL CUTS IN THE ROTOR TO CAUSE THE DESIGNED TRI-HUB BURST FAILURE

The test was performed and the rotor failed at 20,760 rpm giving an energy level of 1,002,558 in-lbs. The triangular structure failed at one of the joints due to a shearing action between the steel "washer" plate and one of the disk segments. The disk segment actually sheared a corner off the plate and escaped as a result. The other two disk segments were just contained by the panels they impacted. One was lodged in a hole made by a corner of the latter disk segment while the other was stopped by the panel it impacted. In this panel, six of the original 32 Kevlar fabric plies survived unbroken. The first of these six adjacent, unbroken plies was located five plies in from the outside surface. The four outermost plies failed presumably as a result of the panel's bending contribution to their tensile strain.

An overall posttest photo is shown in figure 40. The broken blades cut only a few of the inside plies while deep penetration was made by the corner of the disk segment. A close-up of the sheared corner of the washer plate is shown in figure 41. The pinching of the Kevlar laminate between the disk segment and the hard washer plate seemed to shear all the plies in the local area. As the disk segment penetrated the resulting hole, the neighboring "hoop" direction fibers probably failed sequentially in tension, tearing the entire panel away from its bolted tab end.

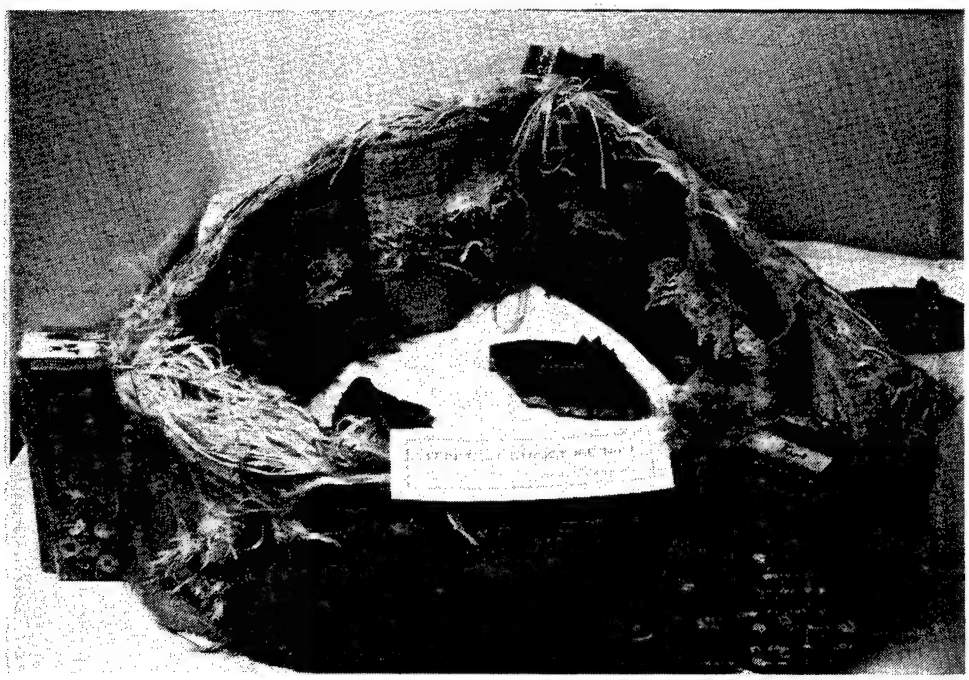

FIGURE 40. SPIN TEST STRUCTURE 1 AFTER TEST. FACESHEET BASE REMAINS ATTACHED IN MANY AREAS BUT THE NEAR CORNER WAS TORN AWAY

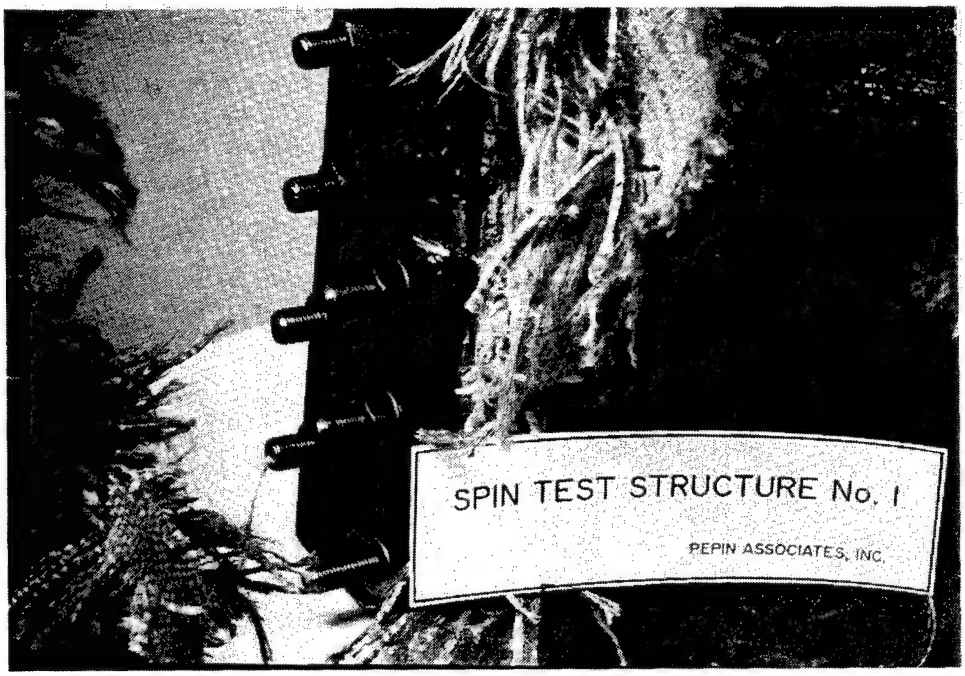

FIGURE 41. CLOSER VIEW OF JOINT SHOWING SHEARED-OFF CORNER OF WASHER PLATE

3.3.2.2 Spin Test Structure 2.

Test structure 2 had the same triangular geometry as structure 1, but unlike structure 1, it used an unbalanced 5:1 plain weave Kevlar 29 fabric as the energy absorber. The inside (closest to the rotor) 18 plies had the strong direction axially while the outside 19 plies had the strong direction of the fabric oriented circumferentially. The thinking behind this approach was that the inside plies would better resist the cutting of the blades and rotor segment while the outside plies would contain the outward expansion of the fragments. The total number of plies was selected to give a panel areal weight equal to that of structure 1. The facesheets consisted of two AS4/3501-6 6K five harness satin fabric plies which were sewn through with the Candidate B architecture and then two like fabric plies which were added before molding so the rigid graphite/epoxy part of the structure was essentially the same as structure 1. The steel washer plates of structure 1 were replaced with a 0.5-in (1.27-cm) Kevlar style 745/epoxy laminate and all panel tabs were impregnated with epoxy using the same wet lay-up and clamping approach. The total weight of structure 2 was 27 lbs (120.1 N) while the weight of a single panel without washer plates or bolts was 6.79 lbs (30.2 N). A pretest photograph is shown in figure 42.

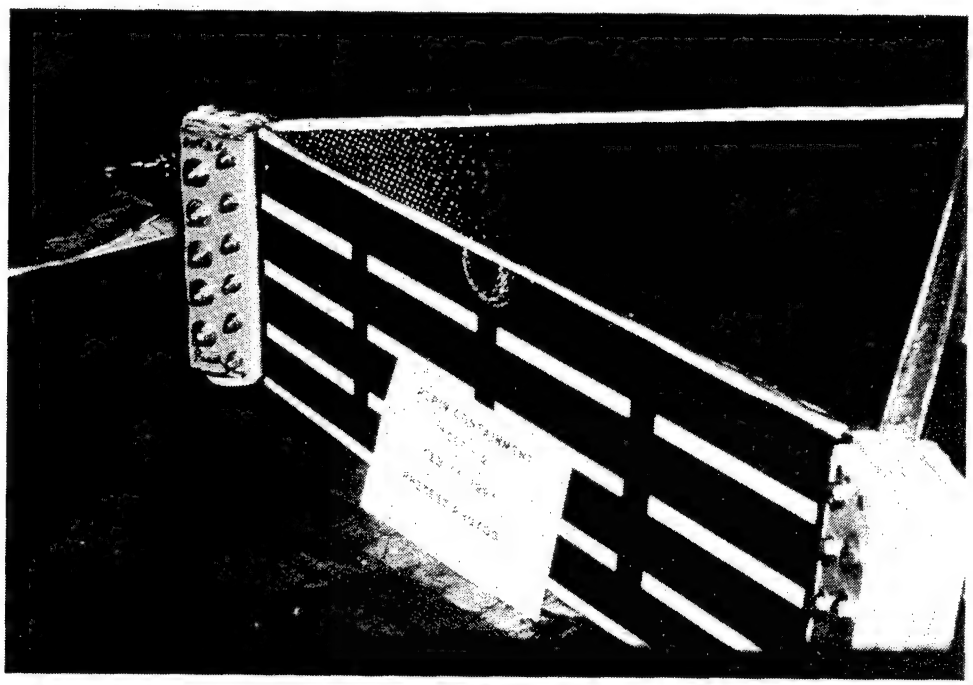

FIGURE 42. PRETEST PHOTOGRAPH OF SPIN TEST STRUCTURE 2 SHOWING KEVLAR/EPOXY WASHER PLATES

The test was run in the usual manner and the rotor failed at 19,800 RPM giving a tri-hub burst energy level of 911,980 in-lbs. The disk fragments hit the triangular structure near the corners and all three large segments seemed to pass quite easily through the structure. Although the

outer plies were preferentially reinforced in the "hoop" direction the fragments easily spread these "hoop" yarns since there were not many transverse yarns linking them together. As a result only the fibers near the penetrating rotor were damaged indicating that the load was not very well shared with adjacent fibers woven into the fabric. In one area the entire 18-ply inner laminate with the preferential axial reinforcement began to be pulled through the exit hole. Figure 43 shows an overall view of the triangular structure after testing and figure 44 shows a closer view of one of the corners. The one-third disk segment hit the corner and caused some bending and tensile fracture but seemed to be deflected to one side where it exited through the panel. The Kevlar/epoxy washer plates deformed extensively, absorbing some energy and did not cause the pinching problems of the steel plates of structure 1. In summary the 5:1 weave performance was significantly poorer than the tight plain weave of structure 1. This was probably due to the looseness of the weave and poor mechanical communication between adjacent yarns of the fabric allowing fragments to locally spread the weave instead of fracturing many adjacent fibers as was the case for the tight plain weave of structure 1.

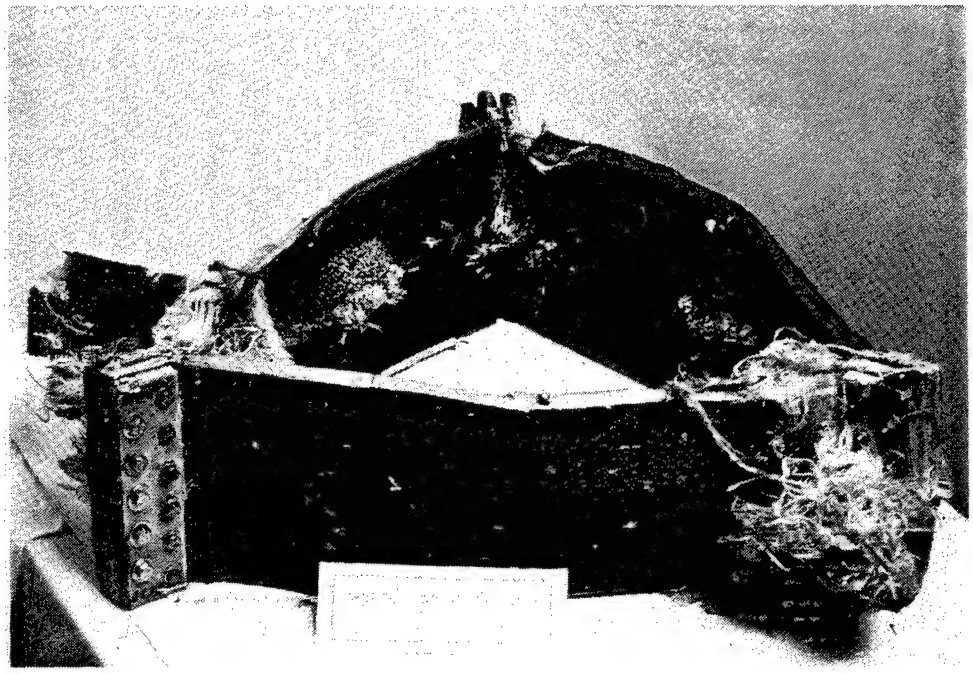

FIGURE 43. PHOTO OF STRUCTURE 2 WITH 5:1 PLAIN WEAVE KEVLAR FABRIC AFTER TEST

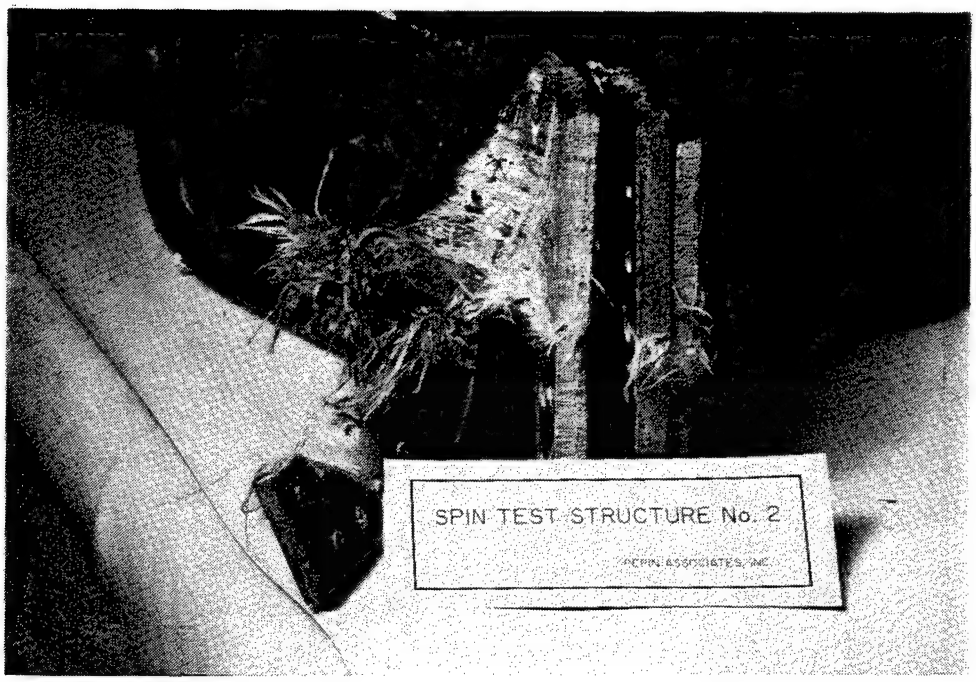

FIGURE 44. PHOTO OF THE CORNER OF STRUCTURE 2 SHOWING BENDING DEFORMATION IN THE IMPACT AREA

3.3.2.3 Spin Test Structure 3.

The third triangular test structure returned to the tight plain weave of Kevlar style 745 as the energy absorbing medium. Four plies more than those in the test structure 1 were used so each panel of the triangle contained 36 plies of this fabric. Two of the three panels had the same facesheet design as the previous structures but the third panel had no facesheets at all. The rods were still inserted so that the panel had the same rigid rod architecture as the other panels, but the facesheets were just omitted. It was felt that the facesheets made little contribution to the ability of the panel to stop the fragments and the panel surface would be more easily visible under high-speed photography if the facesheets were not present. Molded thickness of the facesheet panels was 1.0 in (2.54 cm) while the one without facesheets was 0.85 in (2.16 cm). The washer plates were Kevlar style 745 fabric laminate impregnated with FM 355 film adhesive while the panel tabs were wet impregnated with a room temperature cure epoxy as in the previous structures. The weights are given in table 3 and a photo of the structure is shown in figure 45.

TABLE 3. TRIANGULAR PANEL CONTAINMENT STRUCTURE 3 COMPONENT WEIGHTS

	Facesheet Panels	Core Only Panel (No Facesheets)
Thickness	0.97 in (2.46 cm)	0.85 in (2.16 cm)
Weight without Resin in End Tabs	8.25 lbs. (36.7 N)	6.8 lbs. (30.2 N)
Weight of End Tab Resin	1 lb/panel (4.4 N)	1 lb/panel (4.4 N)
Bolts for Entire Structure	3.73 lbs. (16.6 N)	
Washer Plates for Entire Structure	3.11 lbs. (13.8 N)	
Total Structure Weight	33 lbs. (146.8 N)	

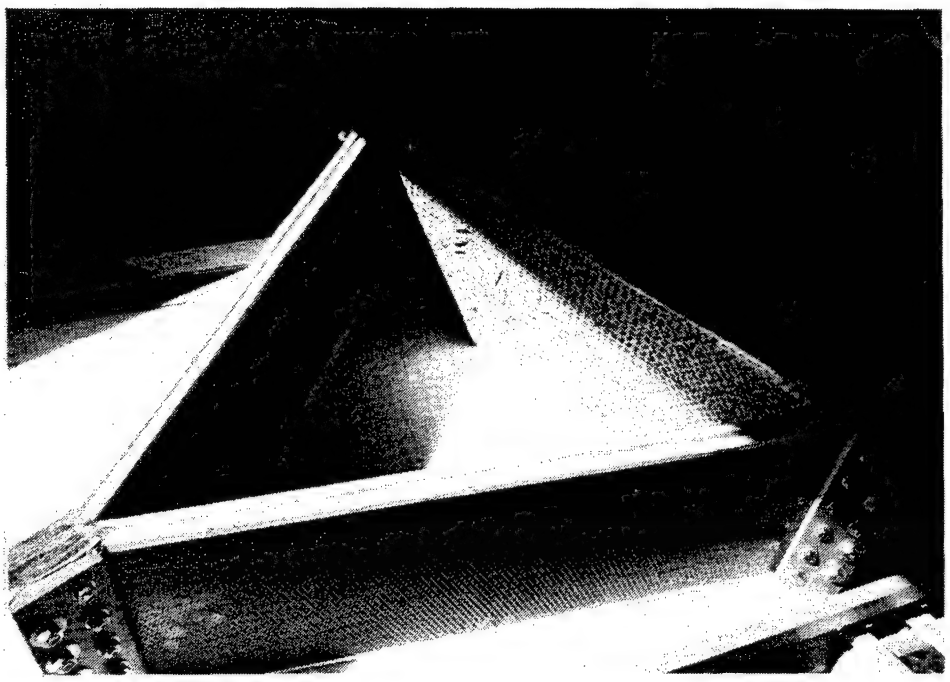

FIGURE 45. PHOTO OF STRUCTURE 3 BEFORE TEST

The test was performed with the rotor failing at 20,440 RPM giving an energy of 971,839 in-lbs. The structure completely contained all rotor fragments. For the two panels with the facesheets, 12 and 13 plies of the Kevlar 29 fabric were broken or penetrated while 16 plies were penetrated for the panel without the facesheets. The high-speed pictures of this test were quite clear and are shown as figure 46A-G. The camera was aimed to get the best look at the panel without facesheets. The disk fragments are seen to impact the panels nearly midway between the joints and the rod loops at the surface are clearly visible. The reflective tape with the black crossing lines tends to remain stationary at the earlier times along with several warp yarns which are

FIGURE 46A-G HIGH-SPEED PHOTOGRAPHS OF STRUCTURE 3 TRI-HUB BURST TEST

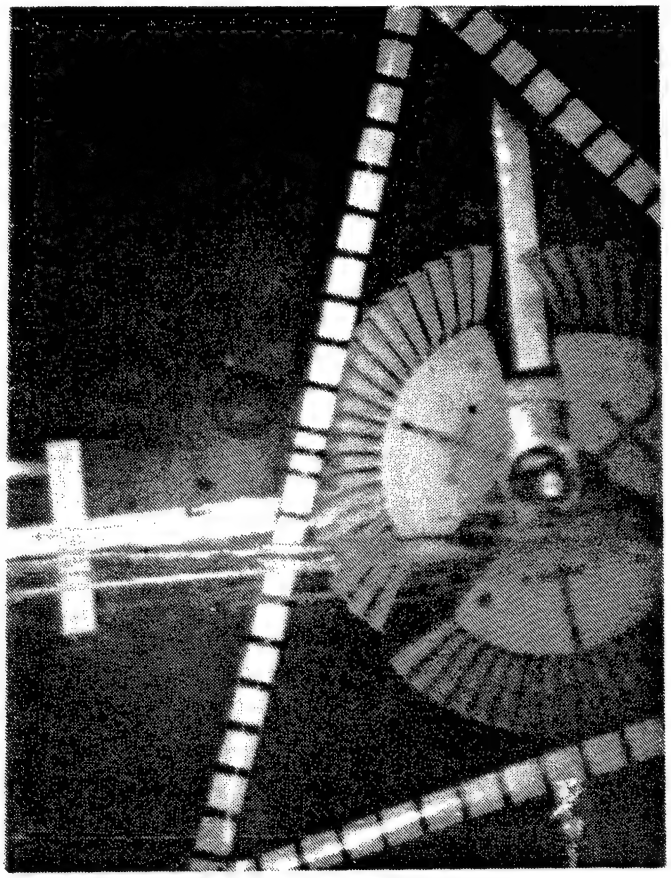

(A) 0 sec

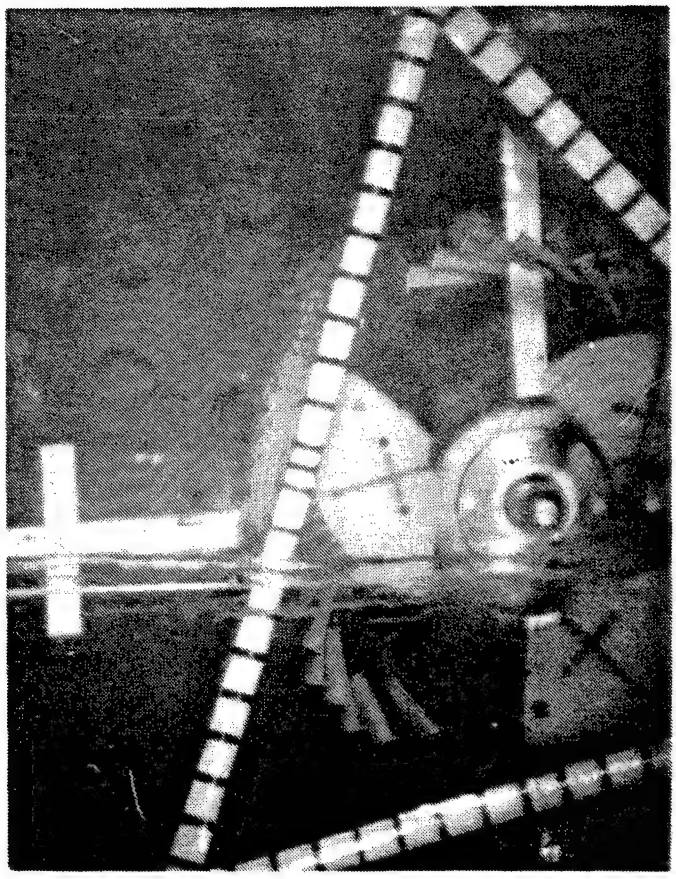

(B) 0.308 msec

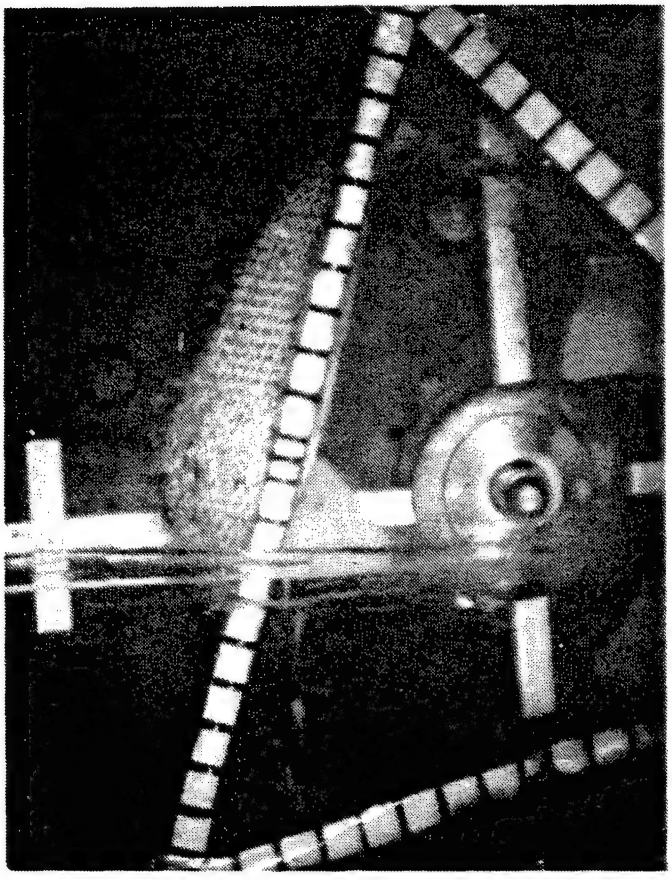

(C) 0.770 msec

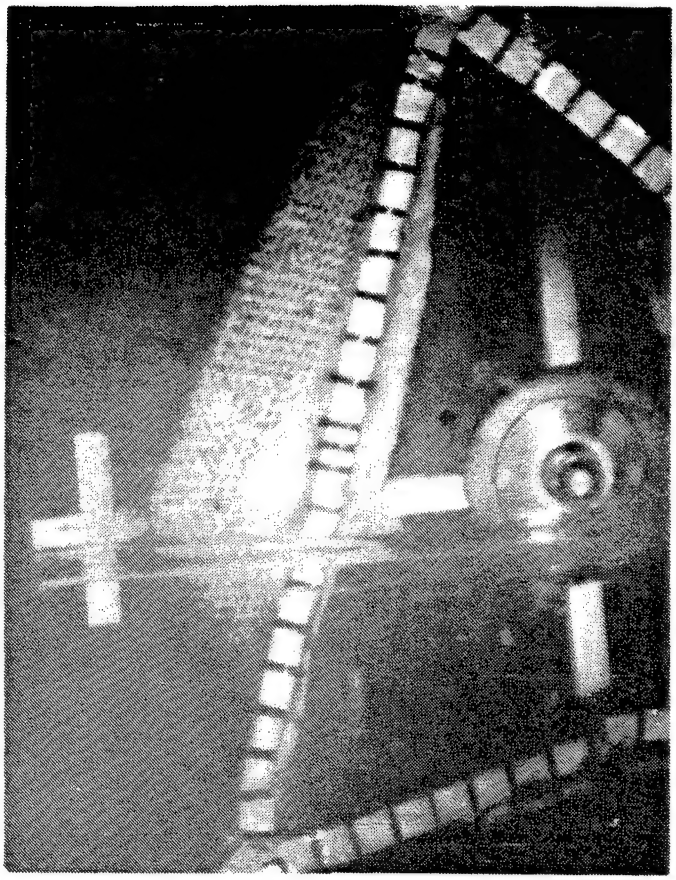

(D) 1.23 msecs

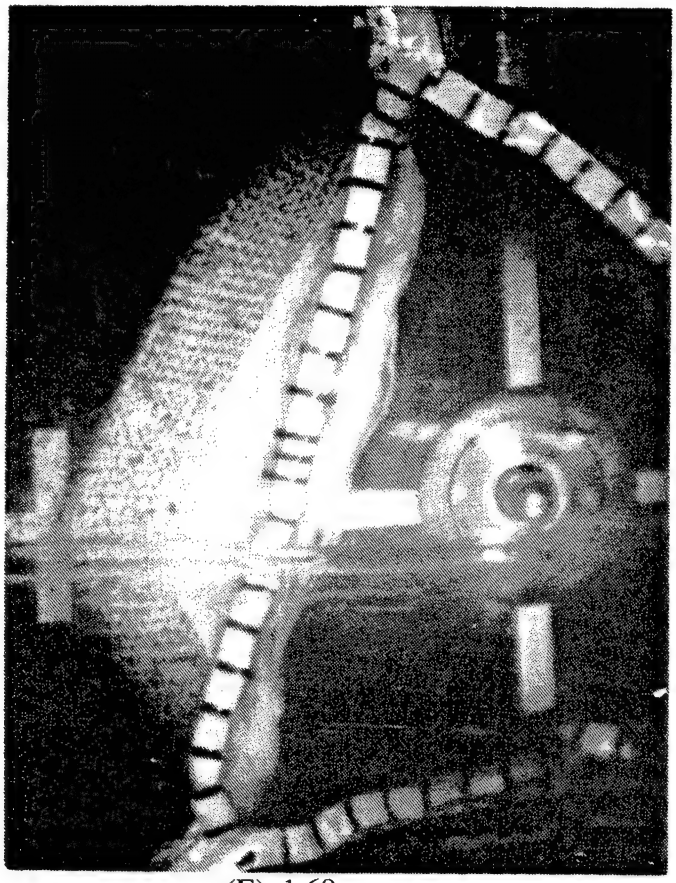

(E) 1.69 msecs

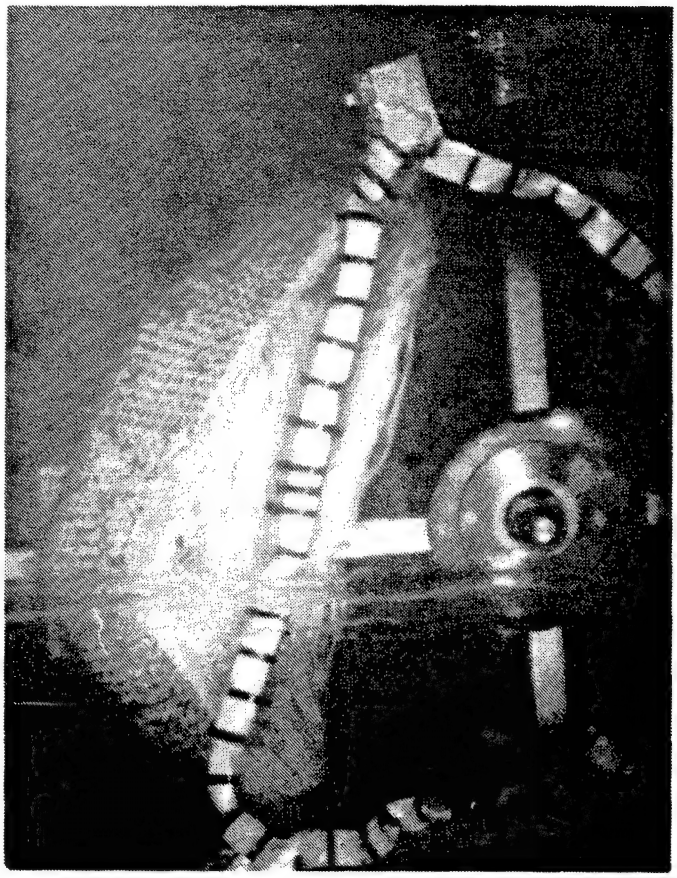

(F) 2.16 msecs

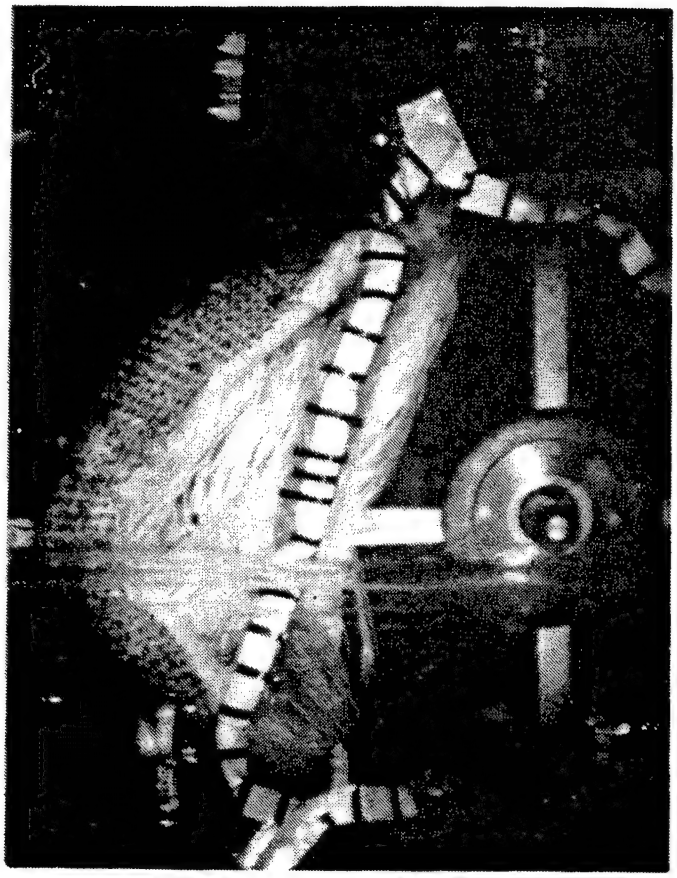

(G) 2.62 msecs

pulled out of the fabric at the edges. The actual edge of the panel is where the last row of carbon loops is seen. The deflection is quite high with the panel expanding out about 9 in. (22.86 cm) from its original flat plane. A video was made from the full set of 36 pictures covering the 2.6 msecs and a wave can be seen traveling the length of the panel from the impact area.

Post test photos are shown in figure 47 and 48. Figure 47 was taken on the floor of the chamber just after the test and shows some of the fiber debris and glass from the broken mirror. Figure 48 shows the base layer of the facesheet still held on with the rod loops. The top layers delaminate and separate at impact. The joints suffered relatively minor damage. Some holes at the midplane were elongated and two or three of the small (5/16 in.) midplane area bolts on each joint were bent by the high restraining forces.

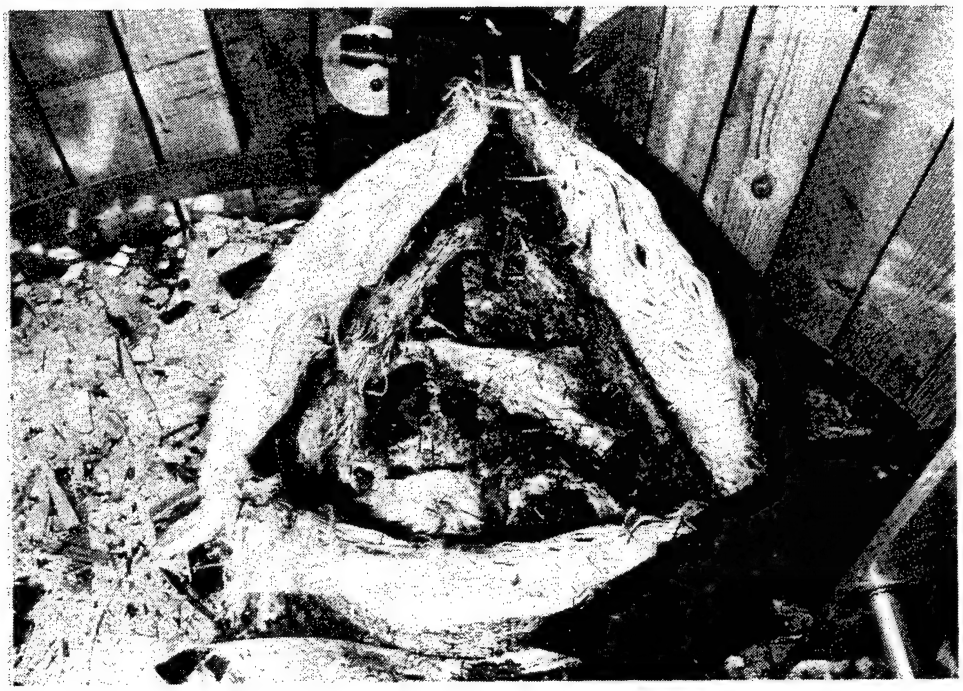

FIGURE 47. STRUCTURE 3 ON FLOOR OF CHAMBER AFTER TEST

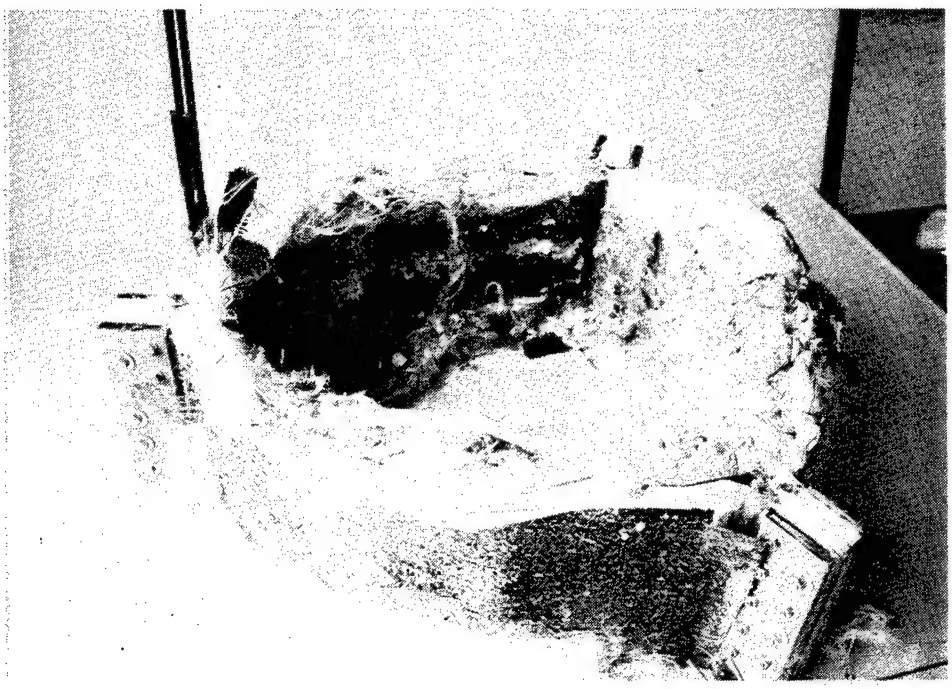

FIGURE 48. STRUCTURE 3 AFTER TEST. FACESHEET BASE IS HELD ON BY THE RODS

3.3.2.4 Spin Test Structure 4.

Test structure 4 was a ring with the same construction as the panel of structure 3 without the facesheets. Nine-inch-wide Kevlar style 745 fabric oriented in the hoop/axial direction was wrapped around a mandrel to form a thirty-six-ply ring which was sewn with the graphite/epoxy towpreg using the Candidate B architecture. The rod rows were sewn in the circumferential direction. The ring, shown in figure 49, had a wall thickness of 0.8 in (2.03 cm), an ID of 14.25 in (36.2 cm), and weighed 10.7 lbs (47.6 N).

The ring was mounted to surround the rotor and the rotor accelerated to 21,080 RPM before it failed. This gave a tri-hub burst energy level of 1,033,704 in-lbs. All three disk fragments completely penetrated the ring as shown in the posttest photo of figure 50. So, although ring 4 and triangular panel structure 3 had identical areal weights and reinforcement architecture, the ring did not have the potential for large deformation before failure as did the panels. Large panel bending deflection and the effective perimeter of the panel structure, 75 in (191 cm), versus 45 in (114 cm) for the ring probably both played a role in the test outcome. The higher total strain energy capability of the larger panel structure and the ability of the panel impact point to accelerate rapidly and deform before significant tensile resistance was felt are apparent advantages of the panel structure. However, it would be interesting to learn how triangular structure 3 would absorb an impact at the corners rather than at the middle of the panel. In this case very little bending deformation would take place, the impact area could not accelerate rapidly, and the tensile load would be immediately felt. So, when comparing ring and panel

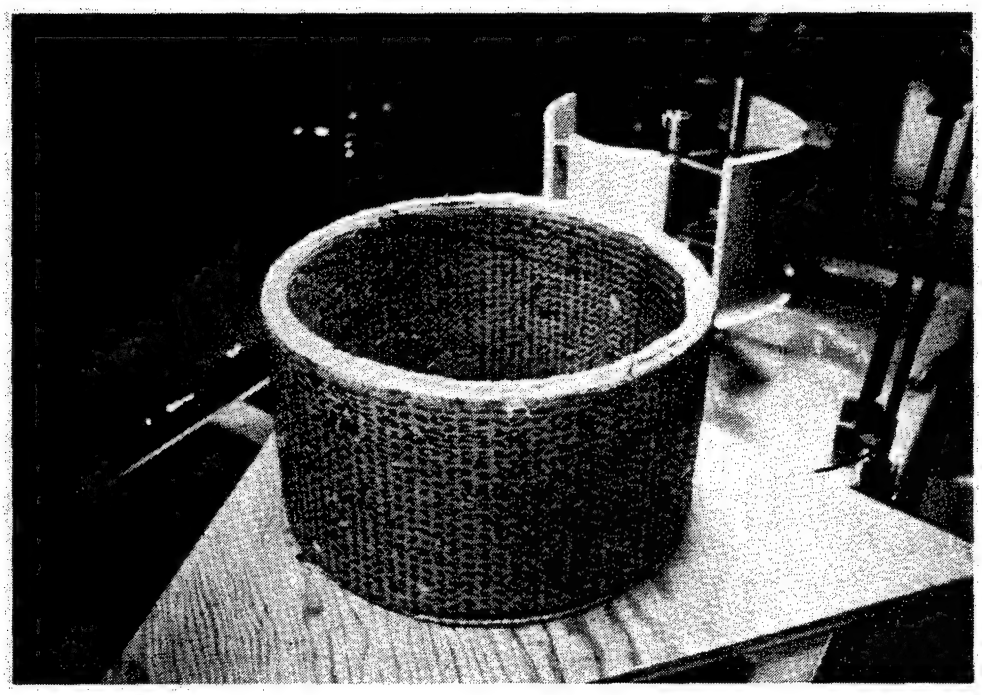

FIGURE 49. TEST STRUCTURE 4 IS A 36-PLY RING SEWN WITH THE CANDIDATE B ARCHITECTURE

structure results the factors which seem to influence the results, are areal weight, effective perimeter, geometry, and for panel structures, the impact point.

FIGURE 50. PHOTO OF STRUCTURE 4 AFTER TEST

3.3.2.5 Spin Test Structure 5.

In order to find the threshold of containment for the ring with 0°/90° Kevlar fabric and ±45° circumferential graphite/epoxy rods, more Kevlar plies were added to the design of structure 4. Spin test structure 5 was the same design as 4 with 50 plies instead of 36. The ID was 14.38 in (36.5 cm), the wall thickness was 1.1 in (2.8 cm), and the weight was 15 lbs (66.72 N). Figure 51 shows structure 5 before testing.

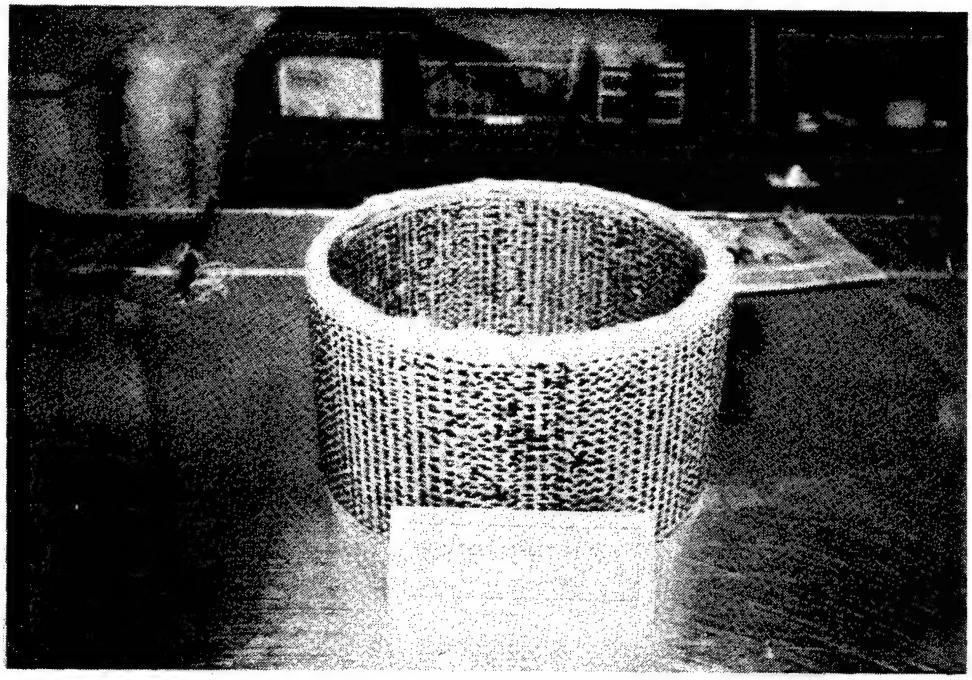

FIGURE 51. STRUCTURE 5 SPIN TEST

The ring was tested in the standard fashion with the rotor failing at 19,980 RPM giving an energy level of 928,637 in-lb. The ring contained the three disk fragments but allowed a blade to be pushed through the ring wall. It appears that a blade or blade segment did not break off as usual but was perpendicular to the deformed wall and seemed to be driven through the wall by the relatively massive 1/3 disk segment. The blade fragment also penetrated the witness ring. A hard facesheet or other liner could be used to blunt such a blade preventing it from being driven through by the disk fragment. The 1/3 disk fragments themselves penetrated 26, 25, and 23 plies with the first listed being the area where the blade penetrated making a hole about its own size. Blade fragments away from the disk impact areas damaged 10 plies on average. This level of damage from the blades was typical of all structures. A similar 50-ply ring was tested by the Army Materials Laboratory under a parallel program with the FAA. Test procedures, facilities, ring architecture, and fabric were the same except the ring had a thin aluminum ID mandrel and no graphite/epoxy through-thickness rods were used. In this test the rotor failed at 19,800 RPM and the 1/3 disk segments penetrated 46, 40, and 36 plies. The rods seemed to have helped or at least not hurt the ability of the dry Kevlar style 745 laminate to stop the disk fragments. Figure 52 is the posttest photo showing the blade exit point near the broken fibers.

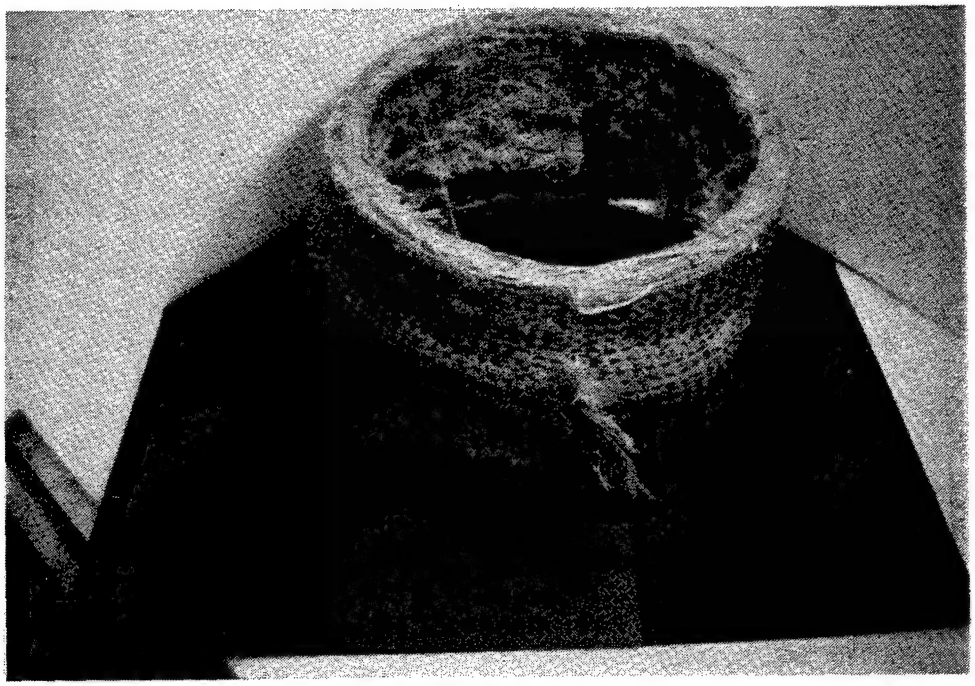

FIGURE 52. POSTTEST PHOTO OF SPIN TEST STRUCTURE 5 SHOWING BLADE EXIT POINT. DISK FRAGMENTS WERE STUCK IN THE RING AFTER THE TEST

The high-speed photographs of this test are shown in figure 53. Maximum radial deformation at the bulge in the ring caused by the 1/3 disk impact is about 3 inches (7.62 cm). The photographs are taken off center to allow room to see the deformation take place. A reflective tape was again used on the edge of the ring and it seems to remain stationary for many time increments during which the large bulge at the midplane appears. The next ring to be tested alters the carbon rod architecture to try to involve more of the ring at an earlier time in the energy absorbing process.

No pretest is shown as photo A begins the impact event. The time between pictures is 0.449 msec giving a total time covered by the photographs of 2.245 msecs.

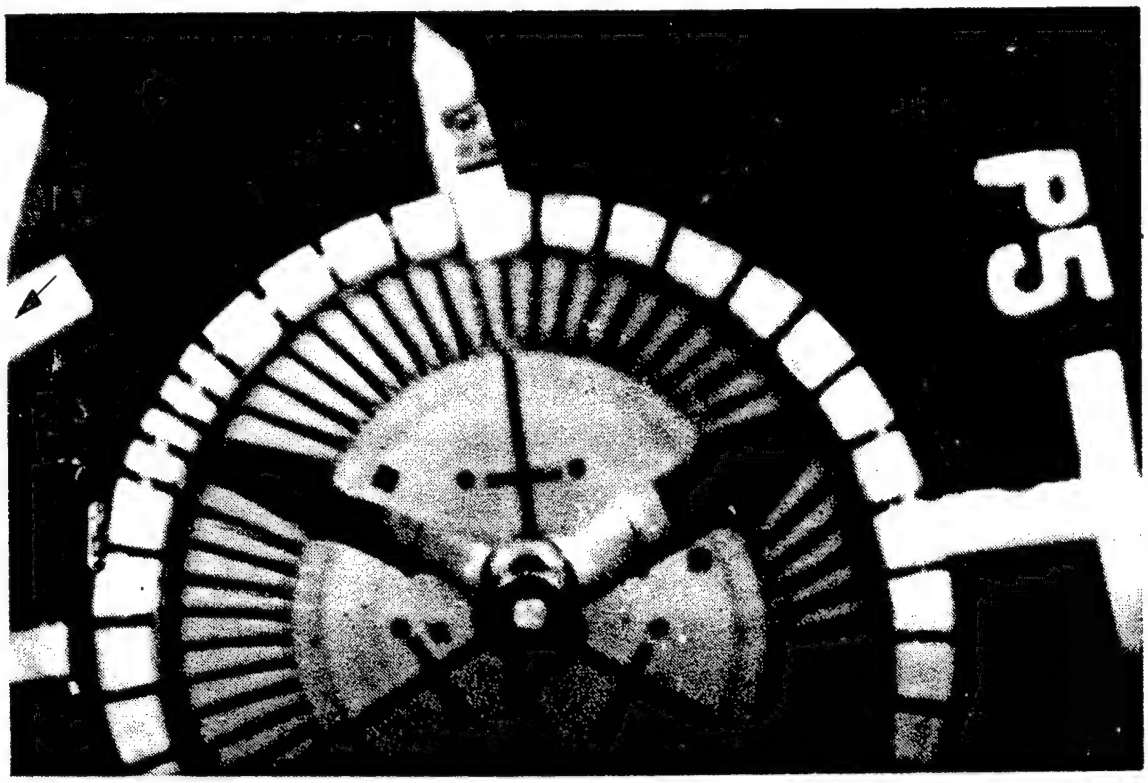

FIGURE 53A-F. (A) HIGH-SPEED PHOTOGRAPHS OF SPIN TEST FIVE

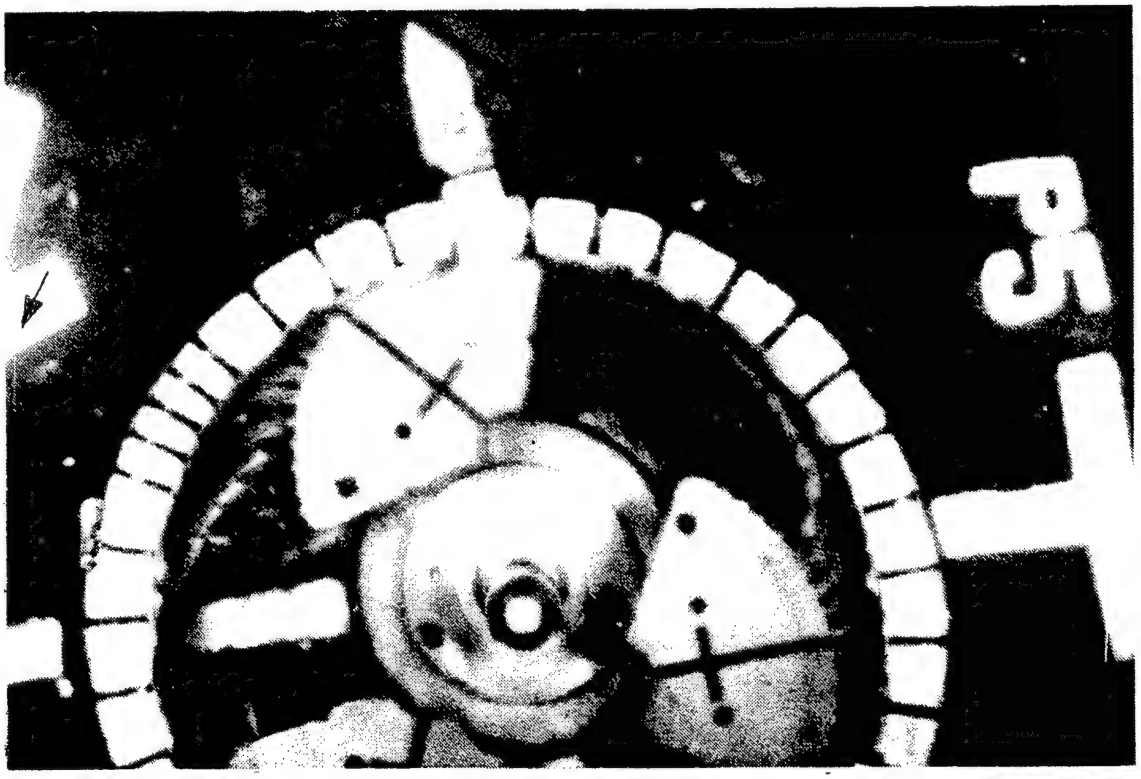

(B)

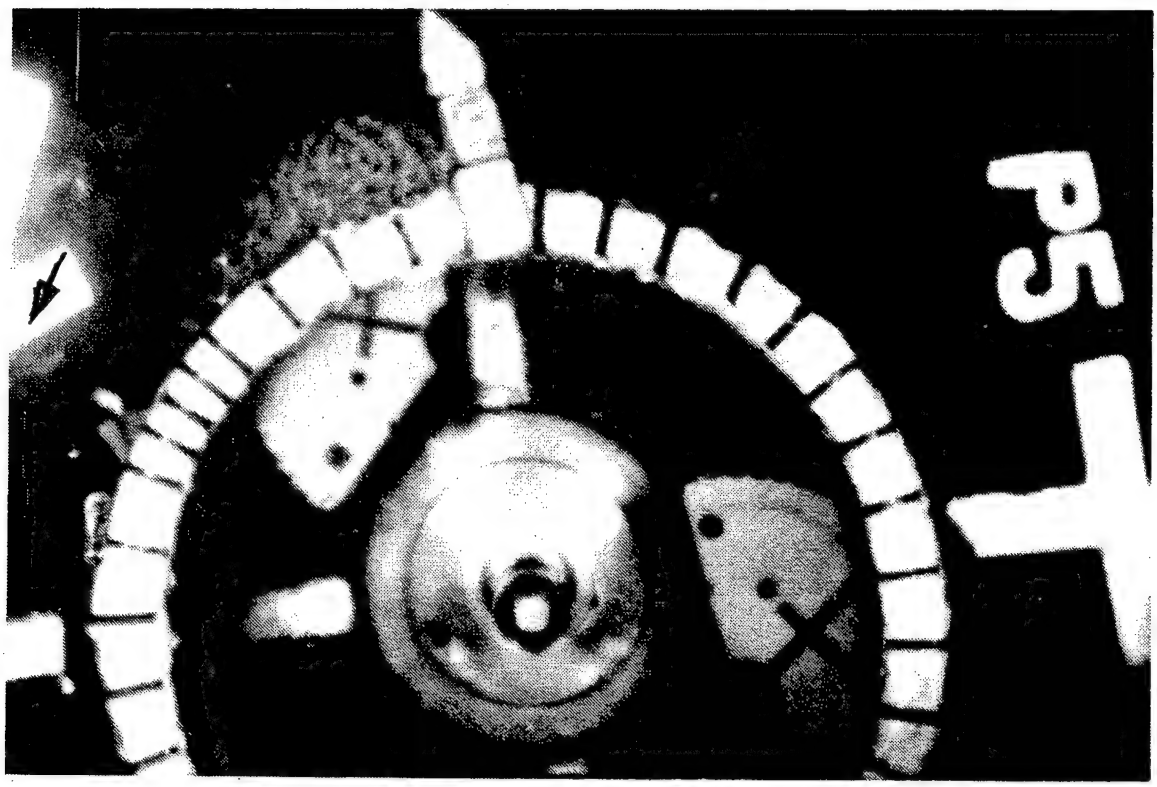

(C)

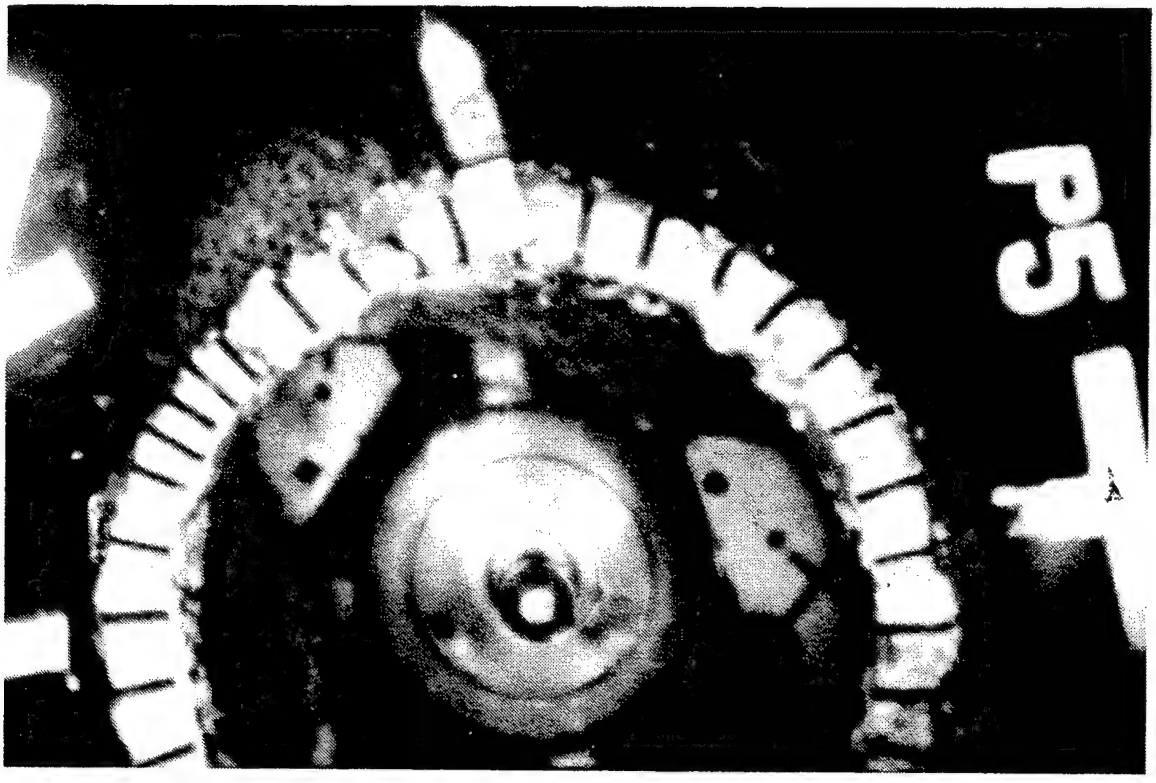

(D)

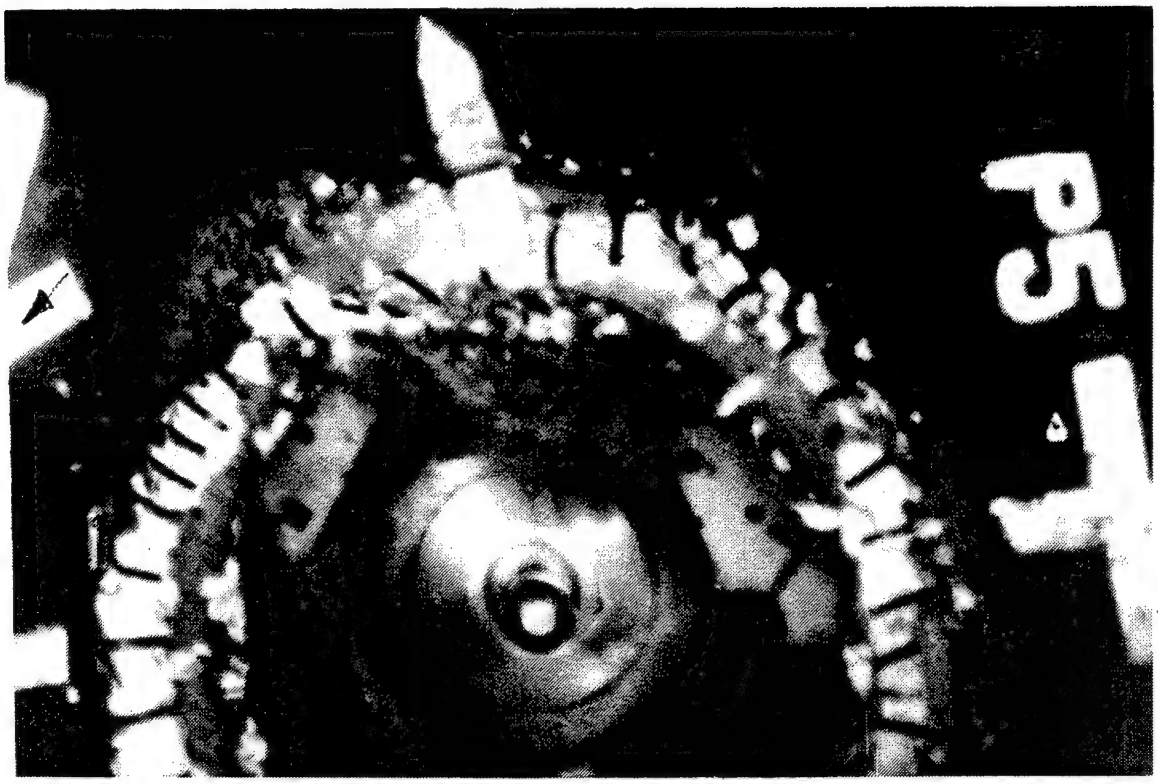

(E)

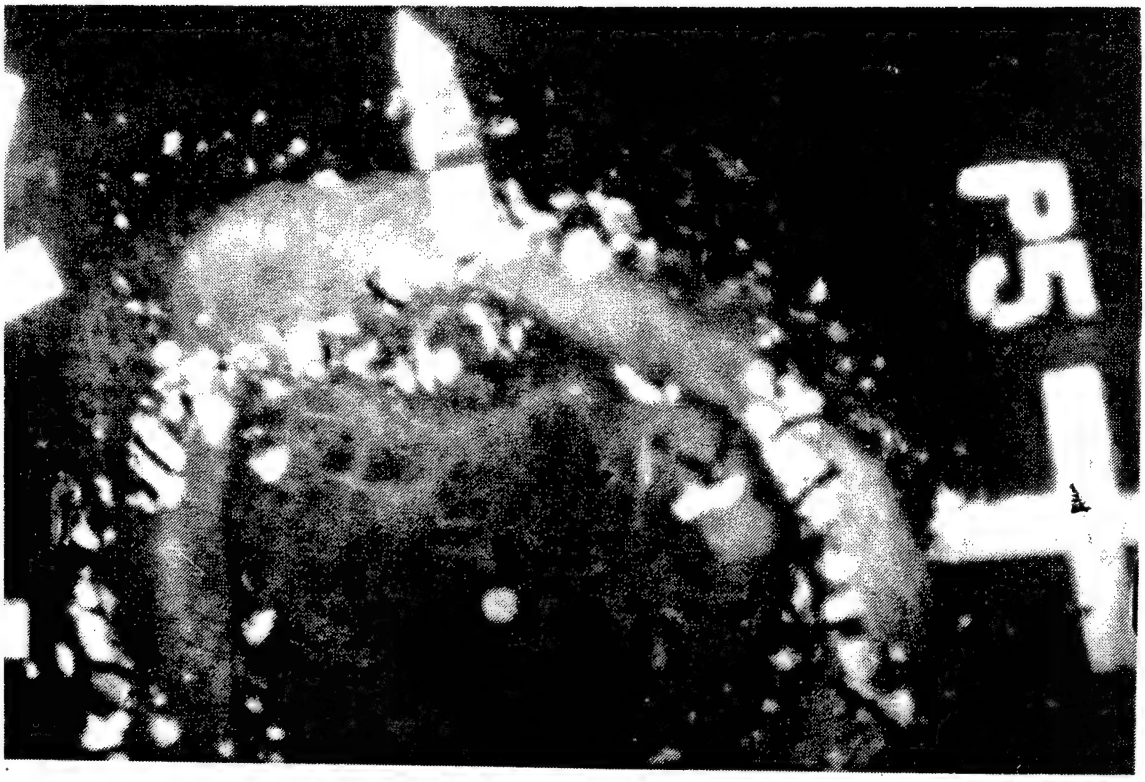

(F)

3.3.2.6 Spin Test Structure 6.

In order to try to involve more of the ring's axial length in absorbing the energy of the fragments impacting at the midplane, the rows of graphite/epoxy rods were inserted axially instead of circumferentially. In a static sense the difference between this geometry and that of the circumferential rod rows was that this geometry increased the axial bending stiffness of the ring wall locally and decreased its circumferential bending stiffness. Whether this modification to the static properties of the core was also reflected in its reaction to the impact event was the question that this test sought to answer. The only difference between ring 6 and ring 5 was this change in through-thickness rod orientation. The weight, number of plies, and construction method were all the same. Figure 54 shows this ring.

Unfortunately the spin test itself for structure 6 was not successful. At about 19,000 RPM the rotor became separated from the shaft. The blades impacted the ID wall of the ring and fractured into many pieces causing damage to the first 11 plies. The still intact disk fell to the chamber floor. The damage to the ring made it unsuitable for retest.

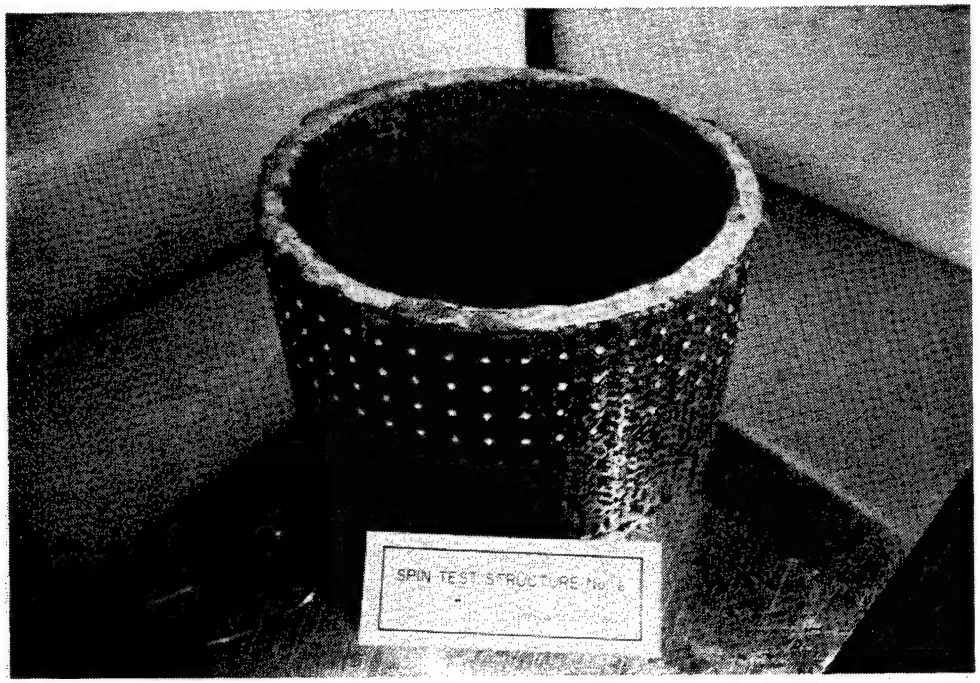

FIGURE 54. PHOTO OF SPIN TEST STRUCTURE 6 SHOWING PAINTED DOTS TO HELP IDENTIFY THE SURFACE WITH THE HIGH-SPEED CAMERA

3.3.2.7 Spin Test Structure 7.

To more closely define the threshold of containment for the ring geometry with circumferential rod rows, a 43-ply configuration was chosen as test structure 7. Again, all the other parameters remained the same as for ring 5 so that results can be compared directly. The wall thickness of this ring was 1.0 in (2.54 cm) and it weighed 12.88 lb (57.3 N).

This spin test went well with the rotor failing at 20,360 RPM giving a tri-hub burst energy of 964,296 in-lbs. This ring did not contain the T-53 tri-hub rotor burst. One of the disk fragments penetrated the ring while the other two were contained within the ring. The two contained fragments penetrated 28 and 29 plies while the latter also caused 3 OD plies to fail in tension. This result can be compared to the 36-ply ring of test 4 where all three disk segments penetrated the ring and the 50-ply ring of test 5 which contained the three disk segments. So the containment threshold for the 0°, 90° (hoop, axial) plain weave laminate of Kevlar style 745 sewn circumferentially with the graphite/epoxy rods is between 43 plies and 50 plies for a 9-inch-long ring. Photos of this ring before and after testing are shown in figures 55 and 56.

FIGURE 55. SPIN TEST STRUCTURE 7

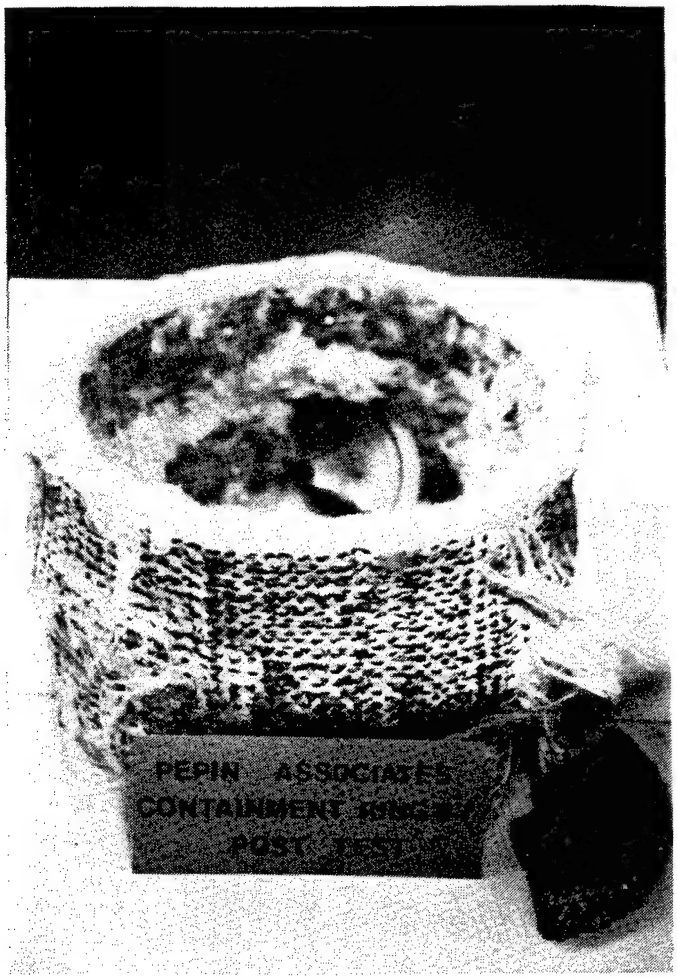

FIGURE 56. PHOTO OF SPIN TEST STRUCTURE 7 AFTER TEST

3.3.2.8 Spin Test Structure 8.

A major goal of this program was to test a containment ring made of PBO (polybenzbisoxazole) fiber and compare these results with those of a similar ring whose energy absorbing fiber was Kevlar 29. Spin test structure 8 was a PBO ring whose weight, geometry, and fiber architecture were designed and fabricated to match those of ring 5 as closely as possible. The PBO fiber was woven into a fabric, wrapped around a mandrel, and sewn circumferentially with the graphite/epoxy towpreg as was done for ring 5.

PBO is a new fiber being developed by Dow Chemical. Its high modulus, strength, and toughness coupled with its close to 300°C temperature stability and excellent fire and toxicity performance make this fiber attractive for a wide range of applications. One of these is containment structure since the temperature stability of PBO is significantly higher than Kevlar and it could be used near a hot section. Table 4 gives a comparison of Kevlar 29, PBO, and S glass mechanical properties at room temperature. The PBO fiber properties given are those of the actual fiber used in the structure 8 ring. Dow is currently fabricating fiber on a small pilot plant scale with strength and moduli significantly higher than those shown.

TABLE 4. COMPARISON OF PBO, KEVLAR 29, AND S GLASS FIBER MECHANICAL PROPERTIES

	Kevlar 29	PBO	S GLASS
Tensile Strength, ksi (MPa)	525 (3620)	674 (4647)	665 (4585)
Tensile Modulus, msi (GPa)	12 (82.7)	36 (248.2)	12.5 (86.2)
Strain to Failure, %	4	2.8	5.4
Density, g/cc	1.44	1.55	2.49

The PBO tows supplied by Dow were close to 1500 denier but there was some variation so they were paired to form as close to 3000 denier tows as possible. The resulting fabric was a 16- by 16-tow/inch plain weave with a weight of 14.43 oz/yd^2 compared to the 13.1-13.4 oz/yd^2 for the Kevlar style 745. Its width was 8.5 inches (21.6 cm) so the ring was 1/2 inch shorter than the Kevlar rings. Without sufficient material to develop the packing efficiency of the yarn, it was difficult to hit the 9 in width exactly. The PBO had to be woven with no waste since only enough material was provided to fabricate one ring. The fabric was woven on an Iwer rapier loom by Techniweave, Inc. of Rochester, NH. Due to the high cost of the developmental fiber (production fiber costs will be competitive) and the requirement that none of the fiber be wasted, the picks were inserted manually. Figure 57 shows the fabric being woven.

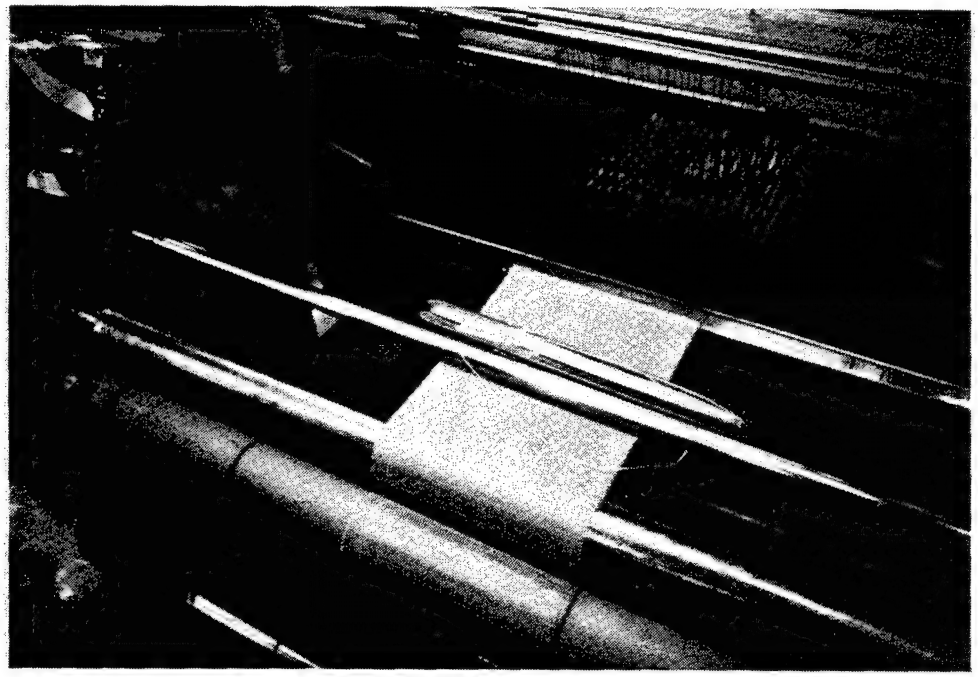

FIGURE 57. PBO FABRIC BEING WOVEN ON AN IWER RAPIER LOOM. NO WASTE COULD BE TOLERATED SO THE PICKS WERE INSERTED MANUALLY

All of the continuous fabric was wrapped tightly around a mandrel to yield a 49-ply ring whose weight before rod insertion, 14.44 lbs (64.2 N), was essentially the same as the Kevlar in the

structure 5 ring. The wall of the PBO ring was thicker because the fabric was 0.031 in (0.79 mm) thick instead of the Kevlar fabric's thickness of 0.024 in (0.61 mm). After insertion of the circumferential rod rows and molding the ring, the final ring weight was 15.72 lbs (69.9 N) and the wall thickness was 1.29 in. (3.27 cm). Due to the thickness of the PBO ring and the dry laminate resistance to insertion of the graphite towpreg, the towpreg was partially covered with a 1500 denier PBO tow. The dry PBO offered much less resistance when rubbed against the PBO fabric laminate making fabrication easier and protecting the graphite towpreg against fraying. This approach was begun when the ring was 15% sewn.

Figure 58 shows the PBO ring before testing and figure 59 is a close-up of the surface showing the towpreg loops, blue Teflon film, and the PBO fabric.

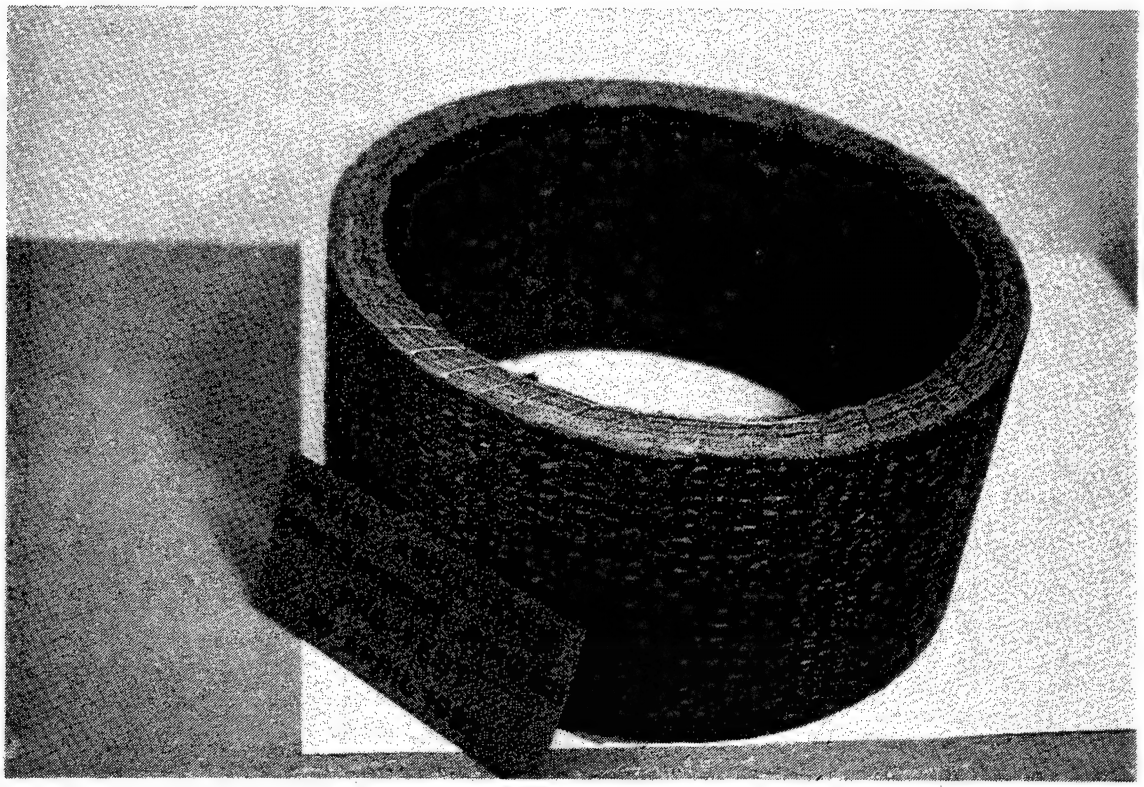

FIGURE 58. PBO RING BEFORE TESTING

The PBO ring was spin tested successfully with the tri-hub burst occurring at 20,580 RPM giving a burst energy of 985,248 in-lb. The ring contained the three disk fragments, but as with the number 5 Kevlar ring, one of the 1/3 disk segments drove a blade through the 49-ply wall such that this blade fragment also penetrated the witness ring. The angle between the rotor disk plane and a vector from the center of the rotor to the witness ring hole is 35° so the blade seems to have been deflected going through the ring. This particular disk segment itself penetrated 19 plies while the other two segments penetrated 16 plies and 25 plies of the PBO fabric. This is compared to the 50-ply Kevlar ring in which 26, 25, and 23 plies were penetrated with the first listed being that segment which pushed the blade through the ring wall.

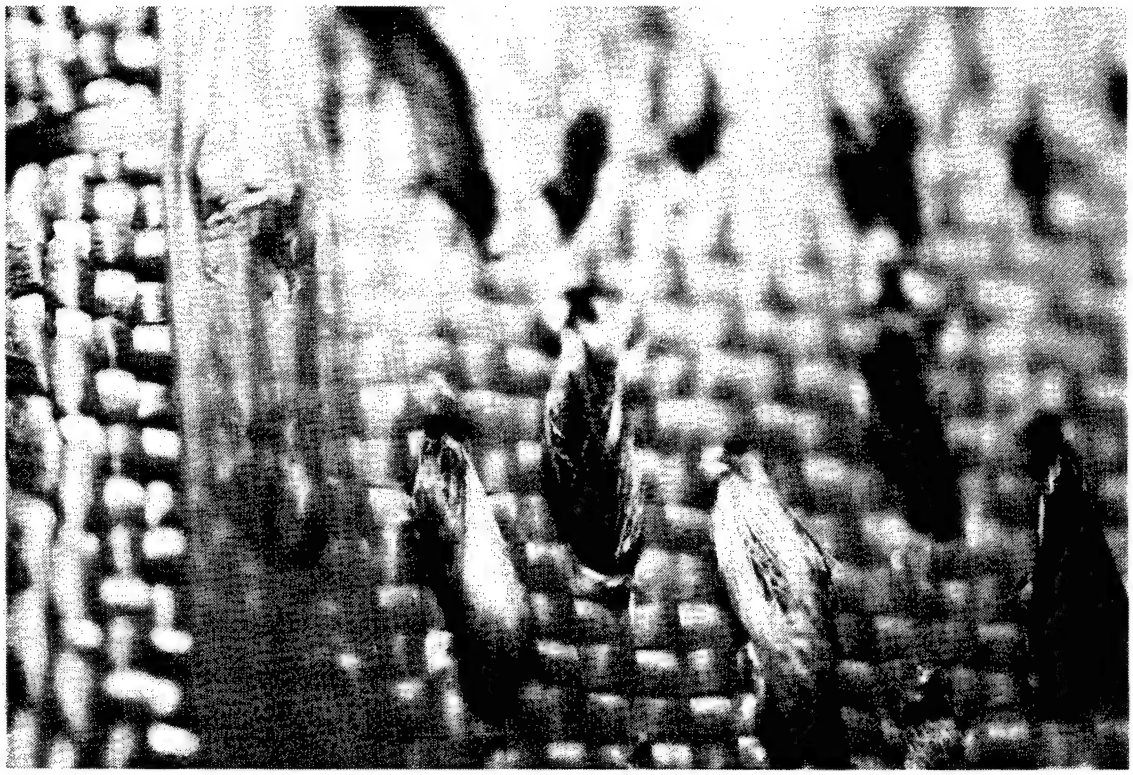

FIGURE 59. CLOSE-UP OF PBO RING SURFACE SHOWING TOWPREG LOOPS, TEFLON FILM, AND PBO FABRIC

Although fewer plies were penetrated in the PBO ring, the results appear similar and further testing would need to be done to confirm the difference in containment threshold between PBO and Kevlar 29. However, PBO's temperature stability still remains a dominant consideration for its use in containment structures. Figure 60 shows the PBO ring after test.

The high-speed photographs of the PBO ring test were not taken because the lighting system failed due to a short circuit in the wiring for these rapidly flashing lights.

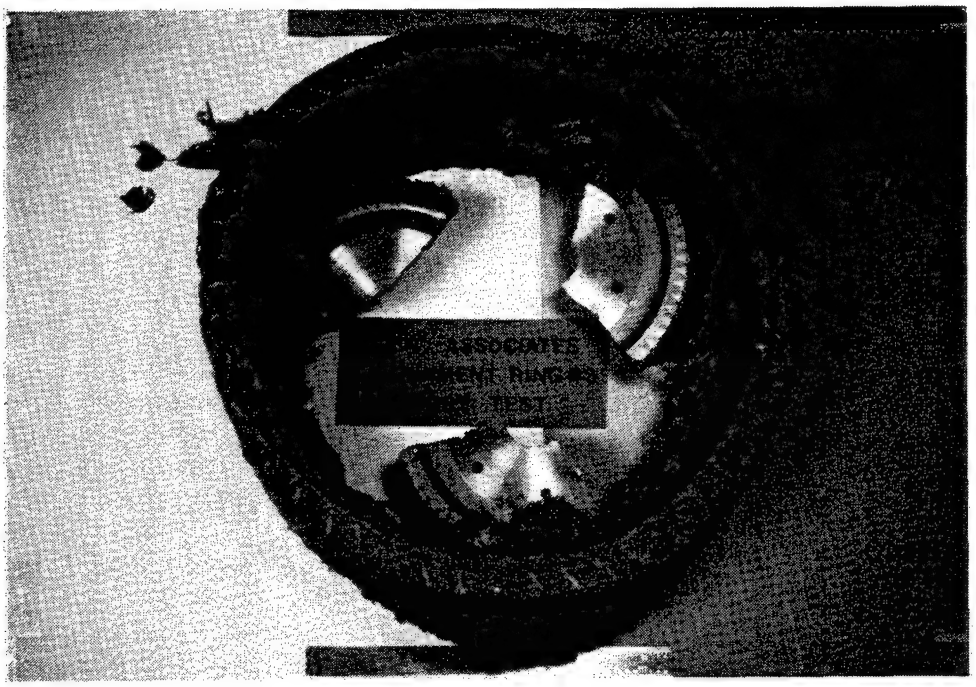

FIGURE 60. PBO RING AFTER TEST

3.3.2.9 Spin Test Structure 9.

Up to this point all of the fabric structures tested have been reinforced in the 0°, 90°, or hoop axial direction. The balanced plain weave fabric was either woven to the 9 inch (22.9 cm) width as with PBO or cut into 9-inch wide strips along the warp direction of a fabric roll as in the case of Kevlar style 745. For containment applications where greater deformation of the containment structure can be tolerated, it may be desirable to use off-axis reinforcement for fabric structures to exchange increased deformation for reduced weight.

General Electric has been testing braided Kevlar for fan blade containment with promising results. In 1976 Boeing successfully tested a ±45° reinforced 40-ply Kevlar ring against a T-58 tri-hub burst with a one million in-lb energy level. This test was done in the NAPC facility. To verify this approach and extend its application to a hybrid core construction, a 43-ply ±45° reinforced ring was wound with Kevlar style 745 fabric and sewn with Candidate B circumferential rods as before. The rod stitches were sewn circumferentially to allow the ring surface to freely shrink axially during the impact. As the ring expands to absorb the fragment energy the fabric stretches as a result of the yarn "scissoring" action which occurs as the yarns become more aligned with the hoop direction. This structure 9 ring was identical to spin test structure 7 except that structure 7 had the fabric oriented in the hoop, axial direction instead of ± 45°.

The structure 9 ring was fabricated by cutting 9-in (22.9-cm)-wide strips at 45° to the edge of a Kevlar style 745 fabric. Each strip was 59.5 inches (151.1 cm) long. These strips were wrapped around the same mandrel used to form the previous rings and the ends of the strips were butted together and lightly stitched to previous layers to hold them in place. These joints were staggered throughout the ring and it took 35 strips to lay-up the 43-ply ring. It was then stitched with the 12K towpreg using the Candidate B architecture as with several previous rings. A photo of the finished ring is shown as figure 61. It had a wall thickness of 0.96 in (2.44 cm) and weighed 13.2 lbs (58.72 N).

FIGURE 61. CONTAINMENT STRUCTURE 9 BEFORE TEST

Although the test setup and rotor configuration for this spin test were the same as for previous tests, the rotor failed at 24,440 RPM instead of the nominal 20,000 RPM. The tri-hub burst energy at this higher value was 1.39 million in-lbs. For the most part the ring contained the rotor burst but one of the disk segments seemed to have flipped over the edge of the ring at a low energy level. It was still moving fast enough, however, to cut and penetrate the witness ring near its edge. This problem may be resolved by interleaving hoop fibers near the ring edges to restrain their radial expansion. The impacting segment would then form more of a "cup-like" surface around itself preventing escape around the edges. Blade fragments penetrated the ring at two of the three disk fragment impact points. In these two areas the disk segments themselves cut through 13 and 18 plies with the remaining plies cut by the penetrating blades. The blade cuts were narrow slit type cuts allowing the blade to penetrate through the remaining plies of the ring behind the force of the impacting disk. The "scissoring" effect of the yarns in the fabric as it stretches caused the ring axial dimension to shrink about 1 inch (2.54 cm) as measured after the test. This axial shrinking was probably greatest at the maximum deformation of the ring during the impact event. The maximum radial deformation measured from the high-speed photos was

4.7 inches (11.9 cm) while the maximum radial deformation of ring 5, a 50 ply 0°,90° ring which contained the three disk segments, was 1.9 inches (4.8 cm). So the obvious price to be paid for a lower weight containment structure using ±45° architecture is increased deformation of the structure to stop the fragments. This may be acceptable for some containment installations but others may have hardware interfering with the potential deformed space. In these cases a heavier 0°, 90° configuration may be required.

Figure 62 shows ring 9 after the test. Notice how puffed out and separated the ring edges are compared to the 0°, 90° rings. Since the ring initially has a small resistance to radial deformations the wall can accelerate rapidly with the impacting fragment. The disk fragment causes a midplane bulge which is transmitted to the ring edges in a wave-like fashion. The rapid acceleration/deceleration of the edges, their relative "softness" radially, and perhaps their ability to shed the graphite/epoxy rods at the edges may all contribute to the expansion of the dry laminate at the edges. This can be seen in the high-speed photos of figure 63A-H. The first photo was taken before the test while the second begins the impact sequence as the blades initially touch the ring wall. The seven photos of the rotor fragments impacting the ring cover 2.85 msecs.

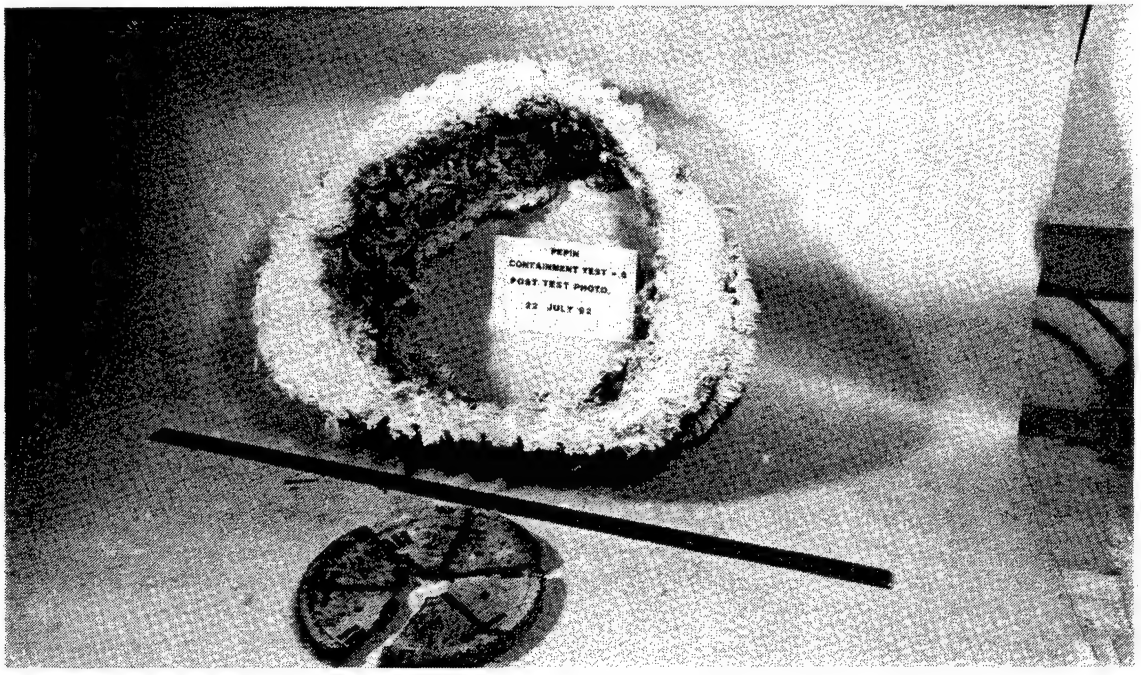

FIGURE 62. CONTAINMENT STRUCTURE 9 AFTER TESTING. ROTOR ENERGY WAS 1.39 MILLION IN-LBS. DISK FRAGMENTS DID NOT PENETRATE ALTHOUGH ONE SEEMS TO HAVE TUMBLED OVER THE EDGE AT A LOW ENERGY LEVEL

High-speed photographs of test 9 are shown in figure 63A-H. The top photo is earlier than bottom photo. Photo A is a pretest photo while B through H record the rotor fragment impact against the containment ring. The time between each photo B through H is 0.475 msecs. (NOTE: The black vertical line through some of the pictures is a tear in the film.)

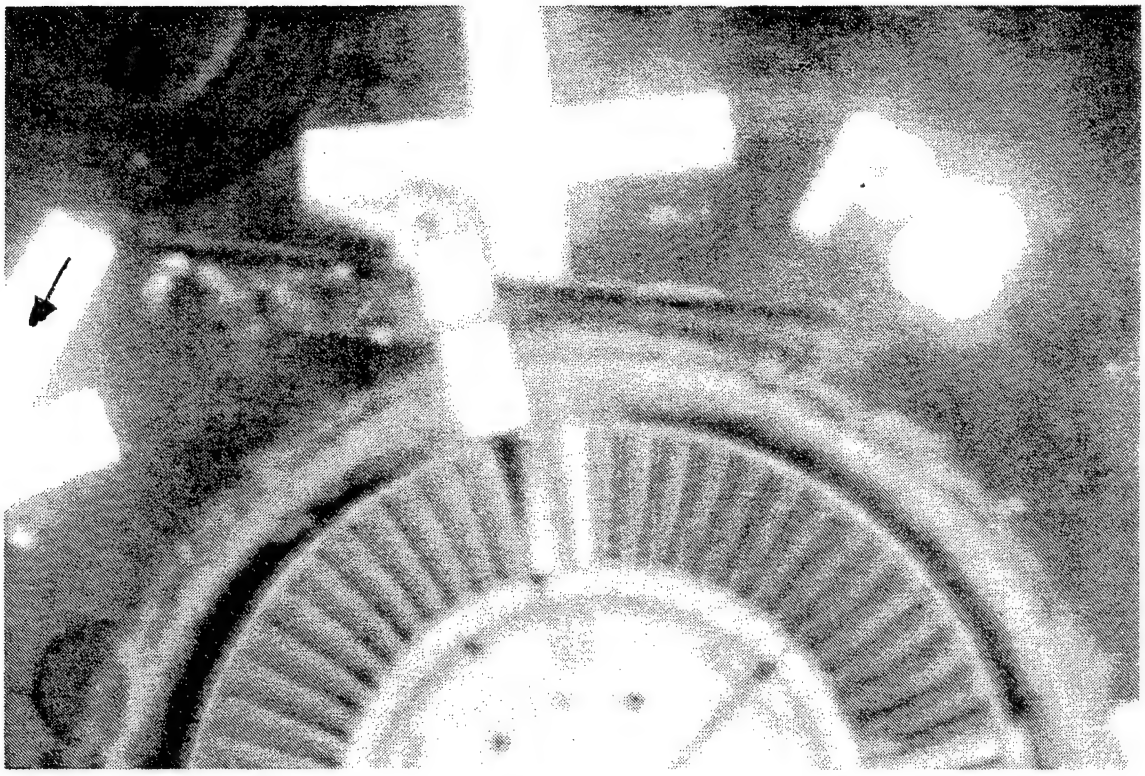

FIGURES 63A-H. (A) HIGH-SPEED PHOTOGRAPHS OF TEST 9

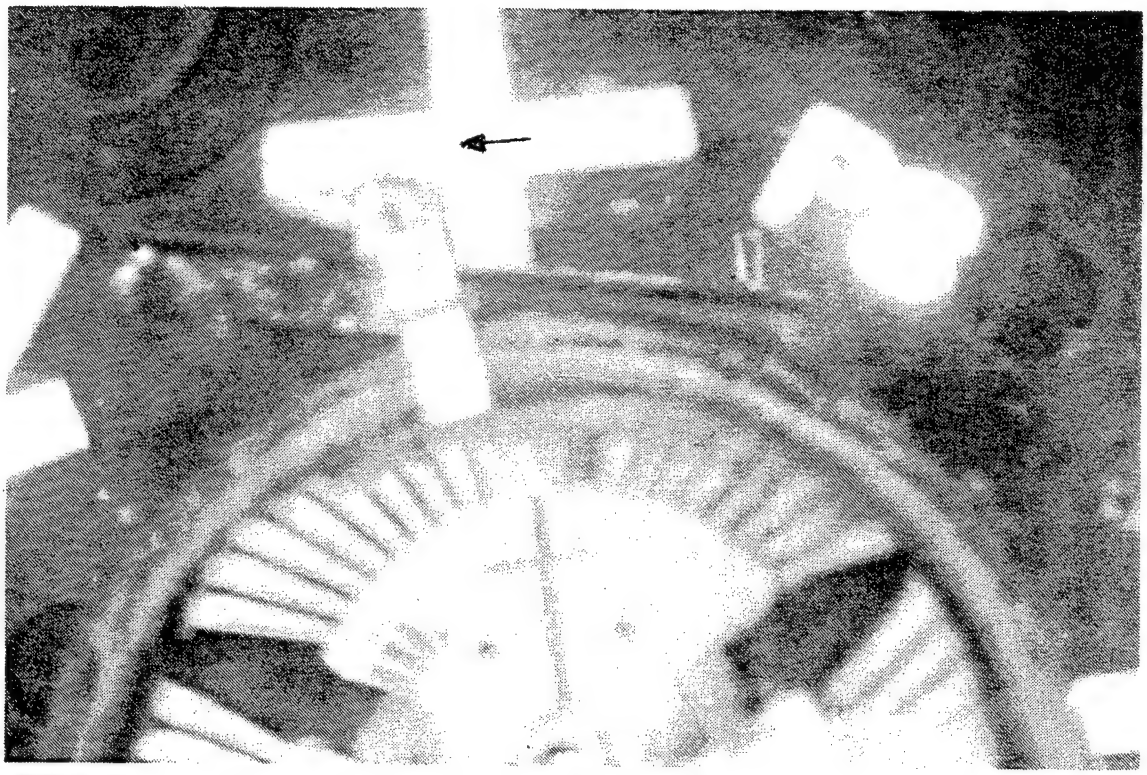

(B)

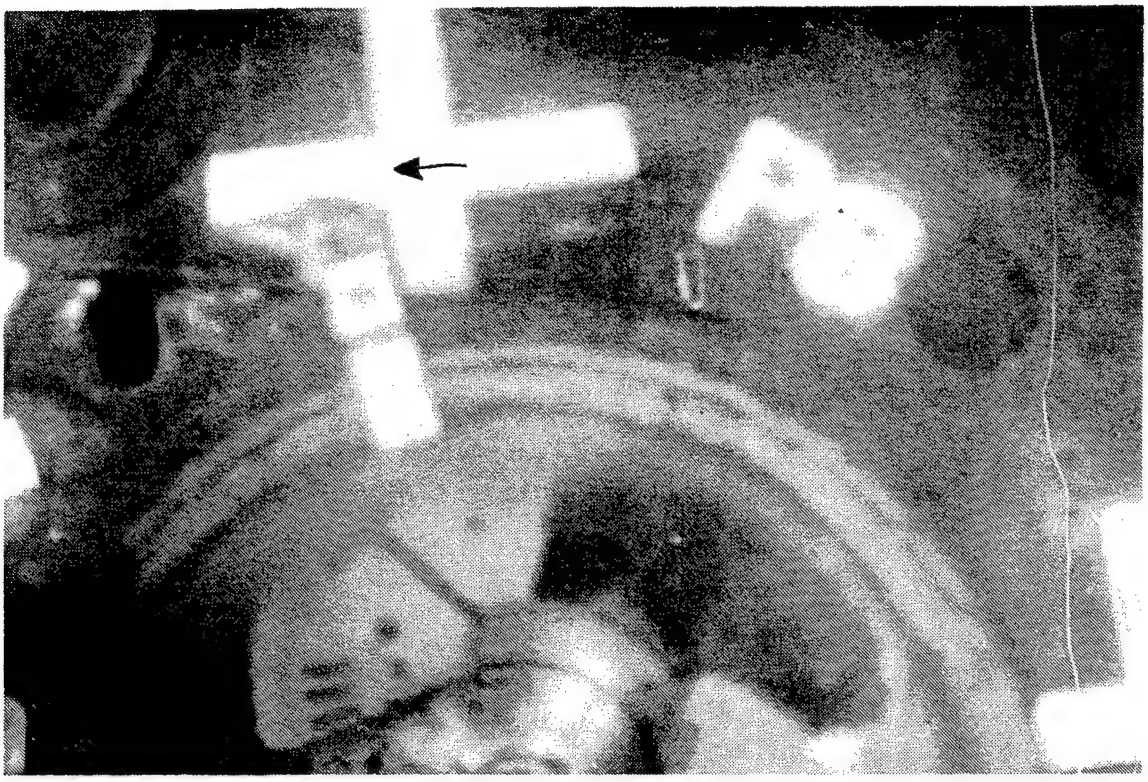

(C)

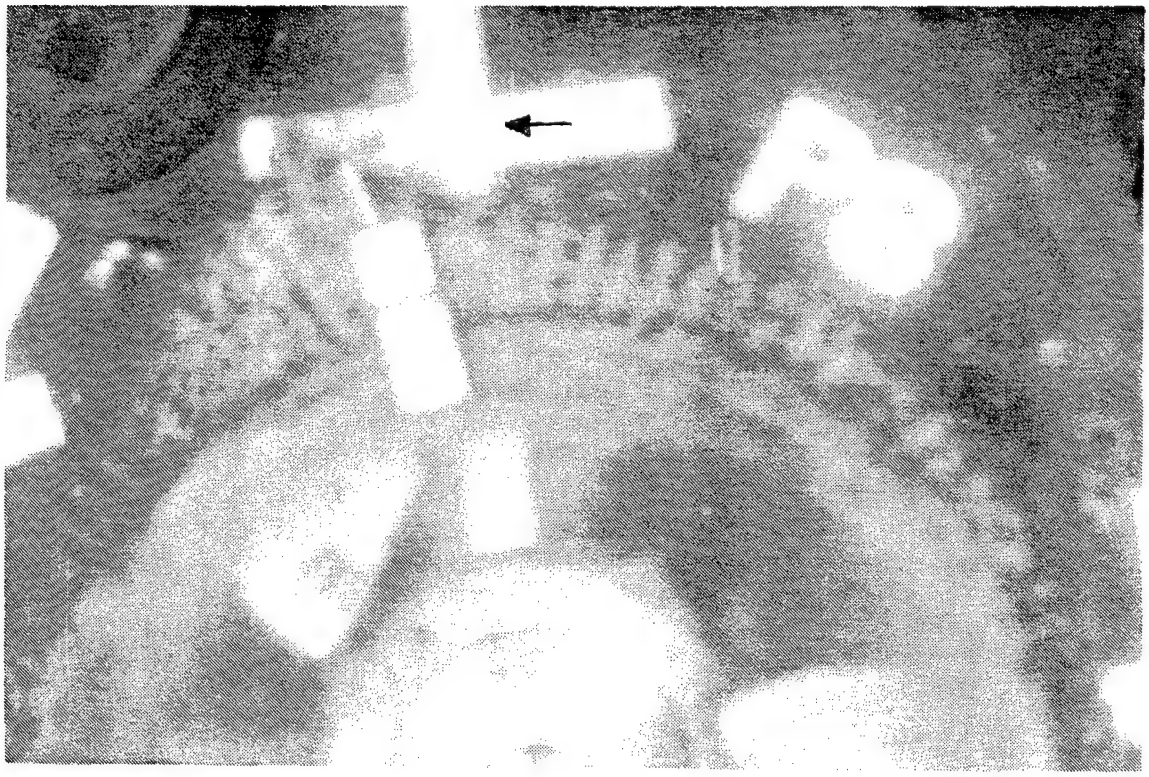

(D)

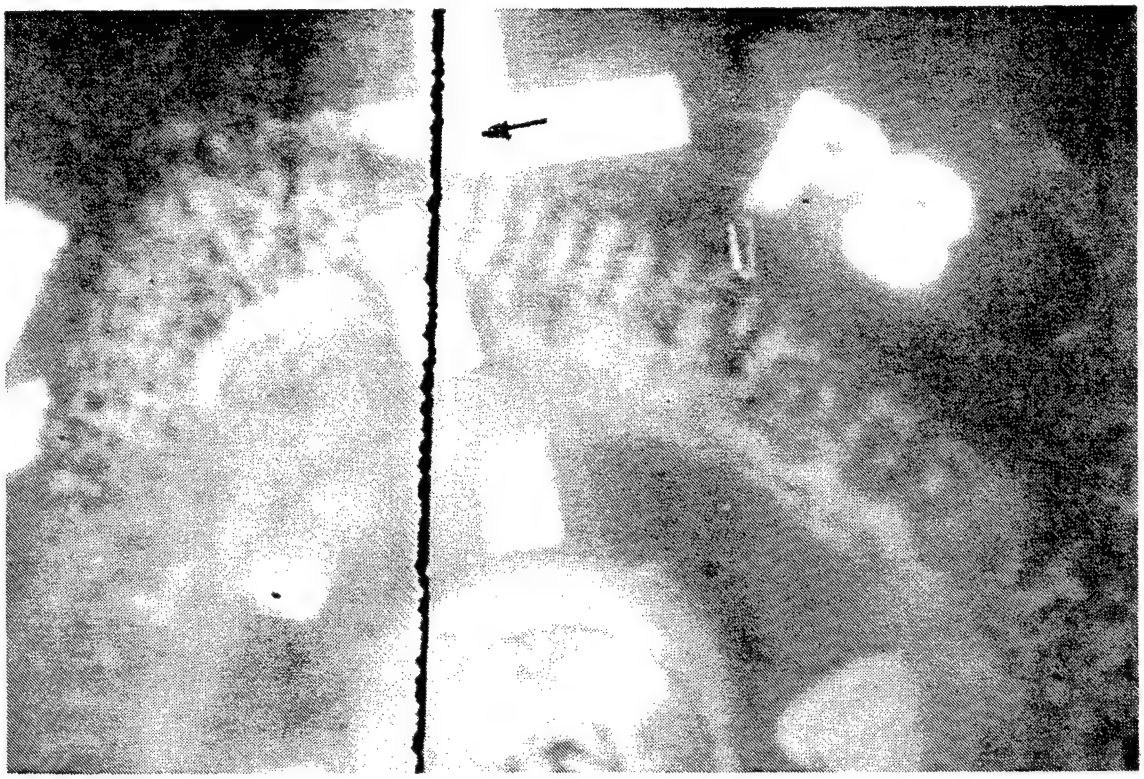

(E)

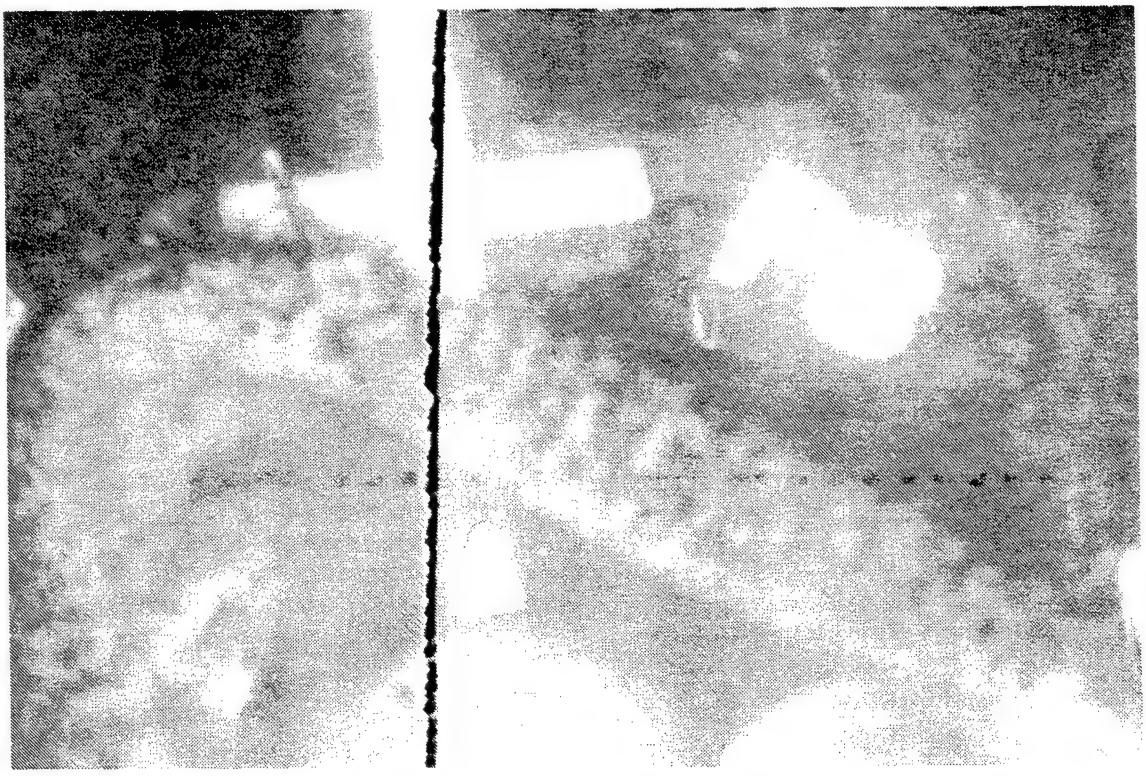

(F)

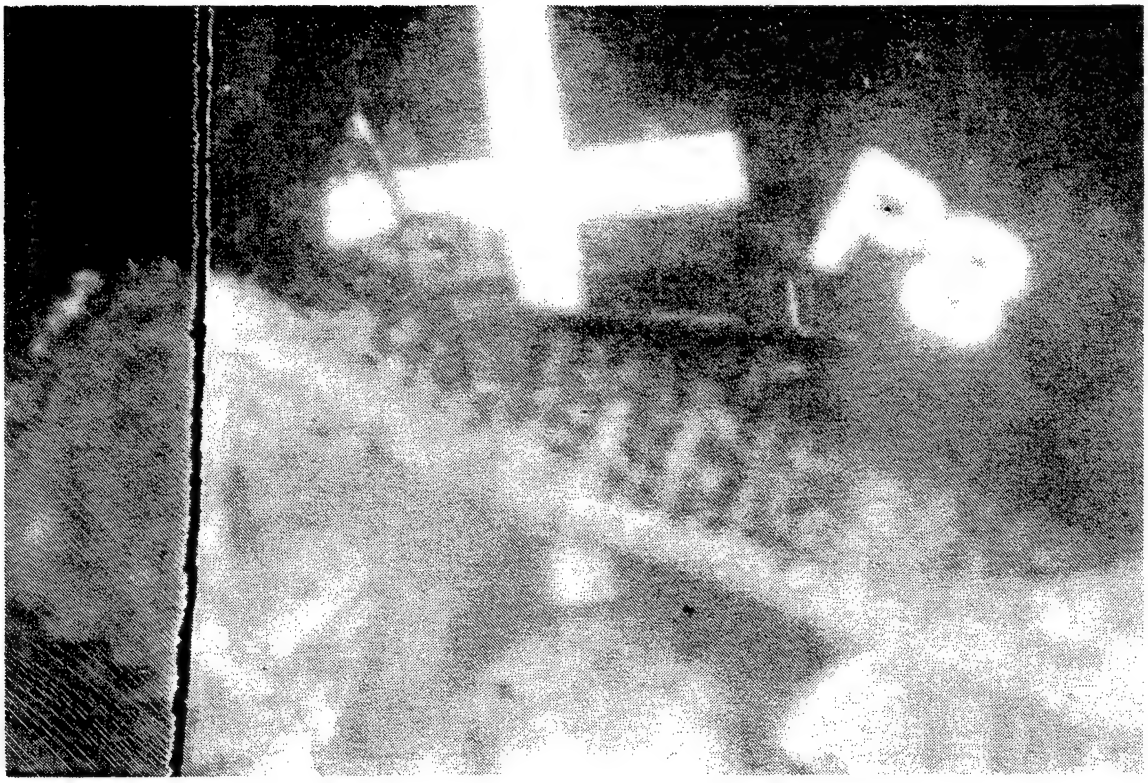

(G)

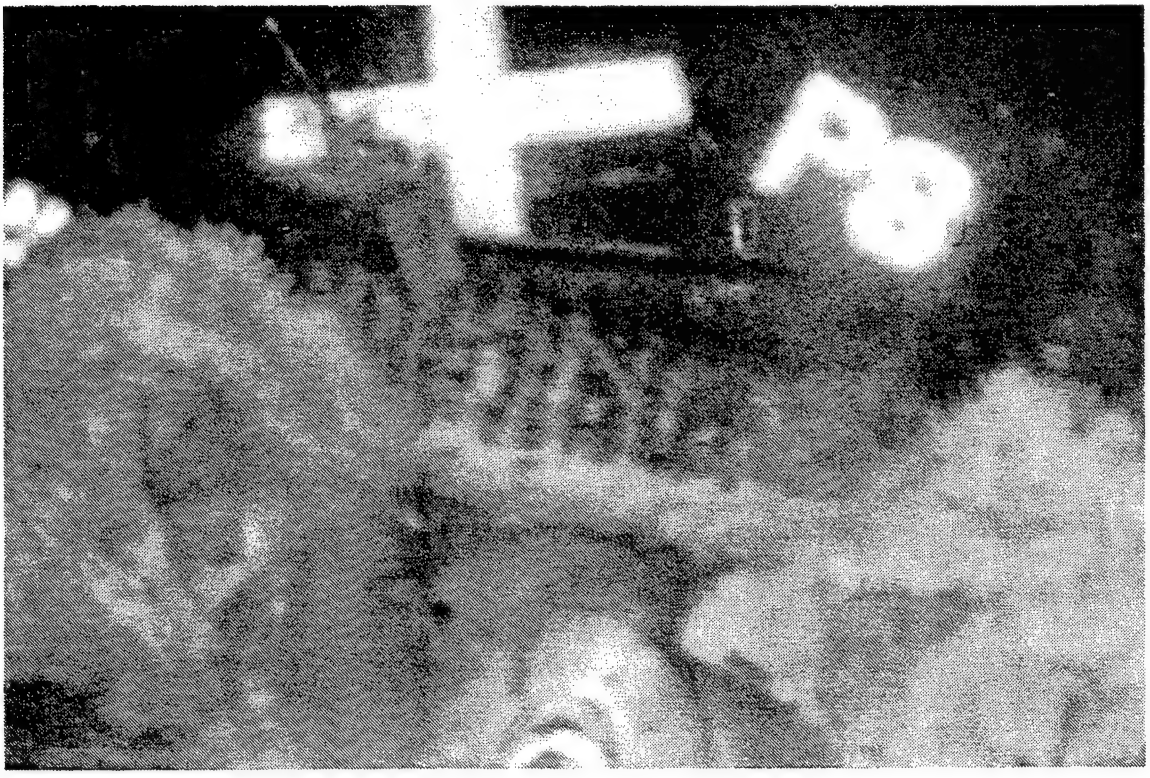

(H)

3.3.2.10 Spin Test Structure 10.

The tenth spin test structure was composed of two curved panels joined by hinge type joints. The potential advantage of these joints is that they would be lighter and allow motion of a panel around a hinge as for a cowling for example. Forty-three plies of Kevlar style 745 fabric formed the energy absorbing component of each panel and the panels were sewn with the candidate B architecture graphite/epoxy towpreg as was ring number 7. The fabric was all oriented in the 0°,90° direction so the basic configuration of the structure is the same as for ring 7. The two joints, one at each end of this lenticular shaped structure, were formed by wrapping the 9-inch (22.9-cm)-wide fabric around two rods as shown in figures 64 and 65. Alternating solid and hollow aluminum doughnuts were slipped over the rod and the fill fibers of the fabric were pulled out only in the joint area leaving the warp fibers to wrap into the open or hollow spaces. The metal ring shown provided the tension as the panel was wrapped. After the panel was wrapped, the warp fibers which were wound into the thin walled open doughnuts were stitched a few times to trap the open doughnuts into the part. The only function of the thin-walled doughnuts was to contain the warp fibers as they made their continuous turn around the joint. The part was then removed from the tooling by sliding it off the solid rod. At this time the solid doughnuts, which merely act as spacers, were removed as well. The spaces which the solid doughnuts occupied accommodate the wound joint section of the opposing panel. The hinge type joint, then, was formed by continuous, unidirectional warp yarns of the fabric making a racetrack-like turn around a pin. The pins for both joints were fabricated by pulling dry Kevlar 29 tows into a thin-walled aluminum tube. The actual tubes had 0.037-inch (0.094-cm) wall thickness and each contained 2079 Kevlar 29 tows of 3000 denier each. The panels were stitched and molded as before and the finished structure is shown in figure 66. The weight of the completed structure was 22.88 lb (101.8 N) and its dimensions are given in figure 32.

One of the joints of this structure was protected by a 30-ply Kevlar style 745 dry laminate pad tucked into the interior corner made by the joint as shown in the photo. The pad was attached with steel hook and loop fastener tapes from Velcro®. These tapes were press molded using FM 355 adhesive. Hook and loop fasteners are finding application in armor and high-vibration environments because the joints remain intact when subjected to these severe situations. Since it was not known initially how the joint would react to a direct impact and if, in fact, a disk fragment would impact a joint at all, only one pad was added. It was felt that something would be learned about the performance of the joint in either case and this information could be applied to future work.

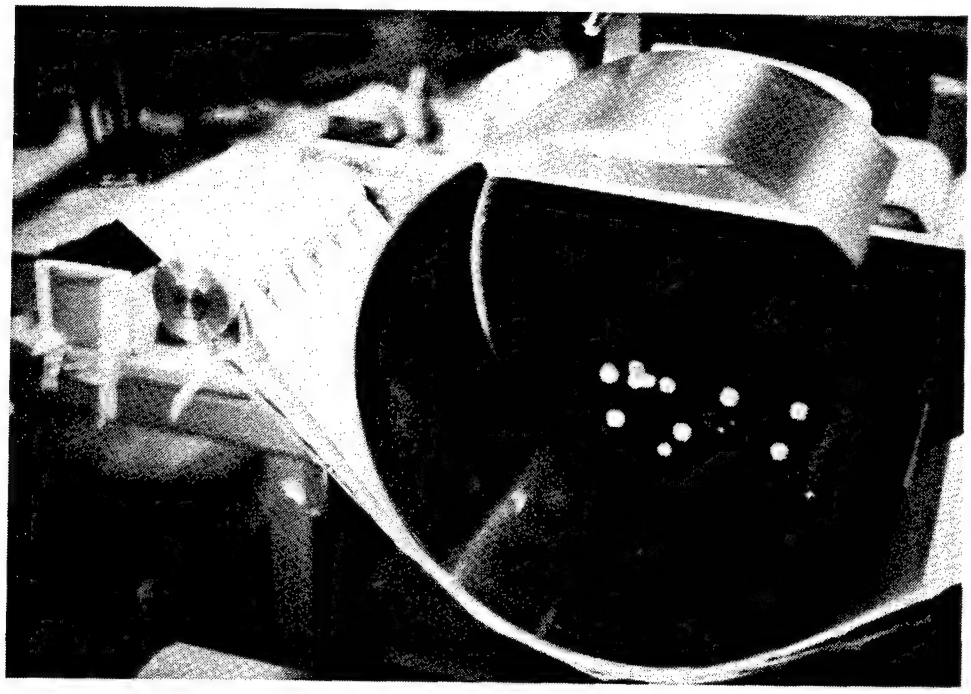

FIGURE 64. PANEL FOR SPIN TEST STRUCTURE 10 BEING FABRICATED. SPLIT STEEL RING PROVIDES TENSION AS THE PANEL IS BEING WRAPPED.

FIGURE 65. CLOSE-UP OF JOINT AREA OF PANEL AS IT IS FABRICATED. HOLLOW, THIN-WALLED DOUGHNUTS DEFINE THE SPACE FOR THE WARP YARNS TO BE WRAPPED. SOLID DOUGHNUTS ARE SPACERS FOR THE SLOTS INTO WHICH THE OTHER PANEL'S YARNS WILL FIT.

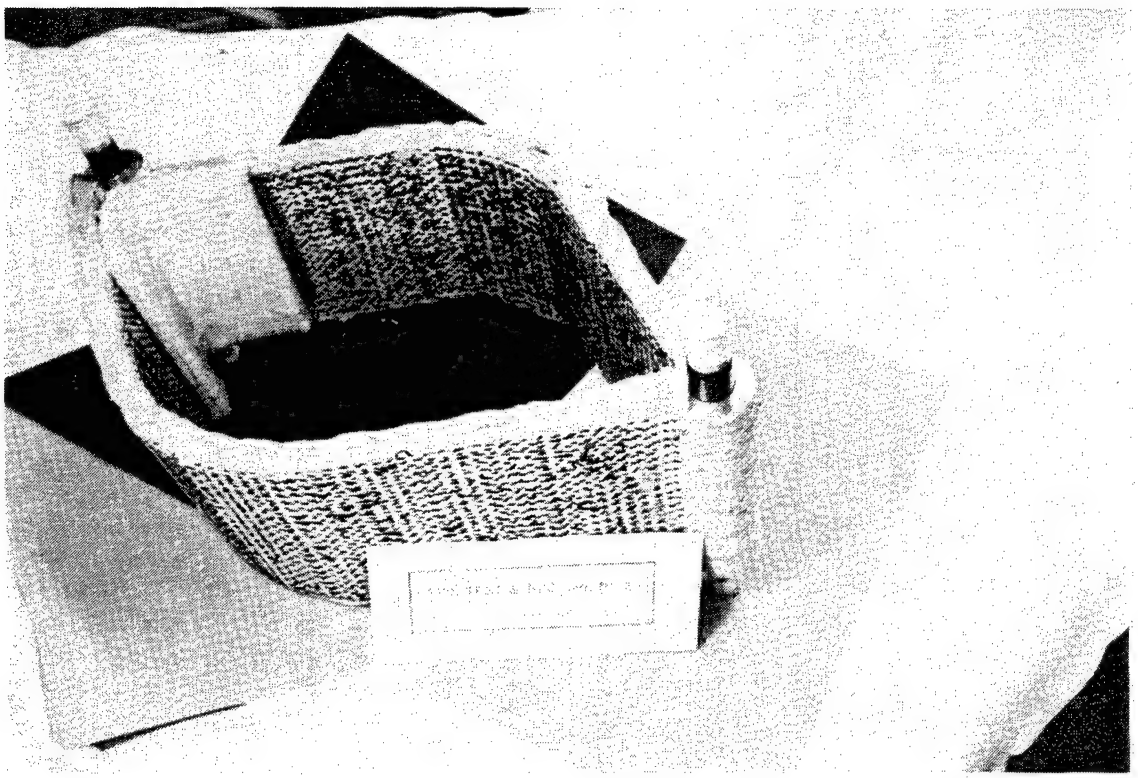

FIGURE 66. FINISHED AND ASSEMBLED SPIN TEST STRUCTURE 10. PINS AT THE JOINTS ARE UNIDIRECTIONAL KEVLAR IN A THIN THIN-WALLED, 1.25-IN OD ALUMINUM TUBE. THE JOINT PROTECTIVE SHIELD IS A 30-PLY DRY LAMINATE ATTACHED WITH VELCR0®.

Spin test structure 10 was successfully tested with the rotor failing at 20,800 rpm giving an energy level of 1.01 million in-lbs. Two of the three disk fragments impacted the panels and were contained within the structure while the third hit the unprotected joint almost directly and went through it. The two contained disk segments penetrated 23 and 13 plies of the 43-ply lay-up. A photograph of the structure after testing is shown in figure 67 while the high-speed photographs are shown in figure 68. The protective pad fastened with the Velcro remained attached to the panels during the impact since it is seen to straighten out with its joint in the high-speed photographs. The joint not impacted supported the dynamic tensile load without much damage. Even though the aluminum doughnuts containing the continuous warp fibers were not restrained axially, only the ones at the ends started to slip off the pins. This hinge type joint, then, seems to have some potential if it can be protected.

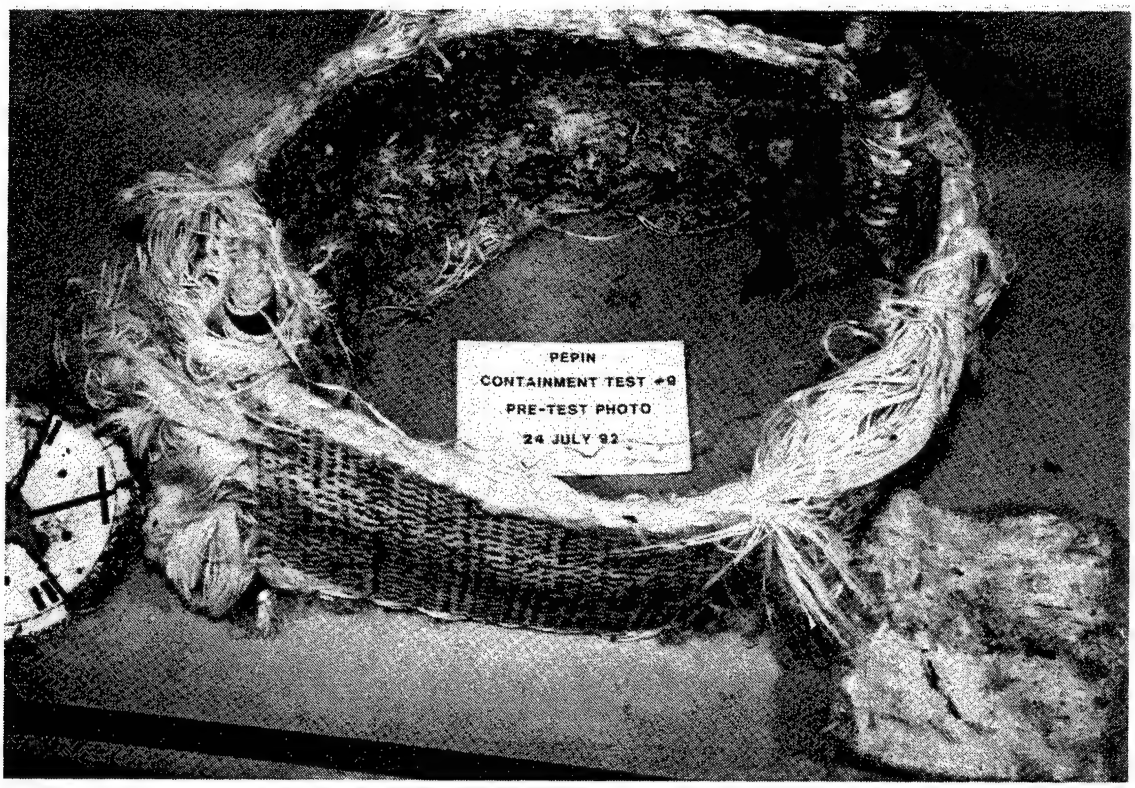

FIGURE 67. SPIN TEST STRUCTURE 10 AFTER TESTING

The first photo is taken before the test while the second records the initial impact. The succeeding photos are in time steps of 0.488 msecs giving a total time between photos B and H of 2.93 msecs.

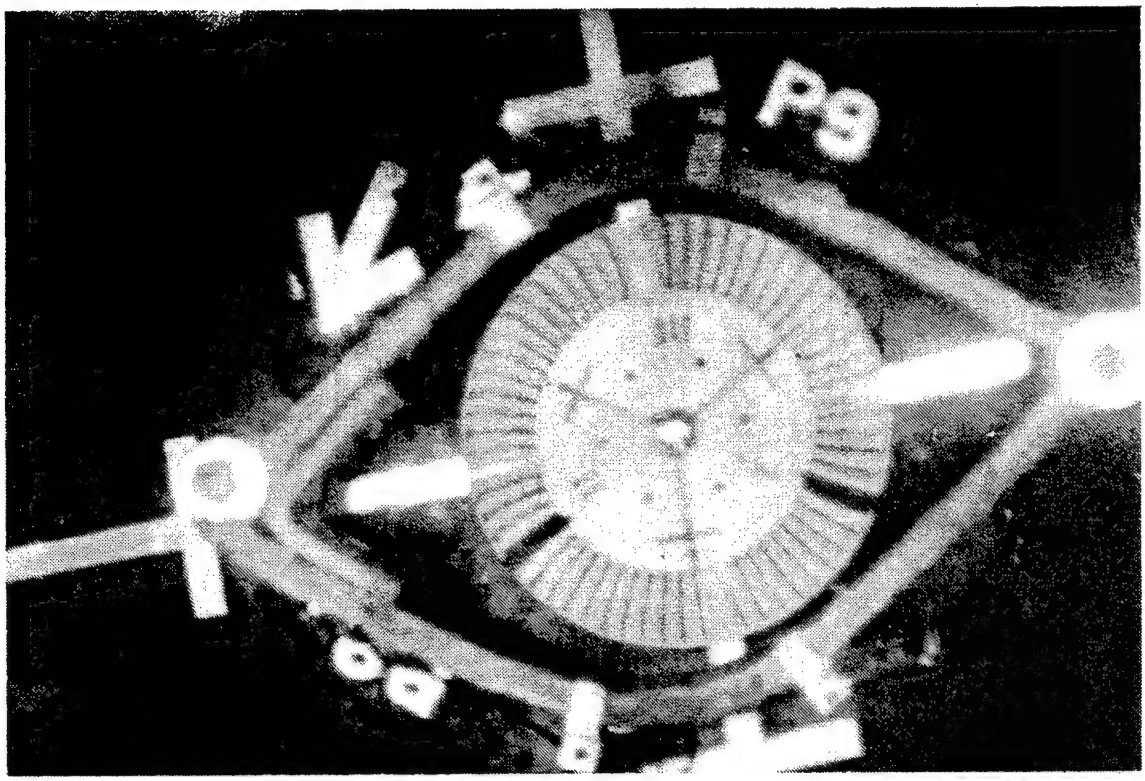

FIGURES 68A-H. (A) HIGH-SPEED PHOTOS OF SPIN TEST 10

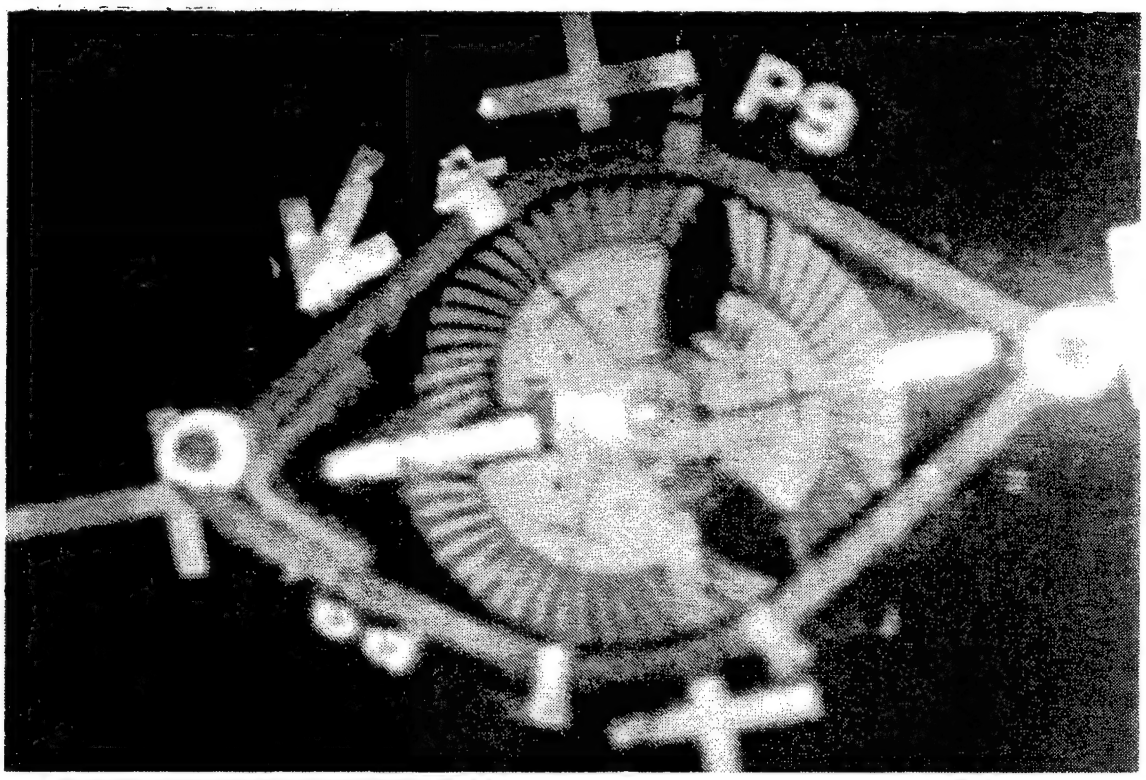

(B)

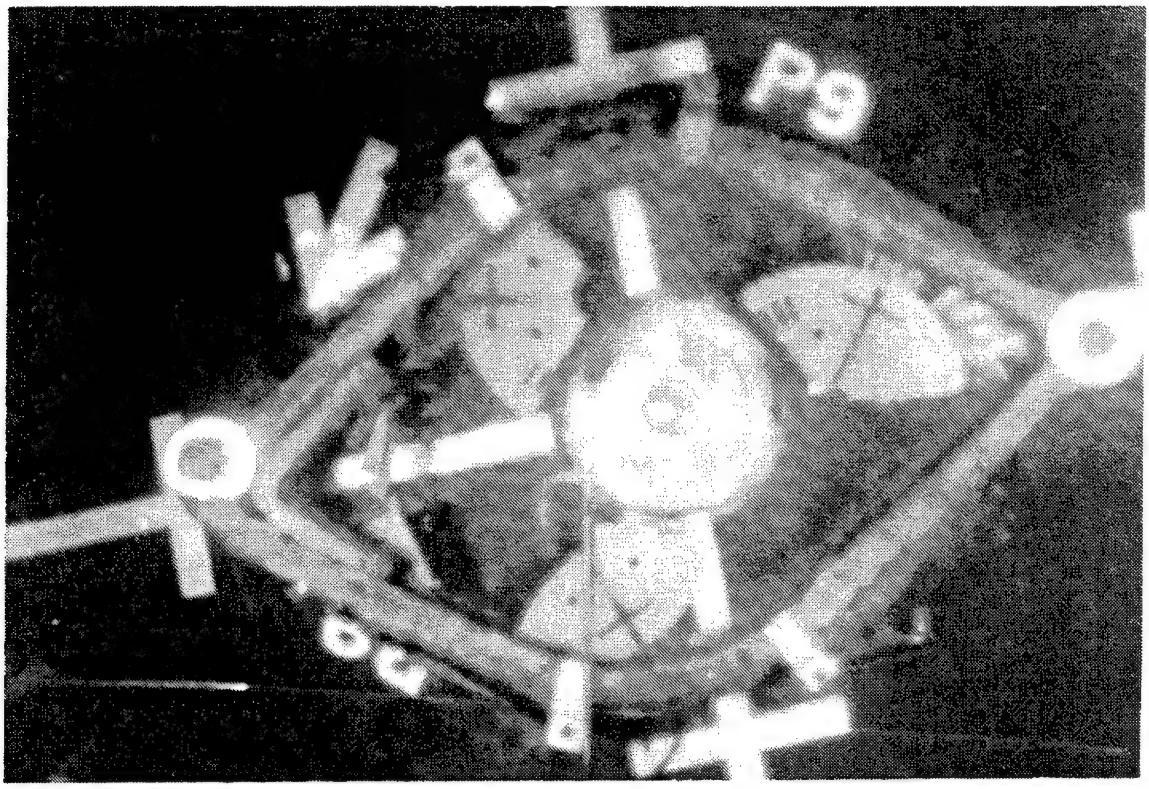

(C)

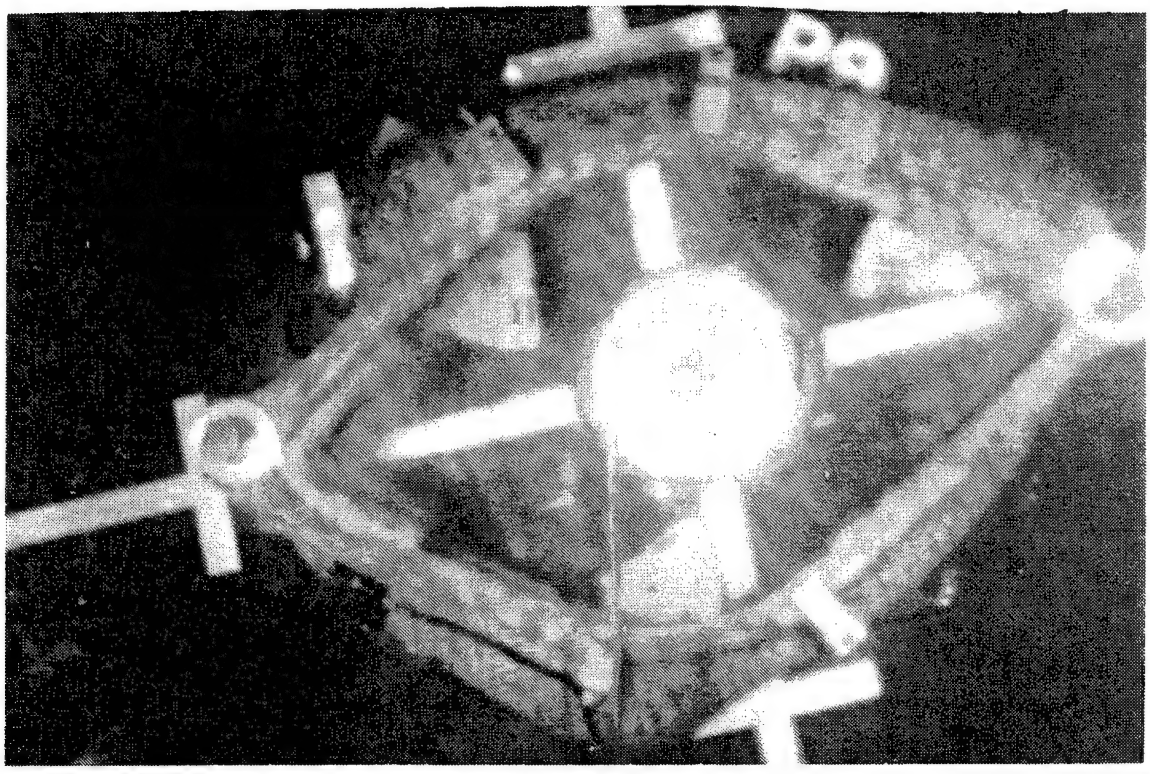

(D)

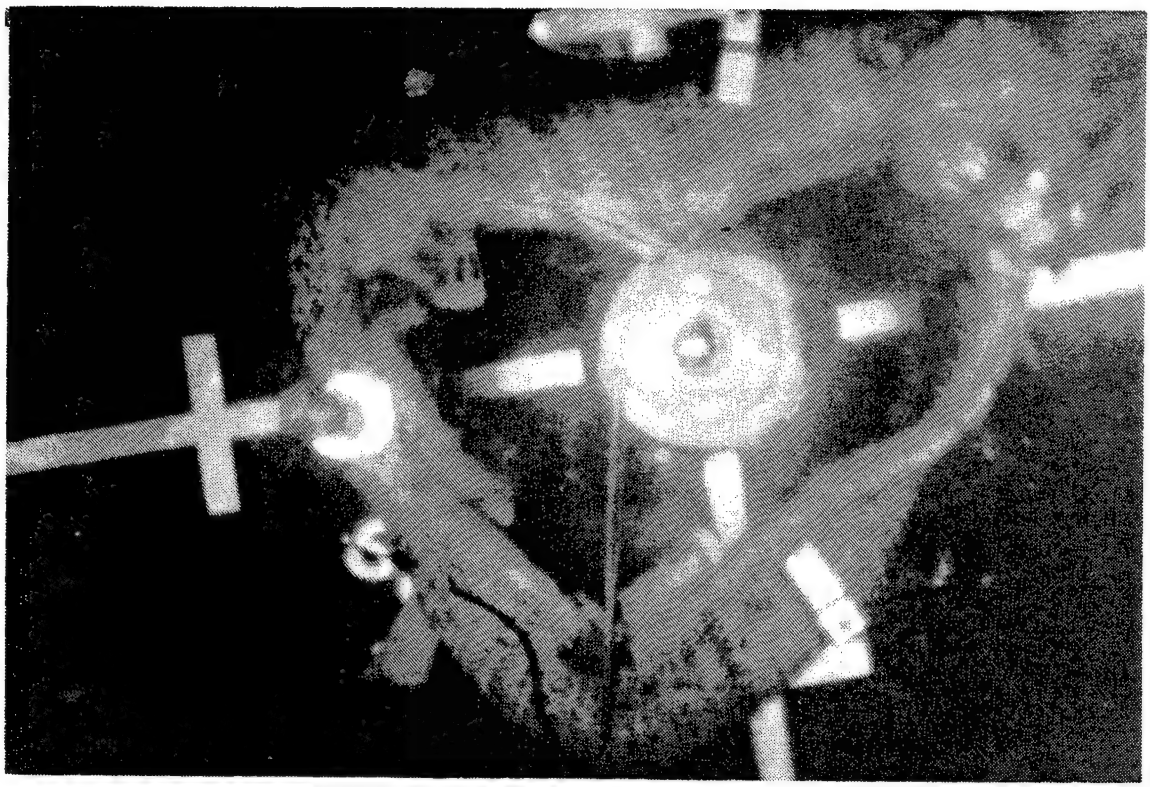

(E)

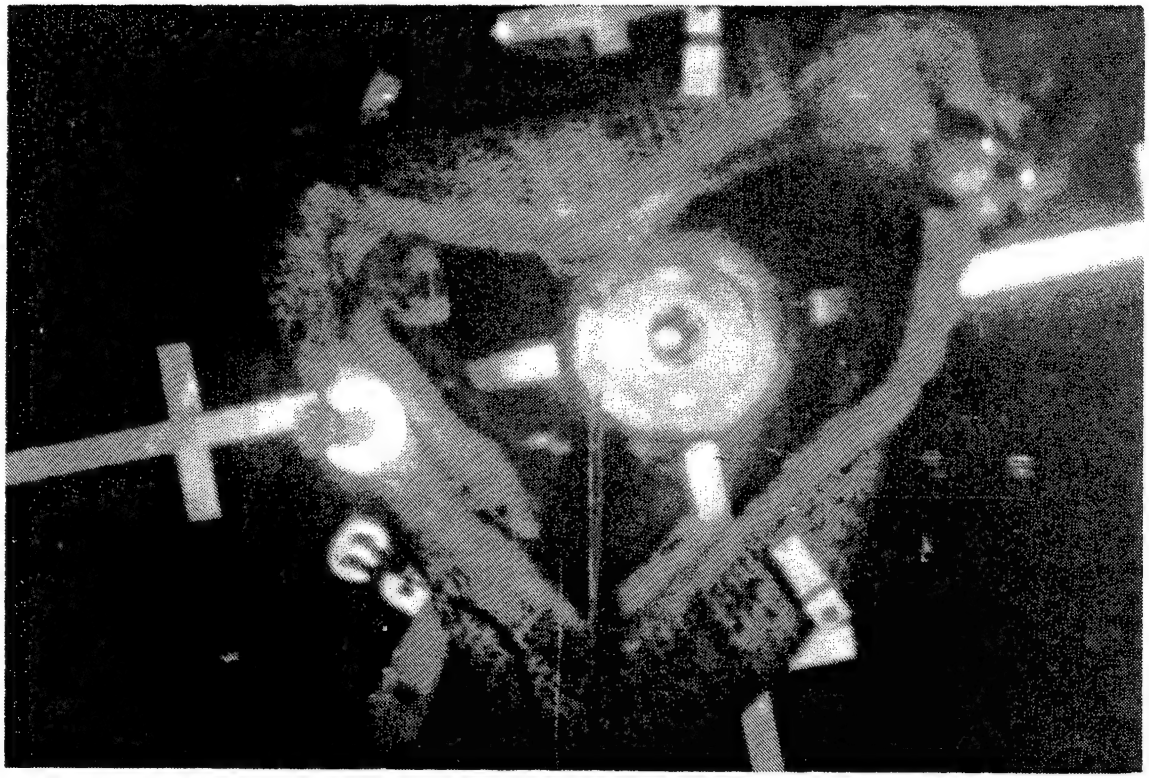

(F)

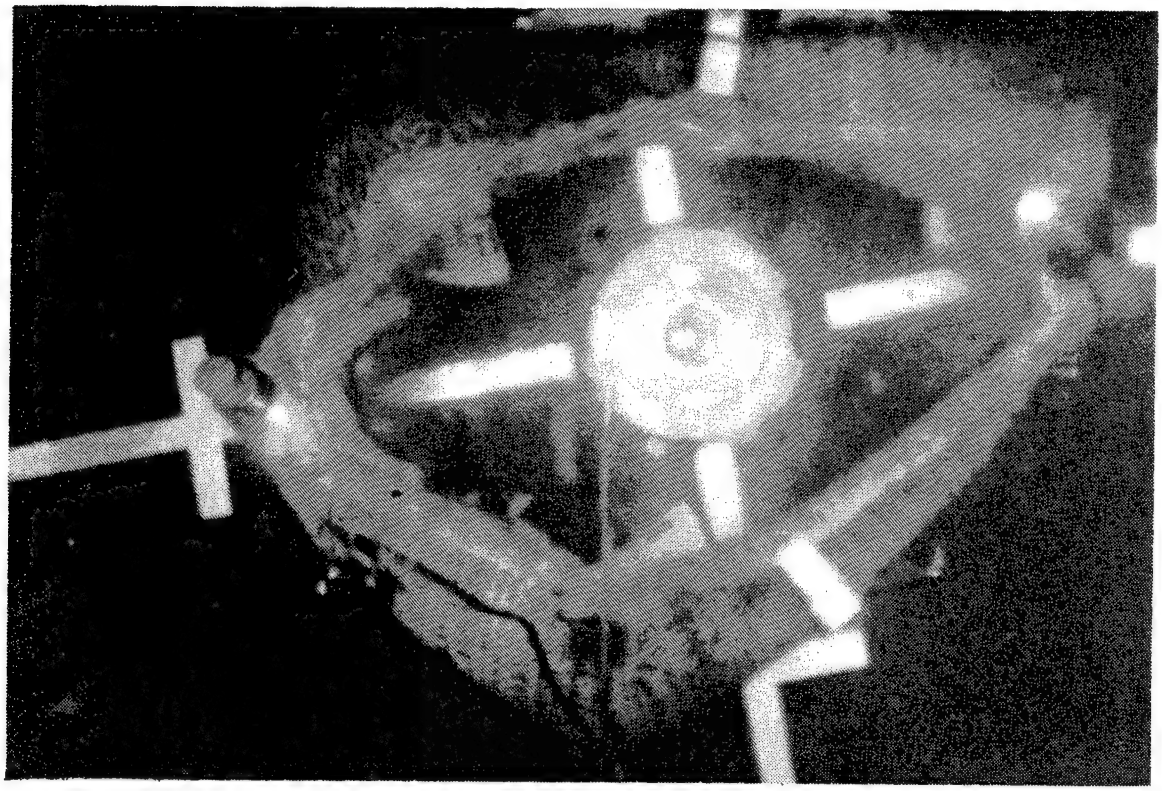

(G)

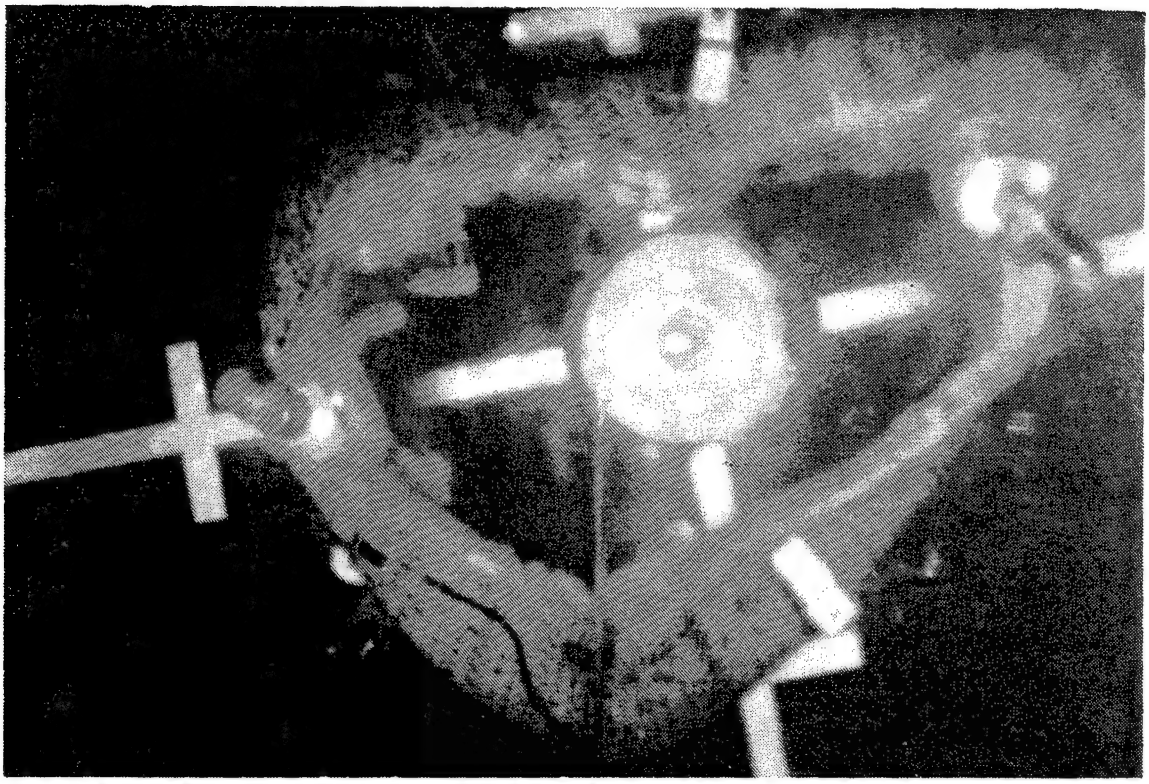

(H)

3.3.3 Spin Test Result Summary.

The following table presents a summary of the ten spin tests performed.

TABLE 5. SPIN TEST SUMMARY

TEST	GEOMETRY	ARCHITECTURE/ ORIENTATION	WEIGHT (LBS)	CONTAINED?	COMMENTS
1	Triangle Bolted	32 Plies K29 Style 745 (0°, 90°)	44.1	No	Disk segment hit steel plate in corners shearing panel
2	Triangle Bolted	37 Plies K29 5:1 PW (0°, 90°)	27	No	Weave too loose; K washer plates
3	Triangle Bolted	36 Plies K29 Style 745 (0°, 90°)	33	Yes	
4	Ring	36 Plies K29 Style 745 (0°, 90°)	10.7	No	3 segments penetrated
5	Ring	50 Plies K29 Style 745 (0°, 90°)	15	Yes	Disk segment hammered blade through wall
6	Ring	50 Plies K29 Style 745 (0°, 90°)	15	Rotor didn't fail	Stitched axially
7	Ring	43 Plies K29 Style 745 (0°, 90°)	12.9	No	1 of 3 segments penetrated
8	Ring	49 Plies PBO PW (0°, 90°)	15.7	Yes	Disk segment hammered blade through wall
9	Ring	43 Plies K29 Style 745 (±45°)	13.2	Yes	One segment tumbled over at low-energy level
10	Lenticular Hinged Panels	43 Plies K29 Style 745 (0°, 90°)	22.9	No	One segment penetrated unprotected joint

This spin test program demonstrated that the hybrid panel core can absorb the energy of high-velocity fragments even though it is pierced by many closely spaced rigid rods. The results of the PBO ring test also showed that PBO is at least as good and perhaps better than Kevlar 29 at room temperature in this containment application. The real advantage of PBO, however, will be at higher temperatures where it will likely be one of the few options for lightweight, fiber-reinforced containment structures. Although these were the primary program goals, several other observations were made which will be helpful in the design of actual containment structures for aircraft and helicopter installations.

The ability of a structure to contain a disk burst is a function of its constituent materials, fiber architecture, effective circumference, geometry, and areal weight. For example, the larger effective circumference and flat panel geometry of the triangular structure allowed it to contain the rotor burst at 36 plies instead of 50. The bending deformation of the flat panels contributed to the energy absorption by spreading the deceleration of the rotor fragments over space and time. It remains to be determined what would happen if the three disk fragments hit the corners of the

triangle directly. In this case the panel bending and large deformation caused by this bending would not play as great a role.

The difference between the ±45° and 0°, 90° fiber architecture was also shown to be quite significant. The ±45° architecture allows a large expansion to take place as the fibers scissor and become more aligned with the hoop direction. As a result a lower areal weight could be used if the larger expansion could be tolerated and the fragments could be captured within the containment structure. One of the disk fragments of test 9 seems to have flipped over the ring edge due to the low hoop restraint of this architecture. Hoop fibers near the edges or a triaxial fabric may solve this problem. The 0°, 90° architecture on the other hand stopped the fragments in a smaller space and formed a pocket which seemed to trap each particular fragment. This was accomplished, however, at the expense of greater weight and numbers of plies. The design of the rigid rod orientation may play a small role in the containment effectiveness of the hybrid panel. Test 6 in which the candidate B rods were sewn axially instead of circumferentially was designed to check this effect but the test itself was not successful as the rotor separated from the shaft before failing. All of the other structures had candidate B circumferential rods. So in addition to showing the effectiveness of the hybrid panel and PBO fiber, the spin test program also developed information about the influences of geometry and fiber architecture on the effectiveness of containment panels and rings.

The spin test program also yielded other specific results. The containment threshold of the 0°, 90° Kevlar style 745 ring was established for the one million in-lb rotor burst between 43 and 50 plies of this material when sewn with the candidate B rod design. This result was about the same or perhaps slightly better than the same ring without the graphite/epoxy rods. It was also learned that, in some cases, blades were hammered through the rings by the disk fragments even though those disk fragments were contained.

This could be solved by hard facesheets to crush the blades or it may be that during an actual engine failure the blades would be stripped off as the disk fragment penetrated the engine case, burner cans, or other surrounding engine hardware. Another observation which will be important in containment structure design is that a hard, massive object in the containment structure's expansion zone can cause the laminate to be pinched between that object and the high-velocity fragment resulting in shear failure of the structure. The first triangular structure tested may have just contained the rotor burst had it not been for this shear failure against a steel washer plate.

Finally, a first step was taken toward design of lightweight joints for containment structures. A bolted joint was used for the three triangular test structures and this seemed to perform satisfactorily although it was heavy because of the bolt weight and weight of the resin used to impregnate the end tabs. The hinge joint was an attempt to eliminate the bolts and resin and, hence, the added weight by using a wound approach with a central pin. The fibers around the joint and through the pin were confined to the required shapes by using thin walled aluminum doughnuts and tubes. Although one of these joints failed upon direct impact in structure 10, the opposing joint sustained the loading. This design then has some promise if it can be protected from a direct impact from a disk fragment.

4. ESTIMATE OF TECHNICAL FEASIBILITY OF APPROACHES PRESENTED.

The mechanical test program and spin test program just described have shown that the hybrid sandwich panel has the ability to efficiently support mechanical loading like most honeycomb sandwich panels used in aircraft and also has the ability to stop high-energy fragments from a failed turbine rotor. In addition this program has shown that PBO can be an effective material for containment at room temperature and should be a very attractive material at high temperature.

It is felt that these concepts have a range of applications in containment design situations. The sandwich panel, for example, could be used as a cowling or nacelle structure or as an internal panel near an engine to selectively protect certain aircraft components. It would have application wherever a structural panel must also act as a barrier to high-energy fragments. With the potential performance of such a panel having been demonstrated, its commercial viability now is a question of efficient manufacture and design flexibility to meet a variety of customer needs. It is believed feasible to develop equipment to rapidly fabricate panels and rings such as those used in this Phase II program as well as structures of metals; e.g., replacing the graphite/epoxy with titanium. These automated fabrication approaches will be pursued to meet requirements of airframe and engine manufacturers.

PBO has a strong potential to be an excellent, lightweight material for containment structures. At present PBO fiber is a developmental material at Dow Chemical and its commercial availability could be several years away. It is believed that its technical performance in containment structures near engine hot sections will be very good but its eventual use in containment structures will be more a function of its overall market viability in many applications. Strong markets in several areas for this fiber will ensure its future production.

5. CONCLUSIONS.

This Phase II work was successful in showing that:

1. The hybrid sandwich panel can effectively support mechanical loads similar to those experienced by commonly used honeycomb panels and can also effectively stop high-energy rotor burst fragments.

2. When used in a containment structure, PBO is at least as effective as Kevlar at room temperature and potentially is one of the few choices for lightweight containment structures at elevated temperature.

3. Reinforcement fiber architecture, areal weight, and containment structure geometry play a strong role in the ability of the structure to stop a given rotor burst. Greater expansion of the ±45° architecture potentially yields a lighter structure but a tailored or triaxial reinforcement design may be necessary to ensure that the fragments are captured in the structure.

4. A continuous, wound hinge type joint can be an effective means to couple adjoining panels if it is protected during a direct impact by a disk fragment.

5. Massive objects in the expansion zone of a containment structure must be avoided to prevent pinching and shear failure of the structure. Blades must also be crushed to avoid their being pushed through the structure by the following disk segment.

6. REFERENCES.

1. FAA Advisory Circular, "Design Considerations for Minimizing Hazards Caused by Uncontained Turbine Engine and Auxiliary Power Unit Rotor Failure," AC20-128A, July 18, 1995.

2. "Report on Aircraft Engine Containment," Society of Automotive Engineers, Inc. Aerospace Information Report AIR 4003, September 1987.

3. Private communication, Mark Fulmer, FM Northeast Region, Burlington, MA, March 1989.

4. Private communication, Rocky Semprebon, Textron Lycoming, E. Hartford, CT, March 1989.

5. Private communication, Greg Harville, Bell 222 Captain, New Hampshire Helicopters, April 1989.

6. Forrester, J., "The Containment Advantages of Braided Kevlar," The Leading Edge, Winter 1990/1991, a publication of GE Aircraft Engines.

APPENDIX A—MECHANICAL TEST SPECIMEN DIMENSIONS

TABLE A.1

Specimen Number	Thickness in (cm)	Kevlar Fabric Length x Width in (cm)	Graphite/Epoxy Length x Width in (cm)	Notes
		THROUGH-THICKNESS COMPRESSION		
A1	0.660 (1.68)	2.86 (7.26) square	2.05 (5.21) square	
A2	0.700 (1.78)	2.80 (7.11) square	2.09 (5.31) x 2.03 (5.14)	
A3	0.680 (1.73)	2.90 (7.37) square	2.06 (5.23) square	
B1	0.587 (1.49)	2.64 (6.71) square	2.25 (5.72) square	99 rods
B2	0.593 (1.51)	2.63 (6.68) x 2.71 (6.88)	2.22 (5.63) square	77 rods
B3	0.587 (1.49)	2.66 (6.76) square	2.22 (5.63) square	77 rods
C1	0.575 (1.46)	2.61 (6.63) square	2.28 (5.79) x 2.20 (5.59)	106 rods
C2	0.580 (1.47)	2.62 (6.68) square	2.23 (5.66) x 2.29 (5.82)	108 rods
C3	0.565 (1.44)	2.61 (6.63) x 2.67 (6.78)	2.26 (5.74) x 2.21 (5.61)	107 rods
		SHEAR		
A1	0.384 (0.98)	2.6 (6.60) x 3.8 (9.65)	2.0 (5.08) x 3.8 (9.65)	
A2	0.372 (0.94)			
A3	0.373 (0.95)			
B1	0.597 (1.52)	Nominal	Nominal	
B2	0.634 (1.61)			
B3	0.613 (1.56)			
C1	0.593 (1.51)	2.64 (6.71) x 3.85 (9.78)	2.03 (5.16) x 3.78 (9.60)	163 rods
C2	0.607 (1.54)	2.63 (6.68) x 3.80 (9.65)	2.14 (5.44) x 3.75 (9.53)	173 rods
C3	0.592 (1.51)	2.66 (6.76) x 3.85 (9.78)	2.12 (5.38) x 3.80 (9.65)	162 rods
		FLEXURE		
A1	0.60 (1.52)	2.3 (5.84) x 9 (22.86)	2.0 (5.08) x 8.75 (22.23)	Nominal
A2	0.68 (1.73)	2.38 (6.05) x 9 (22.86)	2.0 (5.08) x 8.75 (22.23)	
A3	0.60 (1.52)	2.3 (5.84) x 9 (22.86)	2.0 (5.08) x 8.75 (22.23)	Nominal
B3	0.64 (1.63)	2.3 (5.84) x 9 (22.86)	2.0 (5.08) x 8.75 (22.23)	
B3	0.64 (1.63)	2.3 (5.84) x 9 (22.86)	2.0 (5.08) x 8.75 (22.23)	
C1	0.675 (1.71)	2.0 (5.08) x 8.9 (22.61)	2.0 (5.08) x 8.9 (22.61)	497 rods
C2	0.675 (1.71)	2.2 (5.56) x 9.0 (22.86)	2.0 (5.08) x 8.9 (22.61)	491 rods
C3	0.67 (1.70)	2.2 (5.59) x 9.0 (22.86)	2.0 (5.08) x 9.0 (22.86)	492 rods